LICENTIATE THESIS

Statistical Calibration Algorithms for Lidars

Anas Alhashimi

Control Engineering

LULEÅ UNIVERSITY OF TECHNOLOGY

Statistical Calibration Algorithms for Lidars

Anas W. Alhashimi

Department of Computer Science, Electrical and Space Engineering
Division of Signals and Systems
Luleå University of Technology
Luleå, Sweden

Supervisors:

Thomas Gustafsson, Damiano Varagnolo

Printed by Luleå University of Technology, Graphic Production 2016

ISSN 1402-1757
ISBN 978-91-7583-650-8 (print)
ISBN 978-91-7583-651-5 (pdf)

Luleå 2016

www.ltu.se

to my mother and father,
to my wife and my lovely kids,
to my whole family and friends.

Abstract

Robots are becoming increasingly available and capable, are becoming part of everyday life in applications: robots that guide blind or mentally handicapped people, robots that clean large office buildings and department stores, robots that assist people in shopping, recreational activities, etc.

Localization, in the sense of understanding accurately one's position in the environment, is a basic building block for performing important tasks. Therefore, there is an interest in having robots to perform autonomously and accurately localization tasks in highly cluttered and dynamically changing environments.

To perform localization, robots are required to opportunely combine their sensors measurements, sensors models and environment model. In this thesis we aim at improving the tools that constitute the basis of all the localization techniques, that are the models of these sensors, and the algorithms for processing the raw information from them. More specifically we focus on:

- finding advanced statistical models of the measurements returned by common laser scanners (a.k.a. Light Detection and Rangings (Lidars)), starting from both physical considerations and evidence collected with opportune experiments;

- improving the statistical algorithms for treating the signals coming from these sensors, and thus propose new estimation and system identification techniques for these devices.

In other words, we strive for increasing the accuracy of Lidars through opportune statistical processing tools.

The problems that we have to solve, in order to achieve our aims, are multiple. The first one is related to temperature dependency effects: the laser diode characteristics, especially the wave length of the emitted laser and the mechanical alignment of the optics, change non-linearly with temperature. In one of the papers in this thesis we specifically address this problem and propose a model describing the effects of temperature changes in the laser diode; these include, among others, the presence of multi-modal measurement noises. Our contributions then include an algorithm that statistically accounts not only for the bias induced by temperature changes, but also for these multi-modality issues.

An other problem that we seek to relieve is an economical one. Improving the Lidar accuracy can be achieved by using accurate but expensive laser diodes and optical lenses. This unfortunately raises the sensor cost, and – obviously – low cost robots should not be equipped with very expensive Lidars. On the other hand, cheap Lidars have larger biases and noise variance. In an other contribution we thus precisely targeted the problem of how to improve the performance indexes of inexpensive Lidars by removing their biases and artifacts

through opportune statistical manipulations of the raw information coming from the sensor. To achieve this goal it is possible to choose two different ways (that have been both explored):

1. use the ground truth to estimate the Lidar model parameters;
2. find algorithms that perform simultaneously calibration and estimation without using ground truth information.

Using the ground truth is appealing since it may lead to better estimation performance. On the other hand, though, in normal robotic operations the actual ground truth is not available – indeed ground truths usually require environmental modifications, that are costly. We thus considered how to estimate the Lidar model parameters for both the cases above.

In last chapter of this thesis we conclude our findings and propose also our current future research directions.

Contents

Part I

Part II

Acknowledgments

In the name of Allah, the Most Gracious and the Most Merciful. Alhamdulillah, all praises to Allah for the strengths and His blessing in completing this thesis.

Special appreciation goes to my supervisor, the associate senior lecturer Damiano Varagnolo, for his supervision and constant support. His invaluable help of constructive comments and suggestions throughout the experimental and thesis works have contributed to the success of this research. Not forgotten, my appreciation to my main-supervisor, Prof Thomas Gustafsson for his guidance, support and for giving me the opportunity to be here.

First, I would like to express my thanks to the Ministry of Higher Education and Scientific Research and the University of Baghdad for their financial support.

Special thanks goes to all my friends and colleges who have supported and encouraged me during the research especially PhD students at LTU.

Last, but not least, I would like to thank my wife for her understanding and love during the study years. Her support and encouragement was in the end what made this dissertation possible. I would like to thank my parents for allowing me to realize my own potential. They receive my deepest gratitude and love for their dedication and the many years of support they have provided me over the years was the greatest gift anyone has ever given me.

Part I

Chapter 1

Introduction

1.1 Background

The capability of measuring distances is essential to interact effectively with unknown environments. When being in an unknown place, for example, a robot (or animal, or human, it does not matter) must infer where the obstacles are to be able to move without colliding with them.

A classic example of the importance of being able to measure distances is given by autonomous cars: they continuously update maps of the surrounding environment and decide their actions based on the position of the various obstacles. In every industrial and practical applications where the environment is unknown, from autonomous robots that clean floors to robots that fly to do aerial inspection and repair, one thus needs to be able to measure distances.

Among the various distance sensors, Lidars are very promising due to their excellent performance vs. cost ratios. Indeed they are often the main sensors used in applications like navigation, object detection, localization and mapping. Lidars are also the main sensor for Google's and Volvo's self-driving cars; for example, Google's cars are equipped with a Velodyne 64-beam Lidar system [1] (costing around $\$70,000$) mounted on the top (see Figure 1.1) allow vehicles to generate detailed 3D maps of the surroundings (Volvo cars have instead a cheaper solution based on static sensors; nonetheless the basic idea is the same).

There is obviously an increasing interest to have Lidars that are both not only *accurate*, but also *cheap*: accurate and precise Lidars already exist, but they tend to be expensive, and thus not suitable for mass-deployments. On the other hand, also cheap Lidars already exist; of course their negative side is that they have larger biases and noise variances than their expensive counterparts.

The main objective of this thesis is to provide statistical tools that improve the precision and accuracy of Lidars , specially the non-expensive ones, through ad-hoc statistical filters and smoothers that process the raw data collected by the sensors.

Finding these filters and smoothers requires providing accurate statistical models that can explain and agree with both the operation physics and the evidence collected by these devices. Notice that our type of improvement is not aimed to improve the performance of these sensors through increasing the hardware cost (e.g., by adding expensive components or

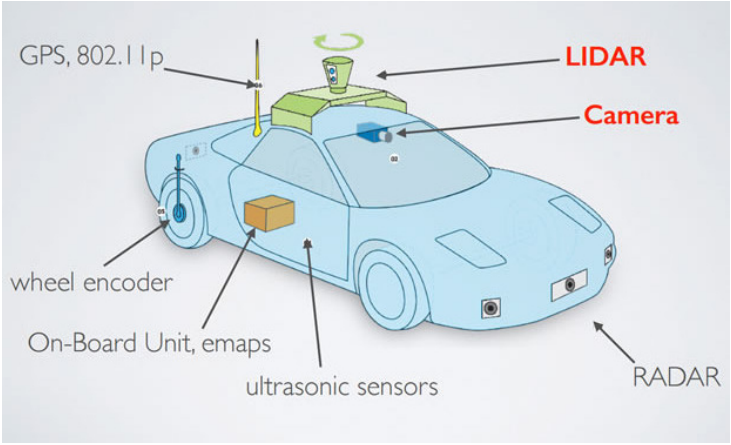

Figure 1.1: A simplified drawing shows the various sensors equipped with the self driving car. The Lidar sensor is mounted on the top to map the surrounding vehicles and objects.

boards): we aim at reaching these improvements using computational manipulations – and even better if these computations may eventually be performed in the boards that already drive the sensors, so to achieve an ultimate goal of costless improvement (or little costs, if one considers the cost of programming new filters in the existing electronic boards).

In this thesis we focus on two different types of Lidars . In the first part we consider ToF Lidars and proposed a statistical model for this type of sensor that compensates both temperature effects on the measurement bias and laser diode mode-hopping phenomena that make the distribution of the measurement noise multi-modal. In brief, we develop a procedure that requires adding a non-expensive temperature measuring board that has negligible cost compared with the ToF Lidar , and with this information we improve the precision and accuracy of the sensor. In the second part of the thesis we focus on triangulation Lidars , and we propose strategies to improve the performance of the measurement process that do not require adding extra hardware. The proposed improvement is achieved through model calibration and estimation procedures that exploit accurate statistical models of the measurement process.

We now formulate in Section 1.2 more precisely the problem that we face in this thesis. After that, we will give a very brief description of the working principles for both ToF Lidars and triangulation Lidars in Section 1.3, to clarify the consequent discussions. We will then present the related work and literature survey in Section 1.4. Finally, we conclude this chapter with outlining the remainder of the thesis in Section 1.5.

1.2 Problem Formulation

In words,

we aim at improving Lidar sensors precision and accuracy through opportune statistical processing tools of the raw measurements coming from the sensor.

Thus we strive for costless (or quasi-costless) improvement of ToF and triangulation Lidars . Our strategy, based on signals processing, requires statistical approaches – and these in their turn require how these sensors work. Therefore, we also aim at:

- developing accurate statistical models that match the evidence collected when using these devices, and that may partially be based on the physics of the sensor;
- finding statistical calibration procedures to learn the parameters of these models;
- designing and characterizing statistical filters and smoothers that are based on the calibrated models above and that improve the precision and accuracy of the sensors measurements when the sensors are used in normal operations.

1.3 Lidar sensors

Before discussing the literature related to the Lidar technologies we describe the basic operation principles for the types of Lidar technologies that will be considered in this thesis. The first type that we consider (Section 1.3.1) is the pulsed ToF Lidars , that have been also considered in paper A. Then we will discuss (Section 1.3.2) triangulation Lidars , that have been also considered in papers B and C.

1.3.1 ToF Lidar

The basic operation of pulsed ToF Lidars is shown in Figure 1.2. In brief, a pulsed infra-red laser beam is emitted by the laser source, travels out of the device, and then is reflected from the object surface into the device again, where its arrival time is detected by an opportune photo-receiver. The time between the transmission and the reception instants is then used to measure the distance between the scanner and the object. Since the laser beam is deflected by a rotating mirror, moreover, the sensor can measure distances in a fan-shaped scan pattern.

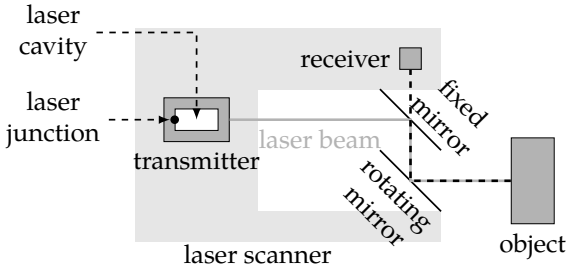

Figure 1.2: Graphical description of the operating principle for pulsed ToF Lidars. A pulsed infra-red laser beam is first emitted from the transmitter. The case of the transmitter, in dark gray, encloses a laser junction and a laser cavity. The emitted laser beam is then deflected by a rotating mirror (resulting in a fan-shaped scan pattern), and finally reflected back by the object. The time of flight τ between the transmission and the reception of the laser beam is then used to estimate the distance d between the scanner and the object.

The measurement of the distance derives from ideal considerations: if the temporal width of the pulse is null, then the distance d between the sensor and the object should satisfy

$$d = \frac{c\,\tau}{2} \tag{1.1}$$

where c is the speed of light and τ is the measured ToF between when the laser pulse is emitted and when it is received. Assume ideally that the laser pulse contains photons with a unique nominal wavelength λ_0. Since

$$c = \lambda_0 f \tag{1.2}$$

with f the light frequency and λ_0 the nominal wavelength, it is sufficient to know λ_0. Thus, from knowing λ_0, one can compute d, since τ is measured.

ToF Lidars require fast and expensive electronic counters to measure very small time differences; they also require precise and calibrated rotating mirrors (also expensive); finally they also require laser diodes that emit precise and calibrated wave lengths – something that requires temperature calibration procedures. All these requirements together make ToF Lidars expensive and bulky devices.

Laser Diode wavelength

The laser diode is the basic element in all ToF Lidars . We now briefly describe the role of its temperature in determining its lasing wavelength; this dependency is indeed of paramount importance, given that it implies variability in Equation (1.2).

From [2] we know that the emitted wave length changes with temperature in discrete steps, as schematically shown in Figure 1.3.

From logical standpoints, this dependency is explained through the following chain of consequences:

- at every given temperature, each laser diode cavity admits a set of specific and given lasing modes. The set of lasing modes is the set of wavelengths for which photons with that specific wavelength are in resonance within the diode cavity;
- certain frequencies cause more pronounced photon avalanche effects than others; the laser diode medium, thus, exhibits a certain gain profile, as shown in Figure 1.4,
- the cavity lasing mode that has a higher gain profile statistically tends to be the winning mode and will statistically be the dominant mode produced by the laser (i.e., the laser pulse will contain coherent photons with identical frequency content). Notice that it is not a deterministic relation: in practice the probability of having a laser pulse with a specific frequency content is directly proportional to its associated gain profile;
- now if the temperature of the laser cavity changes, this will shift the cavity modes (toward increasing or decreasing wavelengths, depending on the temperature change);
- at the same time changing the temperature of the laser cavity shifts the gain curve too; the shift of the gain curve is nonetheless generally bigger in amplitude than the shift in the cavity modes. This implies that the modes not only shift in wavelengths, but also change relative importance.

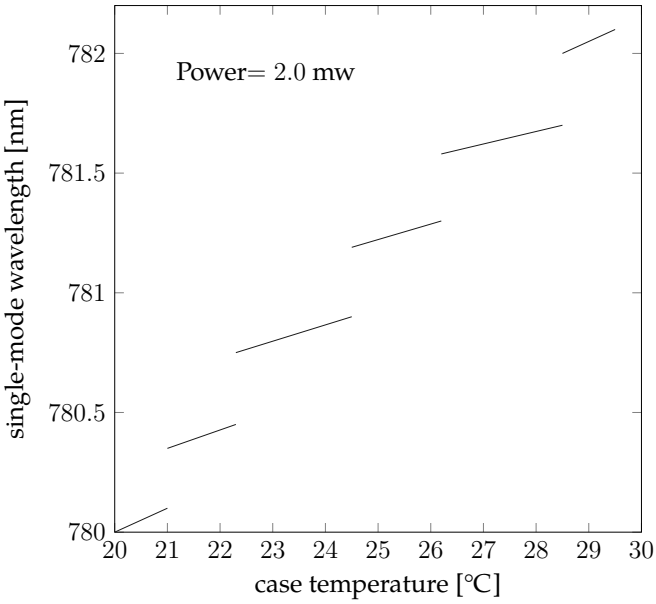

Figure 1.3: Plot of single-mode laser diode wavelength vs. case temperature at constant power operation [2] using a Mitsubishi ML 4402 GaAs index-guided laser diode.

1.3.2 Triangulation Lidar

Triangulation Lidars consist mainly of an infra-red laser transmitter, a pinhole lens, and a pinhole CCD camera. The working principle is extremely simple, and schematized in Figure 1.5: first, the transmitted laser beam hits an object and is then reflected back to the pinhole CCD camera. Then the camera, that is simply a linear sensor, measures the distance b'_k between the dotted line (that is the parallel to the laser beam) and the laser beam reflected from the object. The similarity between the big and small triangles in Figure 1.5 gives then the relation

$$d_k = \frac{bd'}{b'_k} \tag{1.3}$$

where k is the measurement index, d_k is the perpendicular distance to the object, and d' and b are constants given by the geometry of the Lidar .

It is clear from (1.3) that b'_k is inversely proportional to d_k. Obviously, this will induce quantization issues: uniform quantization in measuring b'_k will induce non-uniform quantization in measuring the distance d_k. Moreover any additional measurement noise over b'_k that is uniform over the whole length of the CCD sensor will be mapped into a non-uniform measurement noise over the possible distances d_k. The noise of this sensor is thus intrinsically heteroscedastic, as will be explained in more details in 3.2.

The simple principle of operation of the triangulation Lidars , together with using non-expensive laser diodes and CCD pinhole cameras, make the cost of the device very low compared with the ToF Lidars . Triangulation Lidars are also very light, and this enables using them in aerial applications. However their precision and accuracy is very limited

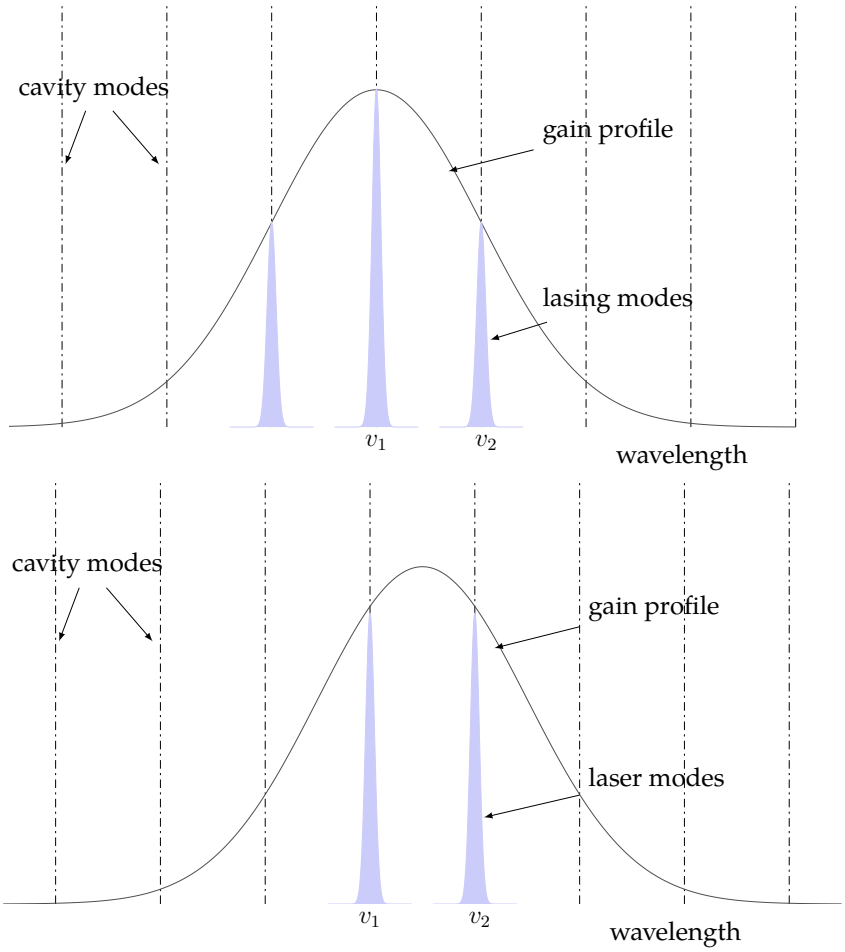

Figure 1.4: The plot explaining the cavity modes, gain profile and lasing modes for typical laser diode. The upper drawing shows the wavelength v_1 as the dominant lasing mode while the lower drawing shows how both wavelengths v_1 and v_2 are competing; this latter case is responsible for the mode-hopping effects.

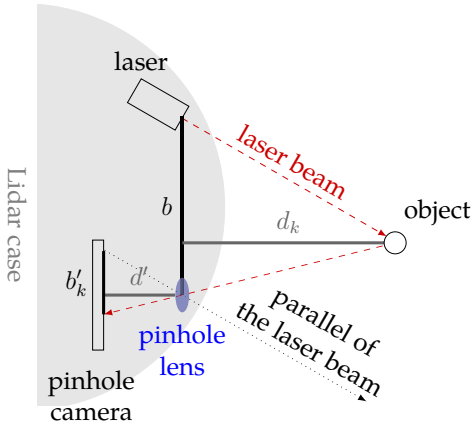

Figure 1.5: Diagram exemplifying the working principle of a triangulation Lidar . The laser emits an infra-red laser signal that is then reflected by the object to be detected. The beam passes through a pinhole lens and hits a CCD camera sensor. By construction, thus, the triangles defined by (b, d_k) and by (b'_k, d') are similar: this means that the distance to the object is nonlinearly proportional to the angle of the reflected light, and as soon as the camera measures the distance b'_k one can estimate the actual distance d_k using triangles similarities concepts.

compared to ToF Lidars .

1.4 Related Work

1.4.1 Lidar Characterization and Calibration

It is convenient to categorize the algorithms in the existing and relevant literature into:

- procedures for the characterization or calibration of the devices. Here characterization means a thorough quantification of the measurement noisiness of the device, while calibration means an algorithm that aims at diminishing this noisiness level;
- when dealing with calibration issues, procedures for the intrinsic or extrinsic calibration. Here intrinsic means that the focus is on estimating the parameters of the Lidar itself, while extrinsic means that the focus is on estimating the parameters resulted from sensor positioning and installation.

We then analyze each item above independently.

Characterization issues: several papers discuss Lidar characterization issues for both ToF [3, 4, 5, 6, 7, 8, 9, 10] and triangulation Lidars [11, 12]. Notice that, at the best of our knowledge, for triangulation Lidars there exist only two manuscripts: [11], that discusses the nonlinearity of Neato Lidars , and [12], that analyzes the effect of the color of the target on the measured

distance. Importantly, [11] models nonlinear effects on the measurements and the variance of additive measurement noises as two independent effects that can be modeled with a second order polynomials on the actual distance. From a statistical perspectives the authors, therefore, decouple the learning process into two separate parts.

Calibration issues: as for the calibration issues there is a relatively large number of papers describing how to calibrate extrinsic parameters either using additional sensors (such as cameras) [13, 14, 15, 16], or just requiring knowledge on the motion of the Lidar itself [17, 18, 19, 20].

Still considering calibration issues, there has been also a big effort on how to perform intrinsic calibration for multi-beam Lidar systems, where the results from one beam is used to calibrate the intrinsic parameters of other beams [21, 22, 23, 24, 25, 26, 27, 28, 29, 30]. As for single-beam Lidar systems, instead, [28] proposes a method for the intrinsic calibration of a revolving-head 3D Lidar and the extrinsic calibration of the parameters with respect to a camera. The technique involves an analytical method for computing an initial estimate for both the Lidar's intrinsic parameters and the Lidar-camera transformation, that is then used to initialize an iterative nonlinear least-squares refinement of all of the calibration parameters.

We also mention the topic of on-line calibration of sensor parameters for mobile robots when doing Simultaneous localization and mapping (SLAM), very useful in navigation tasks. In this category, [31] proposes an approach to simultaneously estimate a map of the environment, the position of the on-board sensors of the robot, and its kinematic parameters. These parameters are subject to variations due to wear of the devices or mechanical effects like loading. An other similar methodology for the intrinsic calibration of depth sensor during SLAM is presented in [32].

1.5 Thesis Outline

This thesis is divided into two parts:

Part I , composed by Chapters 2 and 3, that contains an introduction to the problem and provides additional background information. The theory provided in Chapter 2 serves as a foundation and technical background to the actual scientific contributions of Part II. The discussions in Chapter 3 instead frame the findings in a broader perspective and delineate what are the most likely (and promising) future research directions;

Part II , that contains the three peer-reviewed research papers that have been the scientific outcomes of our academic work up to now. Papers A and B, a journal and a conference papers respectively, have been already published. Paper C, a draft for a journal paper, is currently under review.

CHAPTER 2

Estimation Theory

In this thesis we are concerned with estimation problems. Our objectives are to estimate parameters and states of the measuring systems. In more details, our parameter estimation problems can be decomposed in the classical sub-problems of system identification, model structure and model order selection. Our state estimation problems instead require to have inferred model structures and parameters before attempting to estimate the states. In the following, thus, when we will mention that we aim at estimating states we assume that either the problems of system identification, model structure and model order selection have been already solved, if the model and its parameters are assumed time-invariant, or, otherwise, that these problems are solved simultaneously with the state estimation issue.

2.1 Estimators and Estimators Properties

In modeling and calibrating Lidars we face the very generic problem of estimating parameter values from a stream of discrete-time measurements. Mathematically, we assume to be endowed with a data sequence $\{y\}_1^N$ that has been generated statistically based on an unknown model parametrized by θ. We assume probabilistic models, i.e., the fact that y is generated according to a distribution of the kind

$$y \sim \mathbb{P}[y \mid \theta] \tag{2.1}$$

with $\mathbb{P}[y \mid \theta]$ interpretable either as the probability of observing y when the distribution is parametrized by θ, or the likelihood of the parameter θ given that we observed y.

Our aim is then to estimate the value of θ based on this dataset and on the knowledge of model (2.1); the classical approach is to consider our estimate $\widehat{\theta}$ as a statistic, i.e., a function of the data that does not depend on the estimand θ. In formulas, thus, our estimate will always satisfy a structure of the type

$$\widehat{\theta} = f(y_1, y_2, \cdots, y_N) \tag{2.2}$$

where $f(\cdot)$ is some opportune function of the dataset.

The aim is to have both accurate and precise estimates. These qualities are connected to the concepts of *unbiased* and *minimum variance* estimators. An estimator is then said to be

unbiased if on average it will return the true value [33], or, mathematically,

$$\mathbb{E}\left[\widehat{\theta}\right] = \theta\,, \qquad \forall\theta \in \Theta \tag{2.3}$$

where Θ is the set of admissible (or physically meaningful) θ's. An unbiased estimator is also said to be minimum variance estimator if its variance is minimal, i.e., if it has minimum Mean Squared Error (MSE)

$$\mathrm{MSE}(\theta) = \mathbb{E}\left[\left(\widehat{\theta} - \theta\right)^2\right]. \tag{2.4}$$

A Minimum Variance Unbiased Estimator (MVUE) is thus considered to be optimal (in the squared loss sense) in the family of unbiased estimators of the same parameter.

An other important concept is the one of *efficient* estimator, i.e., an estimator that achieves the so-called *Cramer-Rao bound*, equal (in the case of unbiased estimators) to the reciprocal of the so-called Fisher information matrix

$$I(\theta) := \mathbb{E}\left[\frac{\partial^2 \mathbb{P}\left[y \mid \theta\right]}{\partial\theta^2}\right]. \tag{2.5}$$

The reciprocal of the Fisher information matrix is said to be the Cramér-Rao Lower Bound (CRLB) for the variance of unbiased estimators, and it provides a lower bound for their variances. Efficient unbiased estimators are thus for sure MVUE (while the vice-versa is not true in general). Efficient estimators are also informally said to use all the available information in the dataset related to the estimand.

2.2 Estimation for static systems

We now consider static systems, i.e., systems in which models are independent on the current time. To describe the types of problems we will face in the following we consider the simplest example, i.e., a linear measurement model that satisfies, at the generic time instant k,

$$y_k = \theta x_k + v_k \tag{2.6}$$

where

- θ is the model parameter vector;
- x_k is the model state vector;
- v_k is the model noise.

We will be interested in these two different types of estimation problems:

1. starting from a sequence of measurements $\{y_k\}_{k\in\mathcal{D}}$ and states $\{x_k\}_{k\in\mathcal{D}}$ estimate the model parameter θ;
2. starting from a sequence of measurements $\{y_k\}_{k\in\mathcal{D}}$ and the model parameter θ estimate the states $\{x_k\}_{k\in\mathcal{D}}$.

Before detailing how the two types of problems above apply to our Lidars calibration and estimation issues, we describe the different types of estimators that we will employ.

Maximum Likelihood Estimation

In formulas, Maximum Likelihood (ML) estimators are defined starting from the knowledge of the probabilistic model (2.1) as

$$\theta_{\text{ML}} := \arg\max_{\theta\in\Theta} \mathbb{P}\left[y \mid \theta\right] \tag{2.7}$$

where Θ is the set of admissible θ's, and constitutes a form of prior information. In words, thus, ML estimators correspond to finding in the parameters space Θ that parameter vector θ_{ML} that maximizes the likelihood $\mathbb{P}\left[y \mid \theta\right]$ given the measurement sequence $\{y\}_1^N$ – in practice, find that parameter that fits best the data in the sense of $\mathbb{P}\left[y \mid \theta\right]$.

Under mild hypotheses, as the sample size goes to infinity the ML estimator benefits of two important properties:

Consistency , that means that the ML estimator converges almost surely to the true value of the unknown, i.e.,

$$\widehat{\theta}_{\text{ML}} \xrightarrow{a.s.} \theta \tag{2.8}$$

Efficiency , that means that it achieves the CRLB when the sample size tends to infinity. This means that no consistent estimator has lower asymptotic mean squared error than the ML estimator;

Asymptotic normality , that means that as the sample size increases the distribution of the ML estimator tends to the Gaussian distribution with mean θ and covariance matrix equal to the inverse of the Fisher information matrix.

Given the favorable properties above, it is highly desirable to find ML estimators. Nonetheless not always this type of estimators can be found in closed form, since finding θ_{ML} corresponds to solve a maximization problem (that may also be non-convex). A simple example of when it is impossible to find closed form solutions to problem (2.7) is (often) when the distribution of the model noise v_k is not differentiable with respect to θ. In these cases one must often rely on numerical optimization procedures.

Example 2.1 (the ML estimator for a range sensor subject to Gaussian noise)
Consider the range measurement vector $\boldsymbol{y} = [y_1, y_2, \ldots, y_N]$ generated using the statistical model

$$y_k = \alpha x_k + \sigma v_k \tag{2.9}$$

where α is the parameter of the model that we would like to estimate and the noise v_k satisfies $v_k \sim \mathcal{N}(0,1)$. The noise variance σ^2 is assumed known, as long as the state vector $\boldsymbol{x} = [x_1, x_2, \cdots, x_N]^T$, representing the true distance from the object. If we want to find the ML estimator for α, and since we have Gaussian noise, i.e.,

$$y_k \sim \mathcal{N}\left(\alpha x_k, \sigma^2\right) \tag{2.10}$$

the likelihood function is

$$\mathbb{P}\left[\boldsymbol{y} \mid \alpha\right] = \prod_{k=1}^{N} \frac{1}{\sqrt{2\pi\sigma^2}} \exp\left(\frac{-1}{2\sigma^2}\left(y_k - \alpha x_k\right)^2\right) \tag{2.11}$$

and the log-likelihood is

$$\log \mathbb{P}\left[\boldsymbol{y} \mid \alpha\right] = -\frac{N}{2}\log 2\pi\sigma^2 - \frac{1}{2\sigma^2}\sum_{k=1}^{N}\left(y_k - \alpha x_k\right)^2 \tag{2.12}$$

taking the zero of the score

$$\frac{1}{2\sigma^2}\sum_{k=1}^{N}\left(-2y_k x_k + 2\alpha x_k^2\right) \tag{2.13}$$

with respect to α gives

$$\widehat{\alpha}_{\mathrm{ML}} = \sum_{k=1}^{N} y_k x_k \left(\sum_{k=1}^{N} x_k^2\right)^{-1} \tag{2.14}$$

Example 2.2 (the ML estimator for the variance of a Gaussian range sensor)
Consider again the measurement vector $\boldsymbol{y} = [y_1, y_2, \ldots, y_N]$ generated using the same model

$$y_k = \alpha x_k + \sigma v_k \tag{2.15}$$

where $v_k \sim \mathcal{N}(0,1)$ is white and Gaussian. Assuming both the parameter α and the state vector $\boldsymbol{x} = [x_1, x_2, \cdots, x_N]^T$ to be known, we want to find the ML estimator for σ. Since we have Gaussian noises, i.e.,

$$y_k \sim \mathcal{N}\left(\alpha x_k, \sigma^2\right) \tag{2.16}$$

the likelihood function is

$$\mathbb{P}\left[\boldsymbol{y} \mid \sigma\right] = \prod_{k=1}^{N}\frac{1}{\sqrt{2\pi\sigma^2}}\exp\left(\frac{-1}{2\sigma^2}\left(y_k - \alpha x_k\right)^2\right) \tag{2.17}$$

and the log-likelihood is

$$\log \mathbb{P}\left[\boldsymbol{y} \mid \sigma\right] = -\frac{N}{2}\log 2\pi\sigma^2 - \frac{1}{2\sigma^2}\sum_{k=1}^{N}\left(y_k - \alpha x_k\right)^2 \tag{2.18}$$

taking the zero of the score with respect to σ^2 gives

$$\sigma^2_{\mathrm{ML}} = \frac{1}{N}\sum_{k=1}^{N}\left(y_k - \alpha x_k\right)^2. \tag{2.19}$$

Least Squares estimators

When it is not possible to calculate the ML estimator in closed form, either because the distribution of the noise is unknown or because finding the maximum of the likelihood function is analytically intractable, an alternative approach is to use Least Squares (LS) estimators. This type of estimation starts from the paradigm of trying to minimize the empirical expected value of the measurement noise. In general, if

$$y_k = f(x_k, \theta) + e_k \tag{2.20}$$

where $f(\cdot)$ is a generic function, x_k is the input and e_k is the process noise, given a Dataset of N input and output pairs $\mathbb{D} = \{y_k, x_k\}_1^N$, the least squares approach aims to find $\widehat{\theta}$ that *best explains the data*. The last concept can then be explained geometrically: we would like to find that vector $\widehat{\theta}$ that minimizes the Euclidean distance with the manifold formed by $f(x_k, \star)$ assuming $\star \in \Theta$ with Θ the set of admissible parameters.

In practice, considering for example the linear system described in Equation (2.7), the LS estimator for the parameter θ is

$$\theta_{\text{LS}} := \arg\min_{\theta \in \Theta} \|\boldsymbol{y} - \theta \boldsymbol{x}\|_2^2 \tag{2.21}$$

$$\theta_{\text{LS}} = \arg\min_{\theta \in \Theta} \sum_{i=1}^{N} (y_i - \theta x_i)^2 \tag{2.22}$$

Importantly, for the Gaussian noises case, ML and LS estimators coincide. In the linear case thus the LS is asymptotically unbiased and (under mild assumptions on the informativeness of the dataset) consistent; in general cases, nonetheless, these properties may fail, so that may be an *inefficient* estimator (i.e., not MVUE).

Maximum A Posteriori (MAP) estimator

The previous estimators were dealing with Fisherian approaches where the estimand θ was treated as a deterministic quantity. In some cases instead it is meaningful to consider θ as a random variable on which we have some prior information in the form of a prior distribution $\mathbb{P}[\theta]$. In this case we can use Bayesian formalisms to combine the prior information $\mathbb{P}[\theta]$ with the likelihood $\mathbb{P}[y \mid \theta]$ and, by using the Bayes rule, find the estimand as that potential estimand that maximizes the posterior, i.e.,

$$\theta_{MAP} := \arg\max_{\theta \in \Theta} \mathbb{P}[\theta \mid \boldsymbol{y}] \tag{2.23}$$

where from the Bayes rule we have

$$\mathbb{P}[\theta \mid \boldsymbol{y}] = \frac{\mathbb{P}[\boldsymbol{y} \mid \theta]\,\mathbb{P}[\theta]}{\mathbb{P}[\boldsymbol{y}]}. \tag{2.24}$$

Notice that, since the term $\mathbb{P}[\boldsymbol{y}]$ is constant for a given dataset, the maximization in Equation (2.23) is equivalent to

$$\theta_{\text{MAP}} = \arg\max_{\theta \in \Theta} \mathbb{P}[\boldsymbol{y} \mid \theta]\,\mathbb{P}[\theta] \tag{2.25}$$

or equivalently,

$$\theta_{\text{MAP}} = \arg\max_{\theta \in \Theta} [\log \mathbb{P}[\boldsymbol{y} \mid \theta] + \log \mathbb{P}[\theta]] \tag{2.26}$$

θ_{MAP} is called the MAP estimator of θ.

Example 2.3 (the MAP estimator for a Gaussian range sensor with Gaussian prior)
Consider the measurement vector $\boldsymbol{y} = [y_1, y_2, \ldots, y_N]$ generated using the model

$$y_k = \alpha + \sigma v_k \tag{2.27}$$

and $v_k \sim \mathcal{N}(0,1)$. Assume the noise variance σ^2 to be known along with the prior $\alpha \sim \mathcal{N}\left(\alpha_0, \sigma_p^2\right)$. Given this information, we want to find the MAP estimator for α.

Since we have Gaussian noise, the likelihood function is

$$\mathbb{P}\left[\boldsymbol{y} \mid \alpha\right] = \prod_{k=1}^{N} \frac{1}{\sqrt{2\pi\sigma^2}} \exp\left(\frac{-1}{2\sigma^2}\left(y_k - \alpha\right)^2\right) \tag{2.28}$$

while the prior is

$$\mathbb{P}\left[\alpha\right] = \frac{1}{\sqrt{2\pi\sigma_p^2}} \exp\left(\frac{-1}{2\sigma_p^2}\left(\alpha_0 - \alpha\right)^2\right). \tag{2.29}$$

Combining the two terms and taking the logarithm returns

$$\log \mathbb{P}\left[\boldsymbol{y} \mid \alpha\right] + \log \mathbb{P}\left[\alpha\right] = -\frac{N}{2}\log 2\pi\sigma^2 - \frac{1}{2\sigma^2}\sum_{k=1}^{N}\left(y_k - \alpha\right)^2 - \frac{N}{2}\log 2\pi\sigma^2 - \frac{1}{2\sigma_p^2}\left(\alpha_0 - \alpha\right)^2. \tag{2.30}$$

Differentiate this w.r.t. to α and then equating to zero gives then the formula

$$\alpha_{\text{MAP}} = \frac{\sigma_p^2 \sum_{k=1}^{N} y_k + \sigma^2 \alpha_0}{\sigma_p^2 N + \sigma^2}. \tag{2.31}$$

2.2.1 The stochastic models used to describe our Lidar sensors

We now list the various models that we use to describe the working principles of the various Lidar sensors analyzed in our work. Along with the description of these statistical models, we discuss the challenges that we face in doing estimation with them, and what are the possible solutions of the various numerical and analytical problems that we may encounter.

Heteroscedastic models

Heteroscedastic models are models where the variance of the noise is a function of the state of the system. A generic heteroscedastic model with additive noise that we encounter in our estimation efforts is

$$y_k = f_1(x_k) + f_2(x_k)e_k \tag{2.32}$$

where $f_1(\cdot)$ and $f_2(\cdot)$ are generic nonlinear functions and $e_k \sim \mathcal{N}(0, \sigma^2)$ is white. We can recognize that the term that is responsible for the heteroscedasticity is the function $f_2(\cdot)$.

Example 2.4 (An example of heteroscedastic models for triangulation Lidars)
For reasons explained in Paper B it is convenient to model triangulation Lidars as

$$y_k = ax_k + bx_k^2 e_k \tag{2.33}$$

where a and b are model parameters, $e_k \sim \mathcal{N}(0,1)$, and x_k is the true distance between the object and the sensor that is assumed to be known in this example. We consider the following two problems:

1) for known $b = b_0$ find the ML estimator for a;

2) for known $a = a_0$ find the ML estimator for b.

The distribution of the measurement is heteroscedastic

$$y_k \sim \mathcal{N}\left(ax_k, b^2 x_k^4\right). \tag{2.34}$$

We transform it into homoscedastic by dividing both sides of the model equation by the term x_k^2 results in the homoscedastic equation

$$\frac{y_k}{x_k^2} = \frac{a}{x_k} + be_k \tag{2.35}$$

which has the distribution

$$\frac{y_k}{x_k^2} \sim \mathcal{N}\left(\frac{a}{x_k}, b^2\right). \tag{2.36}$$

Now on the transformed system we can apply the classical ML procedure

1) the distribution of the transformed system is

$$\frac{y_k}{x_k^2} \sim \mathcal{N}\left(\frac{a}{x_k}, b_0^2\right). \tag{2.37}$$

Following the same procedure in Example 2.1 we directly obtain

$$\widehat{a}_{\text{ML}} = \sum_{k=1}^{N} \frac{y_k}{x_k^3} \left(\sum_{k=1}^{N} \frac{1}{x_k^2}\right)^{-1} \tag{2.38}$$

2) the distribution of the transformed system is

$$\frac{y_k}{x_k^2} \sim \mathcal{N}\left(\frac{a_0}{x_k}, b^2\right). \tag{2.39}$$

Following the same procedure in Example 2.2 we directly obtain

$$\widehat{b^2}_{\text{ML}} = \frac{1}{N} \sum_{k=1}^{N} \left(\frac{y_k}{x_k^2} - \frac{a_0}{x_k}\right)^2 \tag{2.40}$$

Gaussian mixture model (GMM)

Some times the distributions of the noises are multi-modal. In this case it is convenient to use the so-called mixture models [34]. In case of Gaussian distributions, a common approach is to use GMM [34]. This model has a form of the kind

$$y_k = \sum_{i=1}^{m} \Pi_m e_{ik} \tag{2.41}$$

where $e_{ik} \sim \mathcal{N}\left(\mu_i, \sigma_i^2\right)$ and Π_m is a mixing parameter such that $\sum_{i=1}^{m} \Pi_m = 1$. Estimation in Gaussian mixture models frameworks require slight modifications of the analytical strategies saw up to now, as shown in the next example.

Example 2.5 (GMM parameter estimation)
Consider the bimodal distribution

$$y_k = \Delta_k e_k + (1 - \Delta_k)\, v_k \tag{2.42}$$

where $e_k \sim \mathcal{N}(\mu_1, \sigma_1^2)$ and $v_k \sim \mathcal{N}(\mu_2, \sigma_2^2)$. Given the measurements $\boldsymbol{y} = [y_1, y_2, \ldots, y_N]$ and the selection variables $\Delta = [\Delta_1, \Delta_2, \cdots, \Delta_N]^T$ the problem is to find the ML estimator for the model parameters $\theta = [\mu_1, \mu_2, \sigma_1^2, \sigma_2^2, \Pi_1, \Pi_2]^T$. To do so, consider that since the distribution of the measurements is

$$y_k \sim \mathcal{N}\left(\Delta_k\mu_1 + (1 - \Delta_k)\mu_2, \Delta_k\sigma_1^2 + (1 - \Delta_k)\sigma_2^2\right) \tag{2.43}$$

the likelihood is

$$\mathbb{P}\left[\boldsymbol{y} \mid \theta\right] = \prod_{k=1}^{N} \frac{1}{\sqrt{2\pi(\Delta_k\sigma_1^2 + (1 - \Delta_k)\sigma_2^2)}} \exp\left(\frac{-1}{\Delta_k 2\sigma_1^2 + (1 - \Delta_k)2\sigma_2^2}\left(y_k - \Delta_k\mu_1 - (1 - \Delta_k)\mu_2\right)^2\right) \tag{2.44}$$

and the log-likelihood is

$$\begin{aligned}\log\mathbb{P}\left[\boldsymbol{y} \mid \theta\right] = -\frac{1}{2}\sum_{k=1}^{N}\log 2\pi(\Delta_k\sigma_1^2 + (1 - \Delta_k)\sigma_2^2) \\ -\sum_{k=1}^{N}\frac{\left(y_k - \Delta_k\mu_1 + (1 - \Delta_k)\mu_2\right)^2}{\Delta_k 2\sigma_1^2 + (1 - \Delta_k)2\sigma_2^2}\end{aligned} \tag{2.45}$$

which is equivalent to

$$\begin{aligned}\log\mathbb{P}\left[\boldsymbol{y} \mid \theta\right] = -\frac{1}{2}\sum_{k=1}^{N}\Delta_k\log 2\pi\sigma_1^2 - \frac{1}{2}\sum_{k=1}^{N}(1 - \Delta_k)\log 2\pi\sigma_2^2 \\ -\frac{1}{2\sigma_1^2}\sum_{k=1}^{N}\Delta_k\left(y_k - \mu_1\right)^2 - \frac{1}{2\sigma^2}\sum_{k=1}^{N}(1 - \Delta_k)\left(y_k - \mu_2\right)^2.\end{aligned} \tag{2.46}$$

Computing the zero of the score with respect to μ_1 and μ_2 eventually gives

$$\begin{aligned}\widehat{\mu_1}_{\text{ML}} = \sum_{k=1}^{N} y_k\Delta_k\left(\sum_{k=1}^{N}\Delta_k\right)^{-1} \\ \widehat{\mu_2}_{\text{ML}} = \sum_{k=1}^{N} y_k(1 - \Delta_k)\left(\sum_{k=1}^{N}(1 - \Delta_k)\right)^{-1}\end{aligned} \tag{2.47}$$

respectively. Then computing the zero of the score with respect to σ_1^2 and σ_2^2 instead gives

$$\begin{aligned}\widehat{\sigma_1^2}_{\text{ML}} = \sum_{k=1}^{N}\Delta_k\left(y_k - \widehat{\mu_1}_{\text{ML}}\right)^2 \\ \widehat{\sigma_2^2}_{\text{ML}} = \sum_{k=1}^{N}(1 - \Delta_k)\left(y_k - \widehat{\mu_2}_{\text{ML}}\right)^2.\end{aligned} \tag{2.48}$$

The mixing parameter $\Pi_{1,2}$ is actually the probability that a given measurement comes from the distribution e_k or v_k respectively. Therefore,

$$\widehat{\Pi}_1 = \frac{\sum_{k=1}^{N} \Delta_k}{\sum_{k=1}^{N} \Delta_k + \sum_{k=1}^{N} (1 - \Delta_k)} = \frac{\sum_{k=1}^{N} \Delta_k}{N} \tag{2.49}$$

and

$$\widehat{\Pi}_2 = 1 - \widehat{\Pi}_1. \tag{2.50}$$

It is important to notice that it was possible to find the ML estimator for Example 2.5 because the selection variable Δ was given. In practice, this is usually not the case, so that there is the need to estimate the various Δ_k's in order to estimate the remaining model parameters θ. Finding closed-form ML estimators is in this unknown Δ's case not feasible, since the likelihood function is now more complex and bimodal with respect to Δ. In such cases, where there are non-observed latent variables involved in the estimation process, the EM algorithm is usually used.

The Expectation Maximization Algorithm

The EM is an iterative method for computing the ML or MAP estimates of a parameter vector θ where the model depends on both observed and unobserved latent variables [35]. Formally solving an EM problem corresponds to solving

$$\widehat{\theta}_{\text{ML}} := \{\theta \in \Theta \big| \mathbb{P}[Y\ ;\ \theta] \geqslant \mathbb{P}[Y\ ;\ \theta']\ \forall \theta' \in \Theta\} \tag{2.51}$$

where $\mathbb{P}[Y]$ is the likelihood of the observed data and Θ is the closed set of candidate parameter vectors. If the likelihood depends on another unobserved dataset X, then $\mathbb{P}[Y]$ can be expressed in terms of the joint probability as

$$\log \mathbb{P}[Y] = \log \mathbb{P}[X, Y] - \log \mathbb{P}[X \mid Y]. \tag{2.52}$$

A procedure to compute $\widehat{\theta}_{\text{ML}}$ is the following [36]: assume to have a current estimate of the parameters θ, say θ'; then the EM algorithm approximates the joint log likelihood with the expected value of the log likelihood with respect to the current parameter vector θ' and given the measurement vector, i.e., performs the approximation

$$\log \mathbb{P}[X, Y] \approx \mathbb{E}_{\theta'}[\log \mathbb{P}[X, Y] \mid Y]. \tag{2.53}$$

Given this, one can then define the function $\mathcal{L}(\theta, \theta')$ as

$$\mathcal{L}(\theta, \theta') := \mathbb{E}_{\theta'}[\log \mathbb{P}[X, Y] \mid Y]. \tag{2.54}$$

It has been shown in [36] that any θ that increases $\mathcal{L}(\theta, \theta')$ above its value at θ' must also increase the likelihood function $\log \mathbb{P}[Y]$. Therefore, maximizing $\mathcal{L}(\theta, \theta')$ corresponds to maximizing for $\log \mathbb{P}[Y]$. Given these facts, the EM algorithm can be summarized as in the following algorithm:

initialization step: start from an initial guess θ' for the parameter vector θ;

Expectation step : given the current parameter estimate θ', estimate the latent variables X as the expected value of the joint distribution

$$\mathcal{L}(\theta, \theta') := \mathbb{E}_{\theta'} \left[\log \mathbb{P} \left[X, Y \right] \mid Y \right]. \tag{2.55}$$

Maximization step: compute that θ in the parameter space Θ that maximizes the log likelihood function $\log \mathbb{P}[Y]$ or equivalently $\mathcal{L}(\theta, \theta')$ given the currently estimated X, and then set $\theta' \leftarrow \theta$;

return to the Expectation step until reaching certain termination condition based on a predefined parameter accuracy.

For simplicity we avoid dealing with details of the various possible termination rules, and send the interested reader back to [37].

Example 2.6 (estimation of the parameters of a GMM)
Consider the bimodal distribution

$$y_k = \Pi e_k + (1 - \Pi) v_k \tag{2.56}$$

where $e_k \sim \mathcal{N}(\mu_1, \sigma_1^2)$ and $v_k \sim \mathcal{N}(\mu_2, \sigma_2^2)$. Assume the measurement vector $\boldsymbol{y} = [y_1, y_2, \ldots, y_N]$ to be known, and the mixing variable Π to be unknown. The problem is then finding the ML estimator for the model parameters.

Considering that the distribution of the measurements is

$$y_k \sim \Pi \mathcal{N}\left(\mu_1, \sigma_1^2\right) + (1 - \Pi) \mathcal{N}\left(\mu_2, \sigma_2^2\right) \tag{2.57}$$

the log-likelihood is then

$$\begin{aligned} \log \mathbb{P}\left[\boldsymbol{y} \mid \Pi, \theta\right] = \sum_{k=1}^{N} \log \Bigg[& \Pi \frac{1}{\sqrt{2\pi\sigma_1^2}} \exp\left(\frac{-1}{2\sigma_1^2} \left(y_k - \mu_1\right)^2\right) \\ & + (1 - \Pi) \frac{1}{\sqrt{2\pi\sigma_2^2}} \exp\left(\frac{-1}{2\sigma_2^2} \left(y_k - \mu_2\right)^2\right) \Bigg] \end{aligned} \tag{2.58}$$

In this case the latent variables are $\Delta = [\Delta_1, \Delta_2, \cdots, \Delta_N]^T$, and they are such that $\Delta_k = 1$ if y_k comes from e_k and $\Delta_k = 0$ when it comes from v_k. The joint log likelihood is then

$$\begin{aligned} \log \mathbb{P}\left[\boldsymbol{y}, \Delta \mid \Pi, \theta\right] = \sum_{k=1}^{N} \log \Bigg[& \Delta_k \Pi \frac{1}{\sqrt{2\pi\sigma_1^2}} \exp\left(\frac{-1}{2\sigma_1^2} \left(y_k - \mu_1\right)^2\right) \\ & + (1 - \Delta_k)(1 - \Pi) \frac{1}{\sqrt{2\pi\sigma_2^2}} \exp\left(\frac{-1}{2\sigma_2^2} \left(y_k - \mu_2\right)^2\right) \Bigg] \end{aligned} \tag{2.59}$$

or, in other equivalent forms,

$$\begin{aligned} \log \mathbb{P}\left[\boldsymbol{y}, \Delta \mid \Pi, \theta\right] = & \sum_{k=1}^{N} \Delta_k \log \Pi \frac{1}{\sqrt{2\pi\sigma_1^2}} \exp\left(\frac{-1}{2\sigma_1^2} \left(y_k - \mu_1\right)^2\right) \\ & + \sum_{k=1}^{N} (1 - \Delta_k) \log(1 - \Pi) \frac{1}{\sqrt{2\pi\sigma_2^2}} \exp\left(\frac{-1}{2\sigma_2^2} \left(y_k - \mu_2\right)^2\right) \end{aligned} \tag{2.60}$$

$$\begin{aligned}\log \mathbb{P}\left[\boldsymbol{y}, \Delta \mid \Pi, \theta\right] = \sum_{k=1}^{N} \Delta_k \log \Pi + \sum_{k=1}^{N} \Delta_k \log \frac{1}{\sqrt{2\pi\sigma_1^2}} \exp\left(\frac{-1}{2\sigma_1^2}\left(y_k - \mu_1\right)^2\right) \\ + \sum_{k=1}^{N} (1-\Delta_k) \log(1-\Pi) + \sum_{k=1}^{N} (1-\Delta_k) \log \frac{1}{\sqrt{2\pi\sigma_2^2}} \exp\left(\frac{-1}{2\sigma_2^2}\left(y_k - \mu_2\right)^2\right)\end{aligned} \tag{2.61}$$

Given (2.61) we are able to write down the equations defining the EM algorithm introduced above. *Expectation step*: to compute the distribution of Δ_k given the observations $\boldsymbol{y}$ we start using the Bayes rule to obtain

$$\mathbb{P}\left[\Delta \mid \boldsymbol{y}\right] = \frac{\mathbb{P}\left[\Delta\right] \mathbb{P}\left[\boldsymbol{y} \mid \Delta\right]}{\mathbb{P}\left[\boldsymbol{y}\right]}. \tag{2.62}$$

Taking then the expected value

$$\mathbb{E}_{\theta'}\left[\log \mathbb{P}\left[\Delta \mid \boldsymbol{y}\right] \mid \boldsymbol{y}\right] = \frac{\mathbb{P}\left[\Delta\right] \mathbb{E}_{\theta'}\left[\log \mathbb{P}\left[\Delta \mid \boldsymbol{y}\right] \mid \boldsymbol{y}\right]}{\mathbb{P}\left[\boldsymbol{y}\right]} \tag{2.63}$$

we can estimate the latent variables as

$$\Delta = \frac{\Pi \frac{1}{\sqrt{2\pi\sigma_1^2}} \left(\frac{-1}{2\sigma_1^2}\left(y_k - \mu_1\right)^2\right)}{\Pi \frac{1}{\sqrt{2\pi\sigma_1^2}} \left(\frac{-1}{2\sigma_1^2}\left(y_k - \mu_1\right)^2\right) + (1-\Pi) \frac{1}{\sqrt{2\pi\sigma_2^2}} \exp\left(\frac{-1}{2\sigma_2^2}\left(y_k - \mu_2\right)^2\right)} \tag{2.64}$$

Maximization step: taking the zero of the score of the likelihood (2.61) with respect to μ_1 and μ_2 gives

$$\begin{aligned}\widehat{\mu_1}_{\mathrm{ML}} &= \sum_{k=1}^{N} y_k \Delta_k \left(\sum_{k=1}^{N} \Delta_k\right)^{-1} \\ \widehat{\mu_2}_{\mathrm{ML}} &= \sum_{k=1}^{N} y_k (1-\Delta_k) \left(\sum_{k=1}^{N} (1-\Delta_k)\right)^{-1}\end{aligned} \tag{2.65}$$

respectively. Then taking the zero of the score with respect to σ_1^2 and σ_2^2 gives

$$\begin{aligned}\widehat{\sigma_1^2}_{\mathrm{ML}} &= \sum_{k=1}^{N} \Delta_k \left(y_k - \widehat{\mu}_1\right)^2 \left(\sum_{k=1}^{N} \Delta_k\right)^{-1} \\ \widehat{\sigma_2^2}_{\mathrm{ML}} &= \sum_{k=1}^{N} (1-\Delta_k) \left(y_k - \widehat{\mu}_2\right)^2 \left(\sum_{k=1}^{N} (1-\Delta_k)\right)^{-1}\end{aligned} \tag{2.66}$$

respectively. Performing eventually the same with respect to Π then gives

$$\widehat{\Pi}_{\mathrm{ML}} = \frac{1}{N} \sum_{k=1}^{N} \Delta_k \tag{2.67}$$

The above quantities are then the novel θ' to be used again in the expectation step.

2.3 Estimation for dynamic systems

Consider now the linear time-invariant linear Gaussian dynamic system

$$\begin{aligned} x_{k+1} &= Ax_k + Bu_k + w_k \\ y_k &= Cx_k + Du_k + v_k \end{aligned} \tag{2.68}$$

where

- A, B, C and D are the model parameters matrices,
- x_k is the states vector,
- u_k is the system input,
- $w_k \sim \mathcal{N}(0, \sigma_x^2)$ and $v_k \sim \mathcal{N}\left(0, \sigma_y^2\right)$.

The problem here is estimating the system matrices A, B, C, and D.

2.3.1 Parameter Estimation

Starting from a dataset containing the sequence of measurements y_k and states x_k we can estimate the parameters by applying directly ML, LS or MAP estimators.

Example 2.7 (Parameters estimation in dynamical systems)
Consider

$$\begin{aligned} x_{k+1} &= ax_k + w_k \\ y_k &= cx_k + v_k \end{aligned} \tag{2.69}$$

where w_k and v_k are zero mean Gaussian and independent and identically distributed (iid), and to know the input sequence $y_1, \cdots, y_N$ and the states sequence $x = x_1, \cdots, x_{N+1}$. It is then required to find an estimator for the parameters a and c.

To solve this task we notice that by solving the first and second equations we can find the estimators

$$\begin{aligned} \widehat{a} &= x_+ x (x_+ x)^{-1} \\ \widehat{c} &= yx(x_+ x)^{-1} \end{aligned} \tag{2.70}$$

respectively, where $x_+ = [x_2, \cdots, x_{N+1}]^T$, $x = [x_1, \cdots, x_N]^T$ and $y = [y_1, \cdots, y_N]^T$.

2.3.2 State Estimation

Consider the model in (2.68) where the parameters A, B, C and D are known. The problem that we now face is the following: starting from datasets containing the sequence of measurements and some knowledge on the initial conditions of the system, estimate the state of the system during its evolution.

It is known that we can perform this task optimally in the mean-squared sense using what is known as a *Fixed-Interval Kalman smoother*. There are different implementations for this strategy; in the next section we will summarize that one proposed [38].

The Rauch-Tung-Striebel (RTS) Kalman Smother

Consider the linear state space model in (2.68), and assume the noise processes to be distributed according to

$$\begin{bmatrix} w_k \\ v_k \end{bmatrix} \sim \mathcal{N}\left(\begin{bmatrix} 0 \\ 0 \end{bmatrix}, \begin{bmatrix} Q & S \\ S^T & R \end{bmatrix} \right) \tag{2.71}$$

where Q and R are the process and output covariance matrices respectively. Assume that the initial condition is also Gaussian, i.e., $x_1 \sim \mathcal{N}(\mu, P_1)$. Following the same procedure described in [36] we can define the parameter vector θ as

$$\theta := \left[\text{vec}\left\{ \begin{bmatrix} A & B \\ C & D \end{bmatrix} \right\}^T \quad \mu^T \quad \text{vec}\left\{ \begin{bmatrix} Q & S \\ S^T & R \end{bmatrix} \right\}^T \quad \text{vec}\{P_1\} \right] \tag{2.72}$$

where the vec $\{\cdot\}$ operator creates a column vector from a matrix by stacking its columns one on top of the other. Given these definitions it follows that

- $\mathbb{E}_\theta \left[y_k x_k^T \mid Y_N \right] = y_k \widehat{x}_{k|N}^T$
- $\mathbb{E}_\theta \left[x_k x_k^T \mid Y_N \right] = \widehat{x}_{k|N} \widehat{x}_{k|N}^T + P_{k|N}$
- $\mathbb{E}_\theta \left[x_k x_{k-1}^T \mid Y_N \right] = \widehat{x}_{k|N} \widehat{x}_{k-1|N}^T + M_{k|N}$

where $\widehat{x}_{k|N}$, $P_{k|N}$ and $M_{k|N}$ are calculated backwards in time as

$$\widehat{x}_{k|N} = \widehat{x}_{k|k} + J_k(x_{k+1|N} - \bar{A}\widehat{x}_{k|k} - \bar{B}u_k - SR^{-1}y_k) \tag{2.73}$$

$$P_{k|N} = P_{k|k} + J_k(P_{k+1|N} - P_{k+1|k}) \tag{2.74}$$

$$J_k = P_{k|k}\bar{A}_{k+1|k}^T \tag{2.75}$$

for $k = N, \ldots, 1$. The matrix $M_{k|N}$ is moreover initialized as

$$M_{N|N} = (I - K_N C)\bar{A}P_{N-1|N-1} \tag{2.76}$$

and calculated using

$$M_{k|N} = P_{k|k}J_{k-1}^T + J_k(M_{k+1|N} - \bar{A}P_{k|k})J_{k-1}^T \tag{2.77}$$

for $k = N-1, \ldots, 1$. Finally, the quantities $\widehat{x}_{k|k}$, $P_{k|k}$, $P_{k+1|k}$ and K_N can be computed by a standard Kalman filter for the system described by

$$\begin{aligned} \bar{A} &:= A - SR^{-1}C \\ \bar{B} &:= B - SR^{-1}D \\ \bar{Q} &:= Q - SR^{-1}S^T. \end{aligned} \tag{2.78}$$

Notice that in the special cases considered in the papers presented in Part II we will always have systems for which $S = 0$, so that $\bar{A} = A$, $\bar{B} = B$ and $\bar{Q} = Q$. More details about the

equations and proofs leading to these can be found in [36]. The Kalman filter equations can instead be summarized as follows [39]:

$$P_{k|k-1} = AP_{k-1|k-1}A^T + Q \tag{2.79}$$

$$K_k = P_{k|k-1}C^T(CP_{k|k-1}C^T + R)^{-1} \tag{2.80}$$

$$P_{k|k} = P_{k|k-1} - K_kCP_{k|k-1} \tag{2.81}$$

$$\widehat{x}_{k|k-1} = A\widehat{x}_{k-1|k-1} + Bu_{k-1} - SR^{-1}y_{k-1} \tag{2.82}$$

$$\widehat{x}_{k|k} = \widehat{x}_{k|k-1} + K_k(y_k - C\widehat{x}_{k|k-1} - Du_k) \tag{2.83}$$

with $k = 1, \ldots, N$.

2.3.3 Joint Parameters and States Estimation

A classic estimation problem is to either estimate the system parameters or perform state estimation. This is specially true in that cases where the model parameters are not changing with time: one learns the parameters once, and then performs state estimation the next times. In practice, tear and wear effects and external conditions may affect the parameters of a model with time. Therefore, it may be necessary to perform joint parameters-state estimation steps. In such cases we can apply the EM algorithm to estimate both the states (considered as latent variables) and the parameters.

Notice that for linear Gaussian systems the expectation step corresponds to perform a Kalman smoothing to estimate the states using the best available parameters estimate. In the maximization step, instead, the joint state-measurements likelihood function is maximized considering the states as calculated in the Expectation step so that to refine the current parameters estimate.

Chapter 3

Contributions and future directions

3.1 Contributions of the included publications

Paper A: Joint temperature - lasing mode compensation for time-of-flight Lidar sensors

Summary

We propose an EM algorithm that compensates the mode-hopping effects described in Section 1.3.1 by modeling the induced measurement noise as a Gaussian mixture. Thus, from mathematical perspectives, we introduce some latent variables (namely, from which Gaussian the noise comes from) as additional estimands. This EM algorithm is also coupled to a temperature compensation filter built on a physics-based linear model for the thermal dynamics of the laser scanner.

Contributions

Our contributions are:

1. a thorough motivation for why it is meaningful to consider mode-hopping effects in laser scanners, arising from a physical description of the lasing mechanism in laser diodes;

2. a thermodynamical model describing the thermal dynamics of a whole laser scanner, needed by the proposed strategy to account for temperature effects;

3. a statistical model describing the measurement process that decouples the effects of the mode-hopping from temperature effects;

4. a numerically-efficient EM strategy based on the statistical model above;

5. a validation of the proposed compensation strategy on real devices.

Paper B: Statistical modeling and calibration of triangulation Lidars

Summary

We aim at increasing the statistical performance of triangulation Lidars for robotic applications, with the target of improving their cost-effectiveness through statistical processing techniques. We thus first propose a statistical model for the measurement process of these devices that accounts for both nonlinear bias effects and heteroscedasticity in the measurement noise. After this we thus solve the problem of calibrating triangulation Lidars models off-line, using ground truth information, and using an approximated ML strategy. Given the results of this calibration procedure we then propose both ML and LS strategies for solving the on-line estimation problem, and validate the whole procedure processing data from a physical device, showing a 17-fold improvement of the empirical MSE of post-calibration data against pre-calibration data.

Contributions

Our contributions are:

1. a dedicated general model for the measurement process of triangulation Lidars that not only generalizes the existing models [11, 12], but is also motivated by mechanical and physical interpretations of the measurement mechanisms;
2. an approximated ML off-line calibration procedure that uses ground truth data (e.g., from a Motion Capture (MoCap) system). The calibration procedure extends the one proposed in [11] by considering a simultaneous calibration of the various parameters instead of an independent and sequential estimation procedure;
3. two novel ML and LS strategies for correcting the measurements from the sensor with the model inferred during the calibration stage;
4. a validation of the whole calibration and testing framework on a real device.

Paper C: Calibrating triangulation Lidars without groundtruth information in terrestrial applications

Summary

The aim is to start from the statistical model proposed in [40] to construct a groundtruth-less intrinsic parameters calibration procedure that exploit an ad-hoc and approximated EM algorithm.

In more details we ignore temporal calibration problems and focus explicitly on calibration procedures for terrestrial robots. The standing assumptions that ensure the feasibility of the estimation strategy are indeed:

1. the robot moves on a line (even with a time varying speed; the important is that the movement is a line);
2. the robot has knowledge of the actuation signals it gave to its motors (this precludes doing calibrations *by hand*).

We also describe how to integrate in the calibration scheme other ranging sensors like odometry and ultrasonic, so to perform simultaneous calibration, and also describe how to use the results coming from a groundtruth-less calibration procedure to perform Kalman smoothing during the normal operations of these sensors.

We eventually quantify and compare how these novel groundtruth-less calibration strategies perform compared to the groundtruth-based strategies proposed in [40], plus investigate the gains obtained combining Lidars , odometers and sonars. The results indicate that the groundtruth-less leads to results that are similar to the ones obtained with groundtruth-based strategies (sometimes even better!). This is not totally surprising: we indeed postulate that the information on the actuation signal given to the robots' wheels (that was not used in [40]) compensates for the loss of the groundtruth.

Contributions

Our contributions are:

1. an approximated EM and a Kalman smoother-based estimation strategies that allow, under the assumptions of linear motion and knowledge of which actuation inputs have been given to the motors of the robot, to jointly (or separately) calibrate sets of homoscedastic and heteroscedastic sensors such as triangulation Lidars , sonars and odometers without the need for groundtruth information;

2. a validation of the whole calibration and testing framework on a real device;

3. a relative comparison of the relative effectiveness of groundtruth-based and groundtruth-less calibration strategies, to quantify how much important is eventually to either know the groundtruth by means of a motion capture system or the actuation signals that are given to the robot.

3.2 Related but not appended publications

A. Alhashimi, R. Hostettler and T. Gustafsson, "An Improvement in the Observation Model for Monte Carlo Localization," *Informatics in Control, 11th International Conference on Automation and Robotics (ICINCO)*, vol. 2, 2014, pp. 498–505.

An ad-hoc modification for the ToF Lidar sensor model to improve the robot Monte Carlo localization in dynamic environments. The modification is based on filtering (deleting) the measurements that are close to each other within a specified threshold. These measurements are known to be problematic for the likelihood function when reflected from un-modeled dynamic objects.

3.3 Future directions

We have mainly two separate future directions:

refine our strategies: our calibration techniques consider only one beam at a certain specific angle, and ignore that a complete Lidar scan is produced through rotating the beam inside the field of view and sampling it at certain angles with precise angular separation. We are thus currently ignoring the potential benefits of considering multi-beam calibrations instead of single-beam ones, and we will address this deficiency right after completing this thesis. To this aim we notice that cheap Lidars use simple mechanical rotation system that lead in inaccurate positioning of the beam angles, which in turn will result in less reliable measurements (with errors increasing for longer distances and producing evident warping, specially when the scanner scans a flat surface);

make Lidars fly: triangulation Lidars are light weight, have long detection range, have a wide field of view, and (most important of all, probably) are quite cheap compared to other Lidar technologies. All these qualities make triangulation Lidars seem appropriate sensors for flying robots.

However, flying objects are known to be affected by mechanical vibrations and fast aggressive responses; calibrating and using Lidar devices in such operating conditions is thus very challenging. Our future plan is to ease the introduction of such sensors in such harsh conditions. One of our first efforts in this topic will thus be checking how to extend our Lidar calibration techniques by inserting what are the effects of the novel dynamics in our models.

References

[1] H. D. LiDAR, "Datasheet for Velodyne HDL-64E S2," *Velodyne: Morgan Hill, CA, USA. Available online: http://www. velodyne. com/lidar/products/brochure/HDL64E% 20S2% 20datasheet_2010_lowres. pdf (accessed 22 January 2010)*.

[2] T. Heumier and J. Carlsten, "Detecting mode hopping in semiconductor lasers by monitoring intensity noise," *Quantum Electronics, IEEE Journal of*, vol. 29, no. 11, pp. 2756–2761, 1993.

[3] L. Kneip, F. Tâche, G. Caprari, and R. Siegwart, "Characterization of the compact hokuyo urg-04lx 2d laser range scanner," in *Robotics and Automation, 2009. ICRA'09. IEEE International Conference on*. IEEE, 2009, pp. 1447–1454.

[4] A. Reina and J. Gonzales, "Characterization of a radial laser scanner for mobile robot navigation," in *Intelligent Robots and Systems, 1997. IROS'97., Proceedings of the 1997 IEEE/RSJ International Conference on*, vol. 2. IEEE, 1997, pp. 579–585.

[5] K.-H. Lee and R. Ehsani, "Comparison of two 2d laser scanners for sensing object distances, shapes, and surface patterns," *Computers and electronics in agriculture*, vol. 60, no. 2, pp. 250–262, 2008.

[6] R. Sanz-Cortiella, J. Llorens-Calveras, J. R. Rosell-Polo, E. Gregorio-Lopez, and J. Palacin-Roca, "Characterisation of the lms200 laser beam under the influence of blockage surfaces. influence on 3d scanning of tree orchards," *Sensors*, vol. 11, no. 3, pp. 2751–2772, 2011.

[7] P. Tang, B. Akinci, and D. Huber, "Quantification of edge loss of laser scanned data at spatial discontinuities," *Automation in Construction*, vol. 18, no. 8, pp. 1070–1083, 2009.

[8] J. Tuley, N. Vandapel, and M. Hebert, "Analysis and removal of artifacts in 3-d ladar data," in *Robotics and Automation, 2005. ICRA 2005. Proceedings of the 2005 IEEE International Conference on*. IEEE, 2005, pp. 2203–2210.

[9] C. Ye and J. Borenstein, "Characterization of a 2-d laser scanner for mobile robot obstacle negotiation," in *ICRA*, 2002, pp. 2512–2518.

[10] A. Alhashimi, D. Varagnolo, and T. Gustafsson, "Joint temperature-lasing mode compensation for time-of-flight lidar sensors," *Sensors*, vol. 15, no. 12, pp. 31 205–31 223, 2015.

[11] J. Lima, J. Gonçalves, and P. J. Costa, "Modeling of a low cost laser scanner sensor," in *CONTROLO'2014–Proceedings of the 11th Portuguese Conference on Automatic Control*. Springer, 2015, pp. 697–705.

[12] D. Campos, J. Santos, J. Gonçalves, and P. Costa, "Modeling and simulation of a hacked neato xv-11 laser scanner," in *Robot 2015: Second Iberian Robotics Conference*. Springer, 2016, pp. 425–436.

[13] Q. Zhang and R. Pless, "Extrinsic calibration of a camera and laser range finder (improves camera calibration)," in *Intelligent Robots and Systems, 2004.(IROS 2004). Proceedings. 2004 IEEE/RSJ International Conference on*, vol. 3. IEEE, 2004, pp. 2301–2306.

[14] C. Mei and P. Rives, "Calibration between a central catadioptric camera and a laser range finder for robotic applications," in *Robotics and Automation, 2006. ICRA 2006. Proceedings 2006 IEEE International Conference on*. IEEE, 2006, pp. 532–537.

[15] O. Jokinen, "Self-calibration of a light striping system by matching multiple 3-d profile maps," in *3-D Digital Imaging and Modeling, 1999. Proceedings. Second International Conference on*. IEEE, 1999, pp. 180–190.

[16] B. Tiddeman, N. Duffy, G. Rabey, and J. Lokier, "Laser-video scanner calibration without the use of a frame store," in *Vision, Image and Signal Processing, IEE Proceedings-*, vol. 145, no. 4. IET, 1998, pp. 244–248.

[17] H. Andreasson, R. Triebel, and W. Burgard, "Improving plane extraction from 3d data by fusing laser data and vision," in *Intelligent Robots and Systems, 2005.(IROS 2005). 2005 IEEE/RSJ International Conference on*. IEEE, 2005, pp. 2656–2661.

[18] G.-Q. Wei and G. Hirzinger, "Active self-calibration of hand-mounted laser range finders," *Robotics and Automation, IEEE Transactions on*, vol. 14, no. 3, pp. 493–497, 1998.

[19] A. M. McIvor, "Calibration of a laser stripe profiler," in *3-D Digital Imaging and Modeling, 1999. Proceedings. Second International Conference on*. IEEE, 1999, pp. 92–98.

[20] Q. Zhang and R. Pless, "Constraints for heterogeneous sensor auto-calibration," in *Computer Vision and Pattern Recognition Workshop, 2004. CVPRW'04. Conference on*. IEEE, 2004, pp. 38–38.

[21] C.-Y. Chen and H.-J. Chien, "On-site sensor recalibration of a spinning multi-beam lidar system using automatically-detected planar targets," *Sensors*, vol. 12, no. 10, pp. 13 736–13 752, 2012.

[22] N. Muhammad and S. Lacroix, "Calibration of a rotating multi-beam lidar," in *Intelligent Robots and Systems (IROS), 2010 IEEE/RSJ International Conference on*. IEEE, 2010, pp. 5648–5653.

[23] G. Atanacio-Jiménez, J.-J. González-Barbosa, J. B. Hurtado-Ramos, F. J. Ornelas-Rodríguez, H. Jiménez-Hernández, T. García-Ramirez, and R. González-Barbosa, "Lidar velodyne hdl-64e calibration using pattern planes," *International Journal of Advanced Robotic Systems*, vol. 8, no. 5, pp. 70–82, 2011.

[24] C. Glennie and D. D. Lichti, "Static calibration and analysis of the velodyne hdl-64e s2 for high accuracy mobile scanning," *Remote Sensing*, vol. 2, no. 6, pp. 1610–1624, 2010.

[25] ——, "Temporal stability of the velodyne hdl-64e s2 scanner for high accuracy scanning applications," *Remote Sensing*, vol. 3, no. 3, pp. 539–553, 2011.

[26] C. Glennie, "Calibration and kinematic analysis of the velodyne hdl-64e s2 lidar sensor," *Photogrammetric Engineering & Remote Sensing*, vol. 78, no. 4, pp. 339–347, 2012.

[27] M. Gordon and J. Meidow, "Calibration of a multi-beam laser system by using a tls-generated reference," *ISPRS Annals of Photogrammetry, Remote Sensing and Spatial Information Sciences II-5 W*, vol. 2, pp. 85–90, 2013.

[28] F. M. Mirzaei, D. G. Kottas, and S. I. Roumeliotis, "3d lidar–camera intrinsic and extrinsic calibration: Identifiability and analytical least-squares-based initialization," *The International Journal of Robotics Research*, vol. 31, no. 4, pp. 452–467, 2012.

[29] X. Gong, Y. Lin, and J. Liu, "3d lidar-camera extrinsic calibration using an arbitrary trihedron," *Sensors*, vol. 13, no. 2, pp. 1902–1918, 2013.

[30] Y. Park, S. Yun, C. S. Won, K. Cho, K. Um, and S. Sim, "Calibration between color camera and 3d lidar instruments with a polygonal planar board," *Sensors*, vol. 14, no. 3, pp. 5333–5353, 2014.

[31] R. Kümmerle, G. Grisetti, and W. Burgard, "Simultaneous calibration, localization, and mapping," in *Intelligent Robots and Systems (IROS), 2011 IEEE/RSJ International Conference on*. IEEE, 2011, pp. 3716–3721.

[32] A. Teichman, S. Miller, and S. Thrun, "Unsupervised intrinsic calibration of depth sensors via slam." in *Robotics: Science and Systems*. Citeseer, 2013.

[33] S. M. Kay, *Fundamentals of statistical signal processing, volume I: estimation theory*. Prentice Hall, 1993.

[34] Y. Anzai, *Pattern Recognition & Machine Learning*. Elsevier, 2012.

[35] A. P. Dempster, N. M. Laird, and D. B. Rubin, "Maximum likelihood from incomplete data via the em algorithm," *Journal of the royal statistical society. Series B (methodological)*, pp. 1–38, 1977.

[36] S. Gibson and B. Ninness, "Robust maximum-likelihood estimation of multivariable dynamic systems," *Automatica*, vol. 41, no. 10, pp. 1667–1682, 2005.

[37] T. Schön, "An explanation of the expectation maximization algorithm," 2009.

[38] H. E. Rauch, C. Striebel, and F. Tung, "Maximum likelihood estimates of linear dynamic systems," *AIAA journal*, vol. 3, no. 8, pp. 1445–1450, 1965.

[39] R. H. Shumway and D. S. Stoffer, *Time series analysis and its applications: with R examples*. Springer Science & Business Media, 2006.

[40] A. Alhashimi, D. Varagnolo, and T. Gustafsson, "Statistical modeling and calibration of triangulation lidars," in *ICINCO*, 2016.

Part II

Paper A

Joint temperature - lasing mode compensation for time-of-flight Lidar sensors

Authors:
Anas Alhashimi, Damiano Varagnolo, Thomas Gustafsson

Reformatted version of paper accepted for publication in:
Sensors 15, no. 12: 31205-31223.

Joint temperature - lasing mode compensation for time-of-flight Lidar sensors

Anas Alhashimi, Damiano Varagnolo, Thomas Gustafsson

Abstract: We propose an EM strategy for improving the precision of ToF Lidar scanners. The novel algorithm statistically accounts not only for the bias induced by temperature changes in the laser diode, but also for the multi-modality of the measurement noises that is induced by mode-hopping effects. Instrumental to the proposed EM algorithm, we also describe a general thermal dynamics model that can be learned either from just input-output data or from a combination of simple temperature experiments and information from the laser's datasheet. We test the strategy on a SICK LMS 200 device and improve its average absolute error by a factor of three.

1 Introduction

ToF Lidars estimate distances by emitting short bursts of laser light and by measuring the time it takes for the reflected photons to arrive back to the device [1]. Despite being based on a very simple principle, they are very much both accurate and precise devices [2]: for example, precisions can reach 10 mm of standard error when the object is 10 m away. Due to these favorable properties, they are commonly used in critical industrial applications where there is the need for high quality measurements.

It is well known that these devices need temperature compensation mechanisms, since changing their temperature leads to changes in the statistics of the returned measurements. The effect of temperature may be huge: experiments by [3] on an amplitude-modulated continuous-wave laser radar pointing at a target six meters away from the sensor showed that measurements at 21 °C and measurements at 45 °C were differing by 40 cm. Since thermal stabilization of a laser scanner may take up to 30 min [4], it is clear that these sensors are affected by a warm-up-induced time drift that must be compensated. Manufacturers of ToF devices thus usually embed opportune algorithms in their products that implement this temperature compensation mechanism. Unfortunately, temperature is not the only physical factor that deserves compensation: as described in detail in Section 2, lasers can suddenly change their lasing mode. This property, called the mode-hopping effect, has a substantial impact on the measure returned by ToF devices, since changing lasing mode means to change the spectral content of the laser burst, *i.e.*, change its time of flight. Remarkably, to the best of our knowledge, the existing literature does not focus on managing this effect, but rather, considers only temperature compensation mechanisms.

We would like to mention here that there are also other methods with high temperature compensation at the nano-scale measurement, such as [5]. The method reduces the offset, the temperature characteristic of the main sensing element, the temperature drift and the noise by the switching method.

1.1 Statement of Contributions

We propose an expectation maximization (EM) algorithm that compensates mode-hopping effects by modeling the induced measurement noise as a Gaussian mixture. Thus, from the mathematical perspective, we introduce some latent variables (namely, from which Gaussian the noise comes from) as additional estimands. This EM algorithm is also coupled to a temperature compensation filter that is built on a physics-based linear model for the thermal dynamics of the laser scanner. Summarizing, thus, our contributions are, with respect to the aforementioned literature:

1. A thorough motivation for why it is meaningful to consider mode-hopping effects in laser scanners, arising from a physical description of the lasing mechanism in laser diodes;

2. A thermodynamical model for the thermal dynamics of a whole laser scanner, needed by the proposed strategy to account for temperature effects;

3. A statistical model describing the measurement process that decouples the effects of the mode-hopping from temperature effects;

4. A numerically-efficient EM strategy based on the statistical model above;

5. A validation of the proposed compensation strategy on real devices.

With the validation, we also show that it is possible to improve the absolute error of a SICK LMS 200 device by a factor of three.

1.2 Organization of the Manuscript

Section 2 analyzes the effects of the laser temperature on the measured distance. Section 3 proposes a general model for the thermal dynamics of a pulsed ToF Lidar. Section 4 presents a general measurement model accounting for both temperature and mode-hopping effects. Section 5 describes how to train the EM algorithm, while Section 6 describes how to use the same algorithm for testing purposes. Section 7 then proposes a likelihood ratio test for calibrating the hyperparameters of the EM algorithm. Section 8 presents some numerical results on commercial devices. Finally, Section 9 draws some conclusions and future research directions.

2 Effects of the Laser Temperature on the Measured Distance

This section lays down interpretations motivating the structure of the novel compensation procedures. We thus here describe the functioning principle of ToF scanners, explain why the measured distance depends on the temperature of the device and motivate why the measurement noise of a Lidar is intrinsically multi-modal.

Consider then the basic operation of pulsed ToF Lidars in Figure 1 and in its caption.

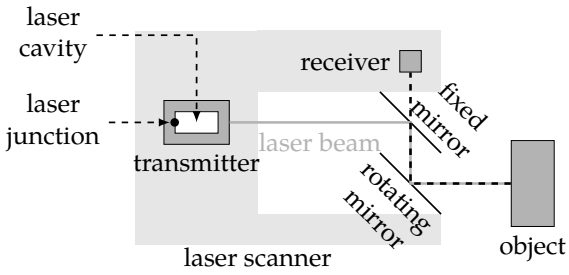

Figure 1: Graphical description of the operating principle for pulsed ToF Lidars. A pulsed infra-red laser beam is first emitted from the transmitter. The case of the transmitter, in dark gray, encloses a laser junction and a laser cavity. The emitted laser beam is then deflected by a rotating mirror (resulting in a fan-shaped scan pattern) and, finally, reflected from the object surface. The time of flight τ between the transmission and the reception of the laser beam is then used to estimate the distance d between the scanner and the object.

The measurement of the distance derives from ideal considerations: if the temporal width of the pulse is null, then the distance d between the sensor and the object should satisfy:

$$d = \frac{c\,\tau}{2} \tag{1}$$

where c is the speed of light and τ is the measured ToF between when the laser pulse is emitted and when it is received. Assume ideally that the laser pulse contains photons with a unique nominal wavelength λ_0. Since:

$$c = \lambda_0 f \tag{2}$$

with f the light frequency and λ_0 the nominal wavelength, and since the light frequency f remains the same through different media, to know c, it is sufficient to know λ_0. Thus, from knowing λ_0, one can compute d, since τ is measured.

We can already now notice the first effect of the temperature of the device on the measurement: according to its datasheet, the nominal wavelength of the laser diode SPL PL90 from OSRAM [6] is 905 nm at 25 °C, and 907.8 nm at 35 °C. Assuming the target to be at a one-meter distance, this 2.8 nm variation in the wavelength λ then results in a 10.3-ps variation in the ToF τ, *i.e.*, a variation in the measured distance of approximately 3.1 mm.

The previous consideration is nonetheless simplistic. We can indeed notice another three distinct effects:

1. In general, lasers do not emit at a unique frequency λ. Indeed, the average spectral distribution of the laser pulses follows a "comb"-like density, like the one in Figure 2.

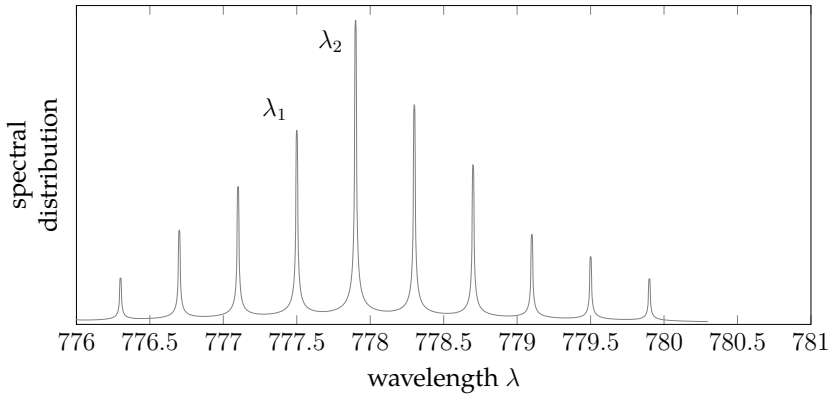

Figure 2: Average spectral distribution for GaAsP lasers at the nominal temperature of 21 °C [7].

2. Lasers are affected by the so-called mode-hopping effect [8] and, indeed, oscillate between different lasing modes (the teeth of the "comb" of Figure 2), for which two different pulses generated under the same temperature and external conditions may have different λ's (e.g., referring to the same figure, the first pulse may contain only photons with wavelengths λ_1, while the second pulse may contain only photons with wavelengths λ_2). In other words, the actual distribution of one specific pulse may contain only a subset of the teeth of the average spectral distribution. Using naively Equations (1) and (2) to estimate d without being aware of the mode hopping, *i.e.*, assuming a certain λ_0 without actually knowing that the average λ jumps between different lasing modes, reflects thus in a multimodal measurement of d, as clearly shown in Figure 3.

3. The average spectral distribution of the laser pulses is not fixed, but rather depends on the temperature of the transmitter [9]. More precisely, the positions and amplitudes of the modes in Figure 2 depend on both the current flowing through the laser junction and the geometry of the laser cavity, but eventually, these two effects are inter-combined: the current flow produces heat that will modify the geometry of the cavity. Eventually, thus, the temperature affects the position and amplitude of the modes of the average spectral distribution. This temperature effect can be clearly seen in Figure 4: even if the device is nominally already compensated in temperature, one can clearly see two different lasing modes shifting in temperature.

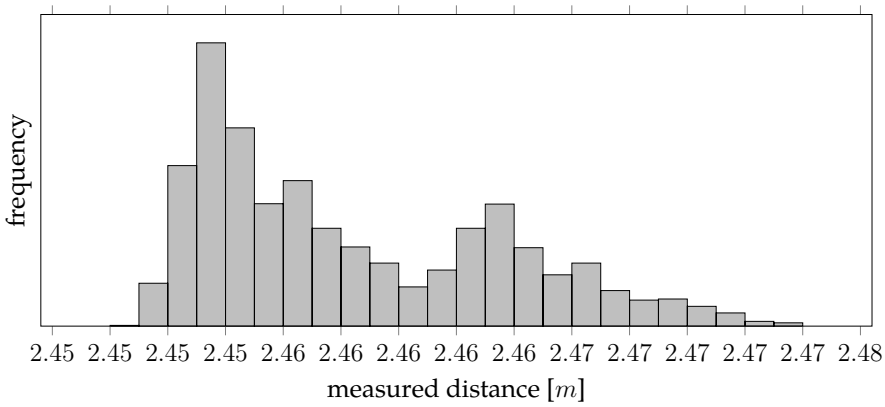

Figure 3: Histogram of consecutive measurements returned by a SICK 200 device in thermodynamical and electrical equilibrium pointing at a fixed object and in a controlled environment.

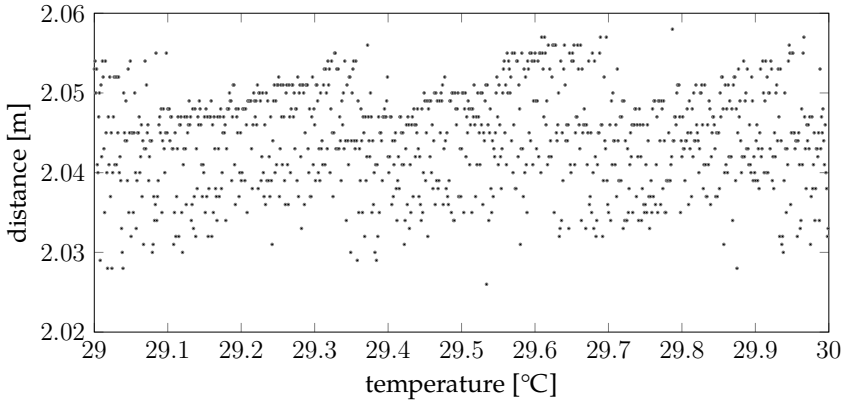

Figure 4: Dependency of the distance measurements on the device temperature for a SICK 200 device pointing to a fixed object in a controlled environment. Despite the true distance and other parameters potentially affecting the measurements being constant in time, the distributions of the measurements are temperature varying. We can notice how the device compensates for the temperature change by adding a temperature-varying negative bias, but that it does not compensate the mode-hopping effect.

To summarize, the actual λ of a laser pulse is in general different from the nominal λ_0 because of two effects: first, the laser may oscillate between different modes; second, these positions of these modes vary with temperature.

3 A General Model for the Thermal Dynamics of a Pulsed ToF Lidar

Instrumental for compensating the effects of temperature offsets highlighted in the previous section, we here discuss a general thermodynamic model describing the temperature dynamics of the whole laser scanner that will lead us to being able to represent the temperature changes of the laser cavity.

3.1 Physical Modeling

Just like any power electronic device, Lidars generate heat that is then exchanged with the environment, so that the temperature of a scanner depends on the temperature of the environment. The main sources of heat inside the LiDAR are thus the laser diode, the motor and the electronic components of the system. The heat generated inside the scanner is then transferred to the surrounding environment through the case. Since our experience indicates that motors and other electronic components induce negligible thermal effects, we consider only the heat produced by the laser diode.

We thus represent the thermal model of a generic scanner as the equivalent electrical circuit shown in Figure 5, interpretable as follows: when the laser is turned on, the heat generated by the laser junction is dissipated in the surrounding environment through first the transmitter case and then, second, through the laser scanner case.

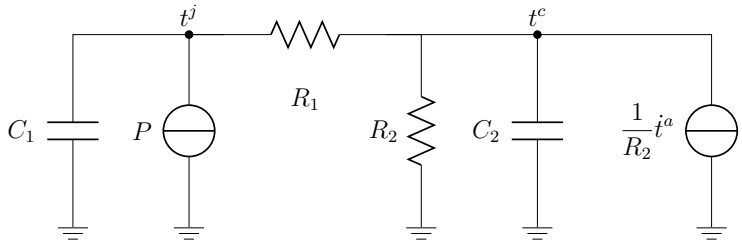

Figure 5: The proposed thermodynamic model for a generic pulsed ToF Lidar.

Considering the notation:

P	Heat power generated by the junction (equal to zero when the device is off)
t^j	Temperature of the junction
t^c	Temperature of the transmitter case
t^a	Temperature of the external ambient
t^s	Noisy measurement of the temperature of the transmitter case
C_1	Thermal inertia of the transmitter case
C_2	Thermal inertia of the laser scanner case
R_1	Thermal resistance between the transmitter case and the laser scanner case
R_2	Thermal resistance between the laser scanner case and the ambient

It follows that the dynamics for the temperatures of the laser junction and scanner case when the laser is on are thus:

$$\begin{cases} \dot{t}^c = \dfrac{t^j}{R_1C_2} - t^c\left(\dfrac{1}{R_2C_2} + \dfrac{1}{R_1C_2}\right) + \dfrac{1}{C_2R_2}\dot{t}^a \\ \dot{t}^j = \dfrac{P}{C_1} + \dfrac{t^c}{R_1C_1} - \dfrac{t^j}{R_1C_1} \end{cases} \tag{3}$$

Discretizing the previous dynamics with a discretization step of T s and letting:

$$\bar{t}_k := \begin{bmatrix} t^c_k \\ t^j_k \end{bmatrix} \qquad \overline{u}_k := \begin{cases} P & \text{if on,} \\ 0 & \text{if off,} \end{cases} \qquad \overline{\nu}_k := t^a_k - t^a_{k-1} \tag{4}$$

implies the following discrete-time state-space representation of the model:

$$\begin{cases} \bar{t}_{k+1} &= A\bar{t}_k + B\overline{u}_k + B'\overline{\nu}_k \\ t^s_k &= C\bar{t}_k + \overline{\mu}_k \end{cases} \tag{5}$$

where t^s_k is a noisy temperature measurement of the case at time k, $\overline{\nu}_k$ and $\overline{\mu}_k$ are independent process and measurement noises, and where:

$$A = \begin{bmatrix} 1 - \dfrac{T}{R_2C_2} - \dfrac{T}{R_1C_2} & \dfrac{T}{R_1C_2} \\ \dfrac{T}{R_1C_1} & 1 - \dfrac{T}{R_1C_1} \end{bmatrix} \qquad B = \begin{bmatrix} 0 \\ \dfrac{T}{C_1} \end{bmatrix} \qquad B' = \begin{bmatrix} \dfrac{T}{R_2C_2} \\ 0 \end{bmatrix} \qquad C = \begin{bmatrix} 1 & 0 \end{bmatrix} \tag{6}$$

Notice that through Equation (5), we introduce t^s_k, *i.e.*, a noisy measurement of the temperature of the transmitter case. This correspond to the practical assumption that perfect knowledge of the actual case temperature t^c_k is in general unavailable, since temperature sensors attached to the case of the scanner will never give noiseless recordings.

3.2 Identifying Model Equation (5)

If one has a dataset of recorded temperatures t^j_k, t^c_k and t^a_k, then one may identify Equation (5) using standard system identification approaches, e.g., a Prediction Error Method (PEM) as in [10]. For the common case where it may be difficult to obtain direct measurements of the quantities, we propose to resort to the following general strategy that uses the datasheet of the laser scanner in conjunction with noisy case temperature measurements t^s_k.

3.3 Estimating t^j from t^s

Assume that model Equation (5) has been identified, either from measured data or using Algorithm 1, and observe that the thermal model is observable, reachable and has stable dynamics. Due to their favorable theoretical and numerical properties, we thus devise to estimate t^j_k from noisy measurements of the case temperature t^s_k via Kalman smoothers/filters, as in [12], *i.e.*, to let:

$$\left[\widehat{t}^j_1, \ldots, \widehat{t}^j_K\right] = W\left[t^s_1, \ldots, t^s_K\right] \tag{7}$$

for an opportune (and potentially time varying) matrix W. As before, notice that the filtering starts from noisy measurements of the case temperature t^s_k, rather than from perfect measurements t^c_k.

Algorithm 1 Identification of model Equation (5) starting from the datasheet of a laser scanner.

1: From the datasheet of the laser scanner infer:
   - its thermal resistance R_1 (directly from the datasheet);
   - its thermal capacity C_1 (by estimating the volume of the laser diode from the datasheet and multiplying it for the heat capacity of the material, also indicated in the datasheet);
2: From measuring the weight and material of the case, infer its thermal capacity C_2;
3: Estimate the generated heat power P by measuring the electrical power absorbed by the device and multiplying this quantity by 0.5 (for the estimated efficiency of generic laser diodes [11]);
4: From situations where the scanner is in thermal equilibrium, calculate R_2 by calculating the difference between the measured case temperature t_k^s and the ambient temperature t_k^a divided by the estimated generated heat power P.

4 A General Measurement Model Accounting for Temperature and Mode Hopping Effects

We recall that our aim is to model the effect of the temperature of the laser junction t_k^j on the measured distance d and understand how noisy case temperature measurements t_k^s help improving the accuracy on the final estimate of d. To this aim, we propose the following measurement model at the generic time instant k:

$$y_k = d + H\left(t_k^j\right)\boldsymbol{\theta} + (1-\Delta_k)\, w_k^1 + \Delta_k w_k^2 \tag{8}$$

where:

- y_k is the distance returned by the sensor;
- d is the true distance from the object (assumed deterministic);
- t_k^j is the temperature of the laser cavity at time k;
- The two modes $w_k^1 \sim \mathcal{N}\left(\mu_1, \sigma_1^2\right)$ and $w_k^2 \sim \mathcal{N}\left(\mu_2, \sigma_2^2\right)$ account for a bimodal Gaussian and white additive measurement noise. The Bernoulli random variable (r.v.) $\Delta_k \sim \mathcal{B}\left(\pi\right)$ selects the active mode at time k, so that π reflects the relative importance of the modes. Intuitively, Δ_k represent which lasing mode has been active during measurement y_k. We notice that here, we consider bimodal noises (*i.e.*, only two lasing modes) just for notational simplicity. It is nonetheless immediate to generalize the subsequent findings for an M-modal case;
- $H\left(\cdot\right)\boldsymbol{\theta}$ is a non-linear transformation of the temperature of the laser junction t_k^j in a measurement bias. In the following Examples A.1 and A.2, we show how different $H\left(\cdot\right)$'s

and $\boldsymbol{\theta}$'s express different maps from the junction temperature t_k^j to the measurement bias.

Notice that, induced by our experience, we let the measurement noise modes w_k^1 and w_k^2 be independent from the laser junction temperature t_k^j. Our experiments indeed indicated that the moments of the noises are not affected by changing temperatures (at least for a range between 0 °C and 40 °C). Notice moreover that model Equation (8) is linear in $\boldsymbol{\theta}$; this restrictive assumption is nonetheless essential for building distance estimation algorithms that are numerically fast.

Example A.1 (Polynomial model)
Let:

$$H_k = H\left(t_k^j\right) := \left[t_k^j,\ \left(t_k^j\right)^2,\ \ldots,\ \left(t_k^j\right)^N\right] \tag{9}$$

and $\boldsymbol{\theta} := [\theta_1, \ldots, \theta_N]$. *Then, the generic model Equation* (8) *specializes into:*

$$y_k = d + \sum_{n=1}^{N} \left(t_k^j\right)^n + (1 - \Delta_k)\, w_k^1 + \Delta_k w_k^2 \tag{10}$$

i.e., a measurement model where the temperature plays the role of an N*-th order polynomial bias (see Figure 6).*

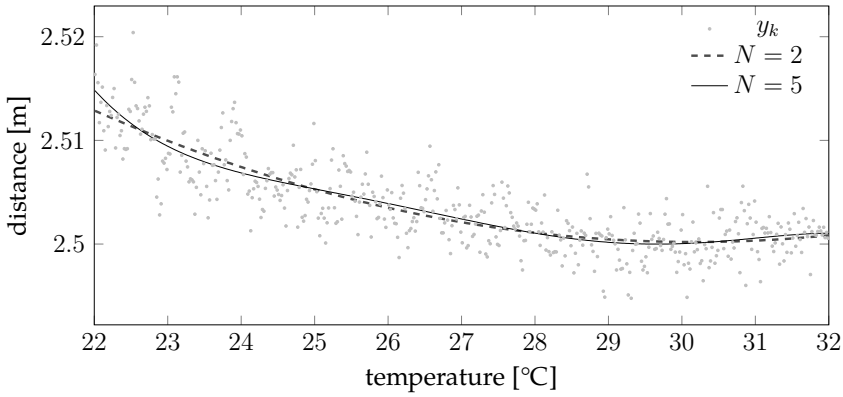

Figure 6: Potential temperature-bias dependencies for the polynomial model of Example A.1.

Example A.2 (Fourier expansion model)
Let:

$$H_k = H\left(t_k^j\right) := \left[\cos\left(2\pi f_0 t_k^j\right),\ \sin\left(2\pi f_0 t_k^j\right),\ \ldots,\ \cos\left(2N\pi f_0 t_k^j\right),\ \sin\left(2N\pi f_0 t_k^j\right)\right] \tag{11}$$

and $\boldsymbol{\theta} := [\theta_1', \theta_1'', \ldots, \theta_N', \theta_N'']$, *where the fundamental frequency* f_0 *is assumed to be known. Then, the generic model Equation* (8) *specializes into:*

$$y_k = d + \sum_{n=1}^{N} \left(\theta_n' \cos\left(2n\pi f_0 t_k^j\right) + \theta_n'' \sin\left(2n\pi f_0 t_k^j\right)\right) + (1 - \Delta_k)\, w_k^1 + \Delta_k w_k^2 \tag{12}$$

i.e., a measurement model where the temperature plays the role of a bias that is periodic with frequency f_0 *(see Figure 7).*

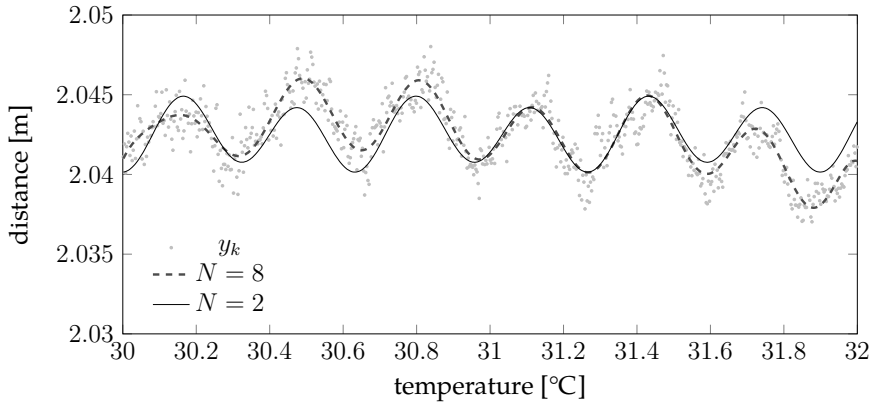

Figure 7: Potential temperature-bias dependencies for the Fourier expansion model of Example A.2.

We then use model Equation (8) for practical purposes following the classical scheme:

- Design the model, *i.e.*, decide the structure for $H(\cdot)$ (e.g., between Example A.1, Example A.2 or also different ones depending on the need) starting from data collected in a controlled environment (see Section 7);
- Train the model, *i.e.*, estimate $\boldsymbol{\theta}$ and the statistics of w_k^1, w_k^2 and Δ_k from data collected in a controlled environment (see Section 5);
- Test the model, *i.e.*, use the previous estimated quantities during the normal operation of the laser scanner, so as to improve the estimation of d from data collected in a non-controlled environment (see Section 6).

The following sections are dedicated in detail to how to implement the previous three points. Notice that Section 7, on the design of the model, is presented after Sections 5 and 6 for notational convenience.

5 Training Model Equation (8)

In this section, we devise a numerical algorithm for learning $\boldsymbol{\theta}$ (*i.e.*, the coefficients multiplying $H(\cdot)$), μ_1, μ_2, σ_1^2, σ_2^2, π (*i.e.*, the statistics of the noises w_k^1, w_k^2 and of the random variables Δ_k) and the values of the mode selection variables Δ_k starting from a dataset containing:

- y_k for $k \in \{1, \dots, K\}$;
- d, *i.e.*, the real distance;
- t_k^s, *i.e.*, measurements of the temperature of the laser scanner case (to be transformed into estimates of t_k^j through Equation (7)).

Let then:

$$\begin{array}{rcl} \boldsymbol{y} & := & \begin{bmatrix} y_1 & \cdots & y_K \end{bmatrix}^T \\ \boldsymbol{t}^s & := & \begin{bmatrix} t_1^s & \cdots & t_K^s \end{bmatrix}^T \\ \boldsymbol{t}^j & := & \begin{bmatrix} t_1^j & \cdots & t_K^j \end{bmatrix}^T \\ \boldsymbol{\Delta} & := & \begin{bmatrix} \Delta_1 & \cdots & \Delta_K \end{bmatrix}^T \\ \overline{\boldsymbol{\theta}} & := & \begin{bmatrix} \boldsymbol{\theta}^T & \mu_1 & \mu_2 & \sigma_1^2 & \sigma_2^2 & \pi \end{bmatrix}^T. \end{array} \tag{13}$$

Given the frequentist assumptions on the unknowns, we would like to perform ML estimation for $\overline{\boldsymbol{\theta}}$, *i.e.*, seek for:

$$\arg\max_{\overline{\boldsymbol{\theta}},\boldsymbol{\Delta}} \ \mathbb{P}\left[\boldsymbol{y}, \boldsymbol{t}^j \ ; \ d, \overline{\boldsymbol{\theta}}, \boldsymbol{\Delta}\right] \tag{14}$$

Since the laser junction temperature $\boldsymbol{t}^j$ is unavailable, Equation (14) cannot be solved. We thus resort to solving the approximated problem:

$$\left(\widehat{\boldsymbol{\theta}}, \widehat{\boldsymbol{\Delta}}\right) := \arg\max_{\overline{\boldsymbol{\theta}},\boldsymbol{\Delta}} \ \mathbb{P}\left[\boldsymbol{y}, \widehat{\boldsymbol{t}^j} \ ; \ d, \overline{\boldsymbol{\theta}}, \boldsymbol{\Delta}\right] \tag{15}$$

where $\widehat{\boldsymbol{t}^j}$ is the estimate of $\boldsymbol{t}^j$ given $\boldsymbol{t}^s$ as in Equation (7). We also notice that, instead of considering the joint density of $\boldsymbol{y}$ and $\widehat{\boldsymbol{t}^j}$, it is sufficient to consider the conditional density of $\boldsymbol{y}$ given $\widehat{\boldsymbol{t}^j}$:

Proposition 1.

$$\left(\widehat{\boldsymbol{\theta}}, \widehat{\boldsymbol{\Delta}}\right) = \arg\max_{\overline{\boldsymbol{\theta}},\boldsymbol{\Delta}} \ \mathbb{P}\left[\boldsymbol{y} \ \middle| \ \widehat{\boldsymbol{t}^j} \ ; \ d, \overline{\boldsymbol{\theta}}, \boldsymbol{\Delta}\right] \tag{16}$$

It is important to notice that the ML problem in Equation (16) contains the latent variables $\boldsymbol{\Delta}$; to estimate them, we thus resort to a tailored EM approach [13]. To this aim, define then the auxiliary variables:

$$\begin{array}{lll} \Sigma_1 := \operatorname{diag}\left(1 - \widehat{\Delta}_k\right) & \widetilde{y}_k := y_k - d & H := \begin{bmatrix} H_1 \\ \vdots \\ H_K \end{bmatrix} = \begin{bmatrix} H\left(\widehat{t}_1^j\right) \\ \vdots \\ H\left(\widehat{t}_K^j\right) \end{bmatrix} \\ \Sigma_2 := \operatorname{diag}\left(\widehat{\Delta}_k\right) & \widetilde{\boldsymbol{y}} := \boldsymbol{y} - d\mathbb{1} & \end{array} \tag{17}$$

with $\mathbb{1}$ being a vector of K ones. The computation of $\left(\widehat{\boldsymbol{\theta}}, \widehat{\boldsymbol{\Delta}}\right)$ is performed through the iteration up to convergence (stopping criteria for EM algorithms are usually based on relative or absolute changes in the parameter estimate or in the value of the log likelihood; see, e.g., [14]; in our implementations, we used the absolute changes in the parameter estimate $\widehat{\pi} < \epsilon$; where ϵ is a small number 1×10^{-5} in the implementation) of the following two steps:

E-step

$$\begin{aligned} \delta_k &= (1 - \widehat{\pi}) \ \mathcal{N}\left(\widetilde{y}_k - H_k\widehat{\boldsymbol{\theta}} - \widehat{\mu}_1, \widehat{\sigma}_1^2\right) + \widehat{\pi} \ \mathcal{N}\left(\widetilde{y}_k - H_k\widehat{\boldsymbol{\theta}} - \widehat{\mu}_2, \widehat{\sigma}_2^2\right), \qquad k = 1, \ldots, K \\ \widehat{\Delta}_k &= \frac{\widehat{\pi}\mathcal{N}\left(\widetilde{y}_k - H_k\widehat{\boldsymbol{\theta}} - \widehat{\mu}_2, \widehat{\sigma}_2^2\right)}{\delta_k}, \qquad k = 1, \ldots, K \end{aligned} \tag{18}$$

M-step

$$\begin{aligned}
\boldsymbol{C} &= \widehat{\sigma}_1^2\,\Sigma_1 + \widehat{\sigma}_2^2\,\Sigma_2 \\
\widehat{\boldsymbol{\theta}} &= \left(H^T\boldsymbol{C}^{-1}H\right)^{-1}H^T\boldsymbol{C}^{-1}\widetilde{\boldsymbol{y}} \\
\widehat{\mu}_i &= \frac{\mathbb{1}^T\Sigma_i}{\mathbb{1}^T\Sigma_i\mathbb{1}}\left(\widetilde{\boldsymbol{y}} - H\widehat{\boldsymbol{\theta}}\right) \qquad i=1,2 \\
\widehat{\sigma}_i^2 &= \frac{\left(\widetilde{\boldsymbol{y}} - H\widehat{\boldsymbol{\theta}}\right)^T\Sigma_i\left(\widetilde{\boldsymbol{y}} - H\widehat{\boldsymbol{\theta}}\right)}{\mathbb{1}^T\Sigma_i\mathbb{1}} \qquad i=1,2 \\
\widehat{\pi} &= \frac{1}{K}\sum_k \widehat{\Delta}_k
\end{aligned} \tag{19}$$

In our numerical experiments, we empirically found it convenient to use the following initial conditions:

$$\widehat{\boldsymbol{\theta}} = \mathbf{0}, \qquad \widehat{\mu}_1 = 0.1, \qquad \widehat{\mu}_2 = -0.1, \qquad \widehat{\sigma}_1^2 = 0.1, \qquad \widehat{\sigma}_2^2 = 0.1, \qquad \widehat{\pi} = 0.5 \tag{20}$$

As for the convergence of the EM to the true ML estimate, we notice that EM algorithms are not in general ensured to have convergence properties. A sufficient condition for convergence is in [15], where the authors show that EM algorithms are convergent if the maximizer of the M-step is unique (a condition that is almost always satisfied in practice). In our case, the M-step maximizer is unique as long as in the update for $\widehat{\boldsymbol{\theta}}$ in Equation (19), the matrix $H^T\boldsymbol{C}^{-1}H$ admits the inverse. In general, e.g., in both the polynomial case of Example A.1 and in the Fourier expansion case of Example A.2, this translates into the need for at least N samples associated with N different laser junction temperatures t_k^j.

6 Testing Model Equation (8)

We now devise a numerical algorithm for estimating d and the values of the lasing mode selection variables Δ_k starting from the model trained in Section 5 (*i.e.*, an estimated vector $\widehat{\widetilde{\boldsymbol{\theta}}} := \left[\widehat{\boldsymbol{\theta}}^T,\ \widehat{\mu}_1,\ \widehat{\mu}_2,\ \widehat{\sigma}_1^2,\ \widehat{\sigma}_2^2,\ \widehat{\pi}\right]^T$ and the statistics of w_k^1, w_k^2 and Δ_k) and a set of measurements y_k and t_k^s for $k = 1, \ldots, K$.

Assuming once again to transform the temperature sensor measurements $\boldsymbol{t}^s$ into estimated laser junction temperatures $\widehat{\boldsymbol{t}}^j = W\boldsymbol{t}^s$ through Equation (7), the problem of estimating d and the Δ_ks can be cast as:

$$\left(\widehat{d}, \widehat{\boldsymbol{\Delta}}\right) = \arg\max_{d,\boldsymbol{\Delta}}\ \mathbb{P}\left[\boldsymbol{y}\ \middle|\ \widehat{\boldsymbol{t}}^j\ ;\ d, \widehat{\widetilde{\boldsymbol{\theta}}}, \boldsymbol{\Delta}\right] \tag{21}$$

As before, we compute this ML estimate through an EM approach:

E-step

$$\begin{aligned}
&\delta_k = (1-\widehat{\pi})\,\mathcal{N}\left(y_k - \widehat{d} - H_k\widehat{\boldsymbol{\theta}} - \widehat{\mu}_1, \widehat{\sigma}_1^2\right) + \widehat{\pi}\mathcal{N}\left(y_k - \widehat{d} - H_k\widehat{\boldsymbol{\theta}} - \widehat{\mu}_2, \widehat{\sigma}_2^2\right), \quad k = 1, \ldots, K \\
&\widehat{\Delta}_k = \frac{\widehat{\pi}\mathcal{N}\left(y_k - \widehat{d} - H_k\widehat{\boldsymbol{\theta}} - \widehat{\mu}_2, \widehat{\sigma}_2^2\right)}{\delta_k}, \quad k = 1, \ldots, K
\end{aligned} \tag{22}$$

M-step

$$\begin{aligned} C &= \Sigma_1 \widehat{\sigma}_1^2 + \Sigma_2 \widehat{\sigma}_2^2 \\ \widehat{d} &= \left(\mathbb{1}^T C^{-1} \mathbb{1}\right)^{-1} \mathbb{1}^T C^{-1} \left(\boldsymbol{y} - H\widehat{\boldsymbol{\theta}}\right) \end{aligned} \tag{23}$$

The same values of μ_1, μ_2, σ_1^2 and σ_2^2 at the end of the training step will be used in the testing step. There is no need to recompute them again. In our experiments, we found it beneficial to start from the initial conditions $\widehat{d} = \dfrac{\mathbb{1}^T \boldsymbol{y}}{K}$ and $\widehat{\Delta}_k = 0.5$. The convergence properties of this EM procedure are then very similar to the EM in Section 5.

7 Designing Model Equation (8)

This section is divided into two parts:

1. Section 7.1, suggesting some hints for designing different structures for $H(\cdot)$ (e.g., choosing the order for Example A.1, for Example A.2 or also designing different functional structures depending on the collected information);

2. Section 7.2, suggesting a numerical algorithm for discriminating between different competing structures for H starting from data collected in a controlled environment.

7.1 Designing $H(\cdot)$

The proposed EM algorithms have the numerically-favorable property of having both the E and the M steps solvable in closed form. It is important to notice that this is induced by the fact that model Equation (8) is linear in $\boldsymbol{\theta}$, *i.e.*,

$$H\left(t_k^j\right)\boldsymbol{\theta} = \left[H_1\left(t_k^j\right), \ldots, H_N\left(t_k^j\right)\right] \begin{bmatrix} \theta_1 \\ \vdots \\ \theta_N \end{bmatrix} = \sum_{n=1}^{N} H_n\left(t_k^j\right)\theta_n \tag{24}$$

Thus, with this structure, the designer can model the effect of the temperature t_k^j on the measurement y_k as the sum of N independent effects, each one represented as an opportune generic function of t_k^j (the weight of which is actually assumed unknown before the training phase).

As shown in Figures 6 and 7, the structures proposed in Examples A.1 and A.2 have quite general generalization capabilities. Nonetheless, the designer can tailor H so that it resembles other structures; our suggestion is to start from raw measured data spanning different temperatures, check visually how the macroscopic temperature trend behaves and then decompose this trend as the sum of different functions that will become the various $H_n(\cdot)$ in model Equation (8).

7.2 Determining the Best $H(\cdot)$ among Different Competing Potential Structures

The process described in Section 7.1 may lead to different competing structures for $H(\cdot)$. In other words, the designer may propose different structures $H^{(1)}$, $H^{(2)}$, *etc.*, and would like to choose the "best" $H^{(i)}$ given a dataset containing $\boldsymbol{y}$, $\boldsymbol{t}^s$ and the true distance d.

We propose to use the classical approach of discriminating the various $H^{(i)}$'s considering their goodness of fit, *i.e.*, to use Generalized Likelihood Ratios (GLRs) [16], for which we first estimate the best estimates $\widehat{\widehat{\boldsymbol{\theta}}}^{(i)}$ and $\widehat{\boldsymbol{\Delta}}^{(i)}$ for each $H^{(i)}$ given the dataset and then select the best hypothesis considering their resulting log-likelihoods. More formally, the suggested procedure is as in Algorithm 2.

Algorithm 2 Selection of the best $H^{(i)}$.

1: **for** $i = 1, 2, \ldots$ **do**

2: Compute $\widehat{\widehat{\boldsymbol{\theta}}}^{(i)}$ and $\widehat{\boldsymbol{\Delta}}^{(i)}$ as in Section 5;

3: Compute

$$\begin{aligned}\ell^{(i)} := \quad & \log(\widehat{\sigma}_1^2)\mathbb{1}^T\Sigma_1\mathbb{1} + \log(\widehat{\sigma}_2^2)\mathbb{1}^T\Sigma_2\mathbb{1} \\ & + \frac{1}{2\widehat{\sigma}_1^2}\left(\boldsymbol{y} - d\mathbb{1} - H^{(i)}\widehat{\boldsymbol{\theta}}^{(i)} - \widehat{\mu}_1^{(i)}\mathbb{1}\right)^T\Sigma_1^{(i)}\left(\boldsymbol{y} - d\mathbb{1} - H^{(i)}\widehat{\boldsymbol{\theta}}^{(i)} - \widehat{\mu}_1^{(i)}\mathbb{1}\right) \\ & + \frac{1}{2\widehat{\sigma}_2^2}\left(\boldsymbol{y} - d\mathbb{1} - H^{(i)}\widehat{\boldsymbol{\theta}}^{(i)} - \widehat{\mu}_2^{(i)}\mathbb{1}\right)^T\Sigma_2^{(i)}\left(\boldsymbol{y} - d\mathbb{1} - H^{(i)}\widehat{\boldsymbol{\theta}}^{(i)} - \widehat{\mu}_2^{(i)}\mathbb{1}\right)\end{aligned} \tag{25}$$

where $\Sigma_1^{(i)} := \operatorname{diag}\left(1 - \widehat{\Delta}_k^{(i)}\right)$ and $\Sigma_2^{(i)} := \operatorname{diag}\left(\widehat{\Delta}_k^{(i)}\right)$;

4: **end for**

5: Select that $H^{(i)}$ that corresponds to the maximal $\ell^{(i)}$.

8 Experiments

We now validate the proposed thermal model and estimation strategy on real data, aiming to show their effectiveness. We thus consider the simple scenario where a target is fixed in front of a sensor, under constant light and electrical conditions, so that the actual distance between the sensor and the target d is fixed. We consider a SICK LMS 200 Lidar, one of the most widely-used Lidars in industry and robotics applications.

8.1 Training and Validation of the Thermal Model Equation (5)

To train and validate the thermal model Equation (5), we conducted the experiment summarized in Figure 8: in a thermally-controlled room at $22°$, we performed several on-off cycles

of the device and measured the corresponding case temperature t_k^s. We then used the data represented as "training data" in the figure, the data-sheet of the SICK LMS 200 LiDAR and Algorithm 1 to train model Equation (5). After that, we drove the trained model with the $\overline{u}_k$ in the "test data" as inputs and obtained a predicted temperature $\widehat{y}_k^s$. The goodness of fit of the predicted temperatures, computed as:

$$100\left(1-\frac{\sum_k\left(\widehat{y}_k^s-y_k^s\right)^2}{\sum_k\left(y_k^s\right)^2}\right) \tag{26}$$

is then 92.79%. This indicates a very good fit, *i.e.*, a good approximation capability of our proposed thermal model (and associated learning algorithm).

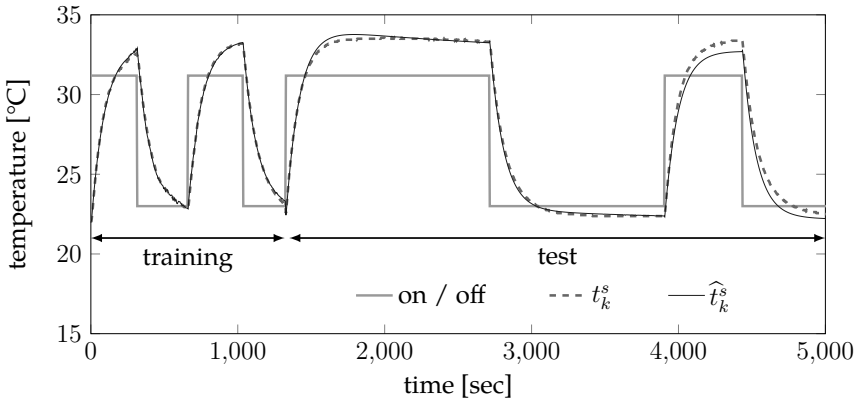

Figure 8: Validation of the thermal model Equation (5) on a SICK 200 Lidar.

8.2 Selection of the Optimal $H(\cdot)$ for the SICK 200 Lidar

We used Algorithm 2 on real data from a SICK LMS 200 to discriminate between different $H^{(i)}$'s in Examples A.1 and A.2, *i.e.*, the hypotheses:

$$\mathbb{H}_i : \boldsymbol{y} \sim (1-\Delta)\mathcal{N}\left(d+H^{(i)}\boldsymbol{\theta}+\mu_1,\sigma_1^2\right)+\Delta\mathcal{N}\left(d+H^{(i)}\boldsymbol{\theta}+\mu_2,\sigma_2^2\right) \tag{27}$$

against the null hypothesis:

$$\mathbb{H}_0 : \mathbf{y} \sim \mathcal{N}\left(d,\sigma^2\right) \tag{28}$$

so that the log likelihood ratio test between two hypotheses can be defined as:

$$\Lambda_i(\boldsymbol{y}) = \frac{\ell\left(\widehat{d},\widehat{\sigma}^2|\boldsymbol{y}\right)}{\ell\left(\widehat{d},\widehat{\sigma}_1^2,\widehat{\sigma}_2^2,\widehat{\mu}_1,\widehat{\mu}_2,\widehat{\boldsymbol{\theta}},\widehat{\Delta}|\boldsymbol{y},H^{(i)}\right)} \tag{29}$$

where we explicitly mention the dependence of the log likelihood ℓ from the various parameters of the considered model.

Figures 9 and 10 show the likelihood ratios obtained for different candidates for polynomial and Fourier expansions, respectively. For the polynomial case, we obtained the highest

likelihood for the polynomial order $N = 16$, while for the Fourier case, we obtained the optimal value for $N = 180$. We motivate this latter order, much higher than that of the polynomial case, to be due to the periodic nature of the Fourier model.

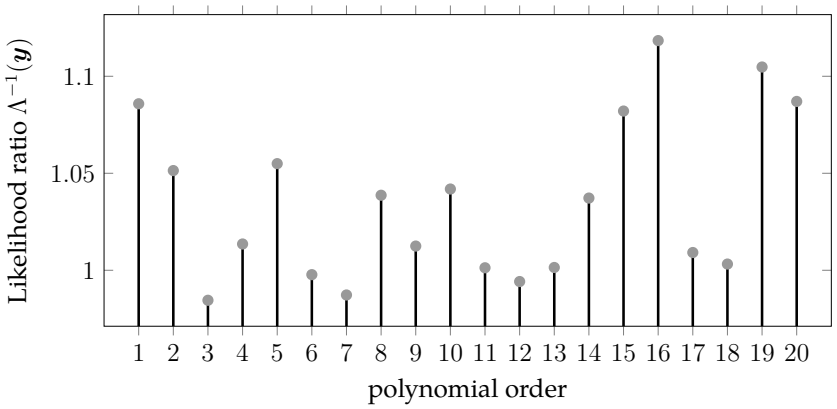

Figure 9: Generalized likelihood ratio (GLR) for Example 10 (polynomial model). The vertical axis values represent the likelihood ratio, and the horizontal axis represents the polynomial order used for generating the $H^{(i)}$ matrix.

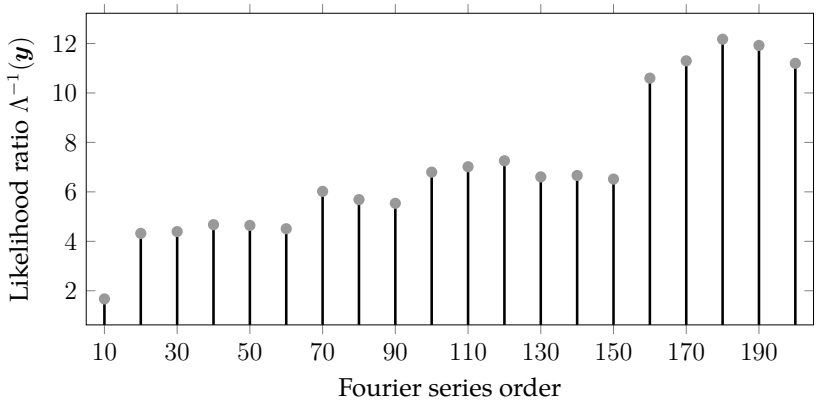

Figure 10: GLR for Example 12 (Fourier model) with different orders. The vertical axis values represent the likelihood ratio and the horizontal axis represents the Fourier series order used for generating the $H^{(i)}$ matrix.

8.3 Assessment of the Performance Improvement for the SICK 200 Lidar

Assume considering the best model order as in Section 8.2 and applying the main EM estimation algorithm for testing purposes. Figure 11 then shows an example of the outcome of this test on real data: first, the figure plots for each raw measurement the associated lasing

modes detected by the EM testing procedure. The same plot shows also the bias induced by the temperature, *i.e.*, $H\widehat{\boldsymbol{\theta}}$.

Once the raw measurements have been associated with the corresponding lasing modes, it is then possible to subtract from them the corresponding noise bias $\widehat{\mu}_1$ or $\widehat{\mu}_2$; in other words, it is possible to remove a certain lasing mode-dependent bias from each of the various measurements. This leads to a new distribution of the measurements, as shown in Figure 12. This figure shows the cumulative distribution of the measurements that we plotted in Figure 11 before and after subtracting the biases induced by the lasing modes. It is clearly visible that after this removal, the cumulative distribution becomes sharper, indicating that the novel dataset has a smaller variance.

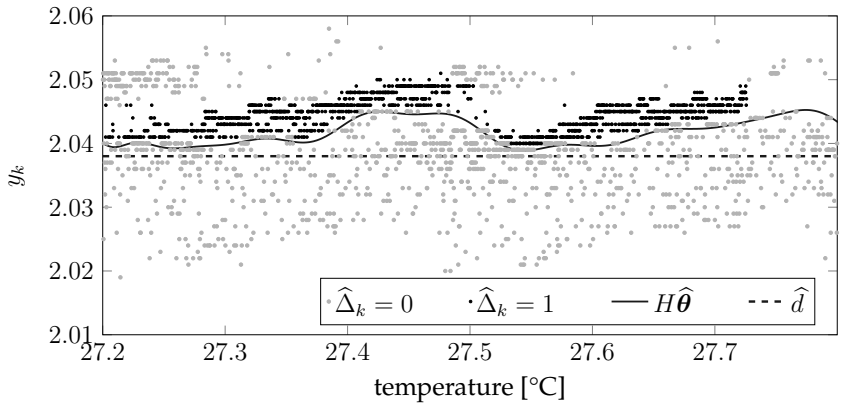

Figure 11: Application of the EM testing algorithm on real data, where the raw measurements are plotted *versus* the temperature of the device. The black dots are the raw measurements that have been associated with lasing Mode 1, while the gray dots are the measurements associated with lasing Mode 2. The solid line denotes the temperature-induced bias on the measured distance.

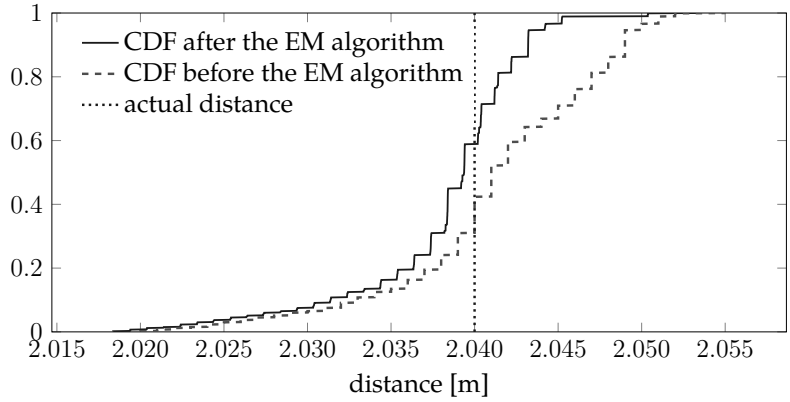

Figure 12: Effects of compensating some raw data with the biases corresponding to the lasing mode of each sample.

8.4 Convergence Properties for the EM Algorithms

We now report some numerical results for the convergence properties of the EM training and test algorithms. More precisely, Figure 13 shows the evolution of the estimates during the training phase, while Figure 14 shows the same evolution for the testing phase. We also plot in Figure 15 the computational burden of performing a fixed number of EM test steps for different measurement vector lengths and show empirically how the computational efforts for testing some points are quadratic with the number of samples. Importantly, this computational effort does not depend heavily on the order of the model.

We show in Figure 16 how the precision and accuracy of the estimate $\widehat{d}$ changes with the number of samples in the test set. More precisely, we show the following cumulative distribution: given the set of 20,000 raw measurements, extract every subset of 200, 400 or 800 consecutive measurements and, for each of these subsets, compute an estimate $\widehat{d}$. The result is intuitive: estimating from more measurements leads to a better estimator (*i.e.*, a cumulative distribution that steepens in correspondence of the true distance).

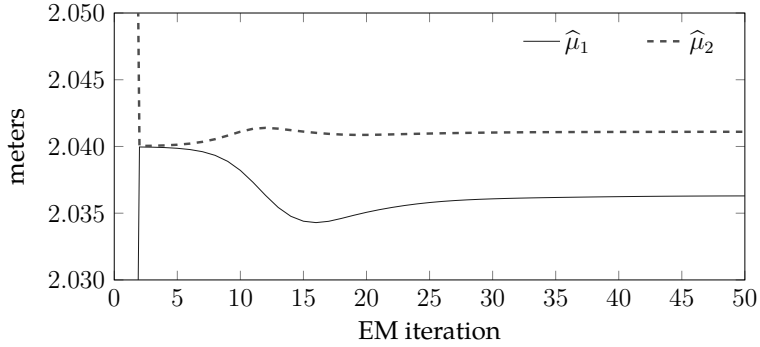

Figure 13: Convergence of the estimated means to their final estimates during the training phase for a training set containing 4000 raw measurements.

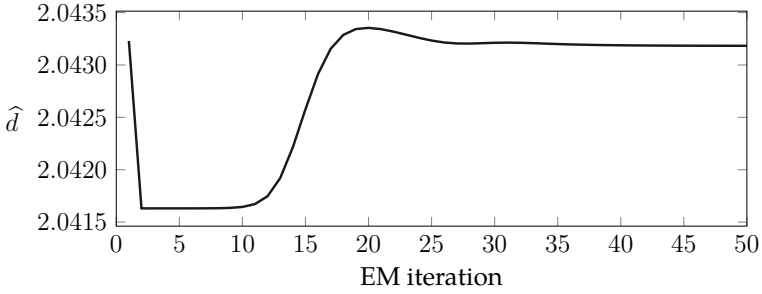

Figure 14: Convergence of the estimated distance to its final estimate during the test phase for a test set containing 4000 raw measurements.

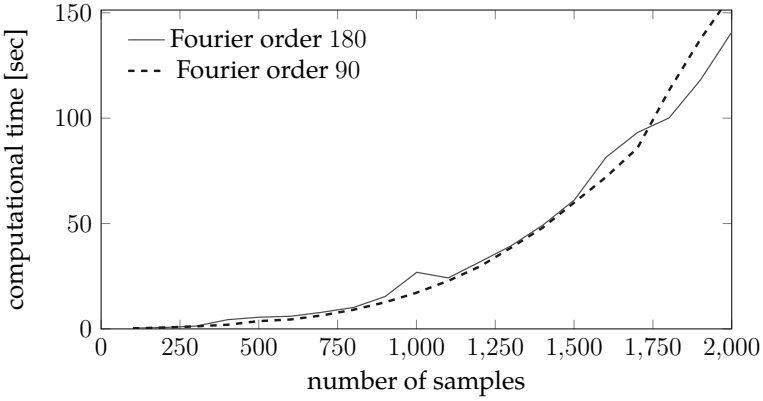

Figure 15: Dependence of the computational complexity for the EM testing phase for two different Fourier order models as a function of the number of samples in the test set.

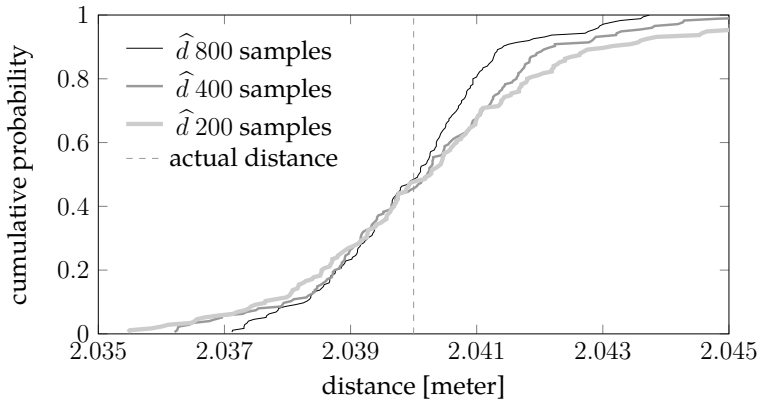

Figure 16: Cumulative distributions of the estimate $\widehat{d}$ for different testing sample sizes. The device temperature ranged in these experiments between 24.8 °C and 28.8 °C.

We show in Figure 17 the realizations of the errors committed by three different estimators: $\widehat{d}$ (our estimator), $\overline{\boldsymbol{y}}$ (the sample average of a window of measurements) and $\overline{\boldsymbol{y} - H\widehat{\boldsymbol{\theta}}}$ (the sample average of a window of measurements corrected by the temperature compensation term $H\widehat{\boldsymbol{\theta}}$). We notice that $\widehat{d}$ commits the smallest errors almost everywhere. To integrate the information, we also plot the temperature of the device in the lower plot. This helps with recognizing that $\widehat{d}$ has better performance, especially where the effect of the temperature is higher.

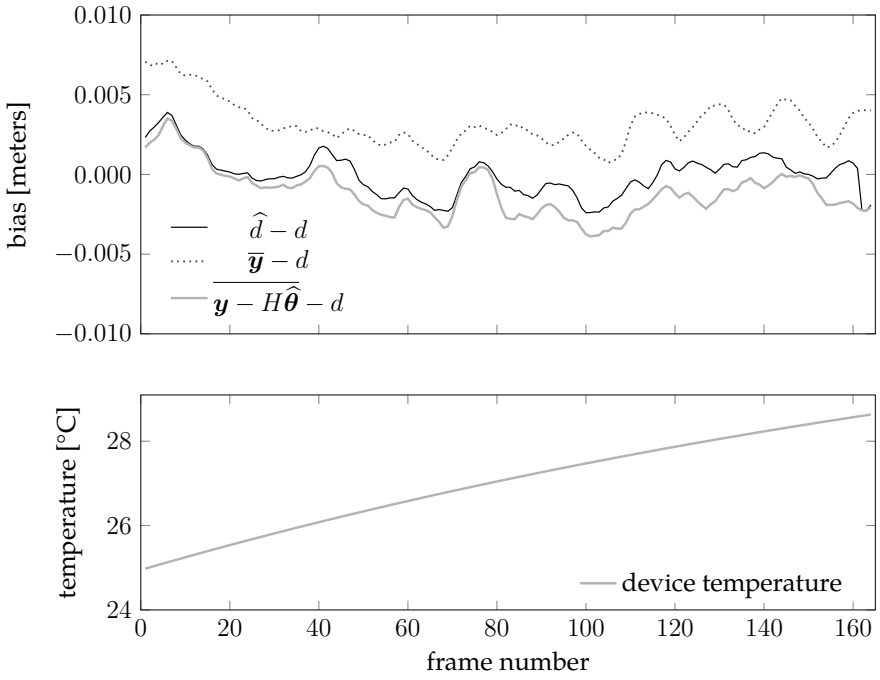

Figure 17: Realizations of the errors committed by the three estimators $\widehat{d}$, $\overline{\boldsymbol{y}}$ and $\overline{\boldsymbol{y} - H\theta}$. In this experiment, the temperature of the device ranged between 24.8 °C and 28.8 °C; the sample size is 1000 points.

We also plot in Figures 18 and 19 how the statistical moments of the empirical error and of the empirical absolute error of these estimators behave with the test sample size. Each point in the plot represents the mean or the variance of an error (or absolute error) sequence similar to those shown in Figure 17. We see that the performance of $\widehat{d}$ improves monotonically, while for the other estimators, this does not happen. Similar results happen also in the plots for the variances, where the proposed estimator outperforms the other two.

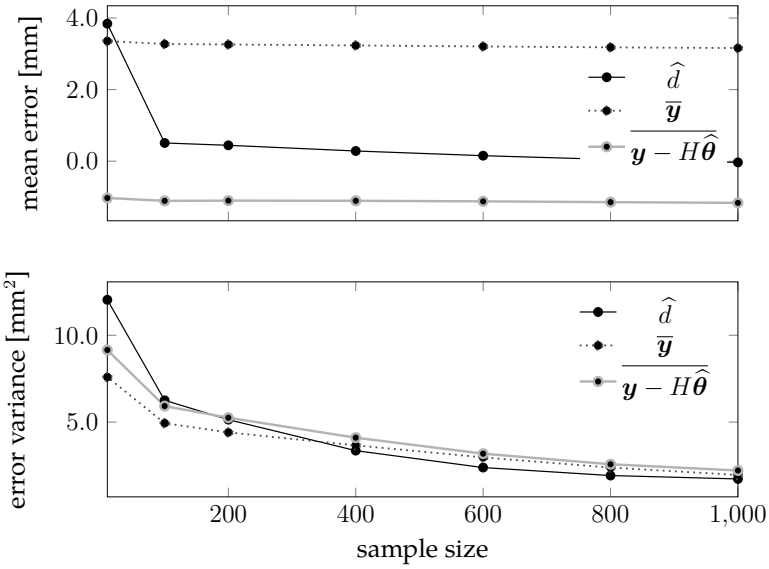

Figure 18: Dependency of the statistical moments of the various estimators on the test sample size. The upper plot shows the mean error, while the lower plot shows the variance of the error. In these experiments, the temperature of the device ranged between 24.8 °C and 28.8 °C.

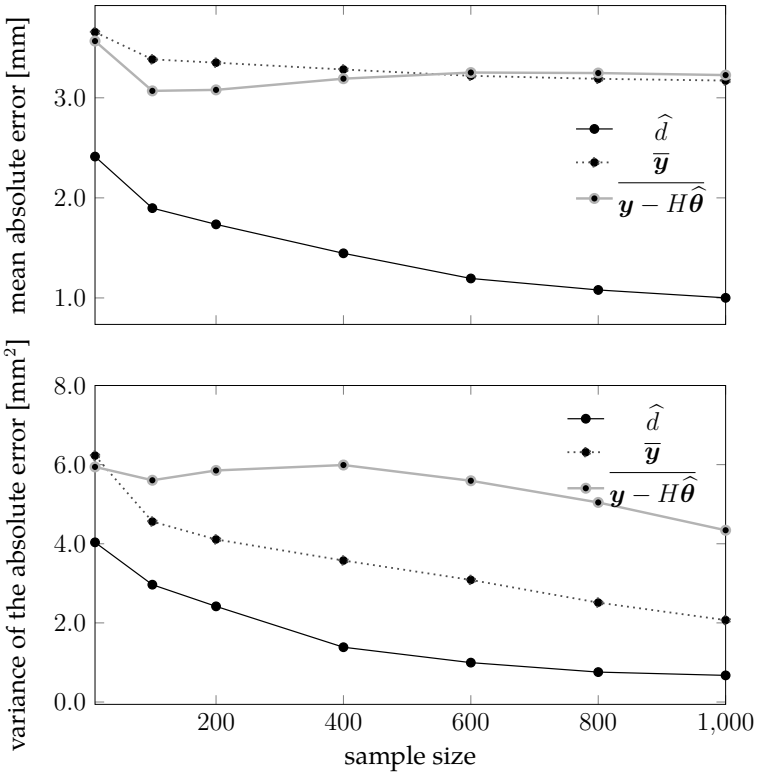

Figure 19: Dependency of the statistical moments of the absolute error of the various estimators on the test sample size. The upper plot shows the mean absolute error, while the lower plot shows the variance of the absolute error. In these experiments, the temperature of the device ranged between 24.8 °C and 28.8 °C.

9 Conclusions

Physical considerations on the mode-hopping effect lead to the consideration that the measurement noise of Time of Flight (ToF) laser scanners is intrinsically multi-modal. In its turn, this implies that estimating the actual distance between scanners and the surrounding objects should be performed using latent variable-based statistical models, where the latent variables correspond to the lasing modes of the laser. Since no literature seems to account for this multi-modality, we aimed at closing this gap.

We thus proposed an Expectation Maximization (EM) algorithm on top of a model that captures biases on the measured distance induced by temperature changes, plus mode-hopping effects through an opportune Gaussian mixture on the measurement noise. Importantly, thanks to a separable model, the EM iterations can be performed analytically. The computational advantages are clear: non-separable models may indeed need to perform the EM iterations numerically, and this would lead to a computational burden hindering the usability

of mode-hopping correction procedures in on-line settings.

The proposed strategy incorporates an accurate model of the temperature dynamics of the laser diode. Moreover, to account for the fact that it may be difficult to collect temperature data on the laser, we proposed a strategy for the identification of the parameters of this model that exploit the datasheet of the laser device and some very simple experiments.

Overall, the proposed temperature compensation strategy led to diminishing the spread of the distribution of real measurements from a SICK LMS 200 around the true value d, as shown in Figure 12, with corresponding decays of the variance of the absolute error from 2.0 mm^2 to 0.68 mm^2 and shift of the expected absolute error from 3 mm to 1 mm, as shown in Figure 19.

We eventually notice that the proposed strategy is still in its infancy: indeed, we considered a frequentist case for which the actual distance d is a deterministic and fixed quantity, aiming at showing that it is possible to improve the overall precision of a laser scanner through accounting for mode-hopping effects. Nonetheless, in real scenarios, d will vary; we thus devise future efforts focusing on strategies for which d is a stochastic process that varies according to some given *a priori* distribution.

Acknowledgments

Acknowledgments: This work is supported by the Framework Programme for Research and Innovation Horizon 2020 under Grant Agreement No. 636834 (DISIRE) and the Swedish research council Norrbottens Forskningsråd.

References

[1] photonics.com, "One photon per pixel produces 3-d lidar image," 2013. [Online]. Available: http://www.photonics.com/Article.aspx?AID=55422

[2] P. Fuchs, "Pulse ranging technology (prt) - highly accurate positioning over large distances," 2015. [Online]. Available: http://www.pepperl-fuchs.com/global/en/23466.htm

[3] M. Hebert and E. Krotkov, "3-d measurements from imaging laser radars: How good are they?" in *Intelligent Robots and Systems' 91.'Intelligence for Mechanical Systems, Proceedings IROS'91. IEEE/RSJ International Workshop on*. IEEE, 1991, pp. 359–364.

[4] A. Reina and J. Gonzales, "Characterization of a radial laser scanner for mobile robot navigation," in *Intelligent Robots and Systems, 1997. IROS'97., Proceedings of the 1997 IEEE/RSJ International Conference on*, vol. 2. IEEE, 1997, pp. 579–585.

[5] V. Matko, "Next generation at-cut quartz crystal sensing devices," *Sensors*, vol. 11, no. 5, pp. 4474–4482, 2011.

[6] O. O. Semiconductor, "Pulsed laser diode in plastic package 25 w peak power spl pl90," OSRAM Opto Semiconductor, Data sheet, 2014. [Online]. Available: http://www.osram-os.com/Graphics/XPic8/00149644_0.pdf/SPL%20PL90.pdf

[7] J. Hawkes and I. Latimer, *Lasers: theory and practice*. Prentice Hall, 1995.

[8] R. Paschotta, "article on 'mode hopping' in the encyclopedia of laser physics and technology," 2008. [Online]. Available: http://www.rp-photonics.com/encyclopedia_cite.html?article=modehopping

[9] B. Tell, K. Brown-Goebeler, R. Leibenguth, F. Baez, and Y. Lee, "Temperature dependence of gaas-algaas vertical cavity surface emitting lasers," *Applied physics letters*, vol. 60, no. 6, pp. 683–685, 1992.

[10] L. Ljung, *System Identification: Theory for the User*, ser. Prentice-Hall information and system sciences series. Prentice Hall PTR, 1999. [Online]. Available: https://books.google.se/books?id=nHFoQgAACAAJ

[11] R. Paschotta, "article on 'laser diodes' in the encyclopedia of laser physics and technology," 2008. [Online]. Available: http://www.rp-photonics.com/laser_diodes.html

[12] B. D. Anderson and J. B. Moore, *Optimal filtering*. Courier Corporation, 2012.

[13] A. P. Dempster, N. M. Laird, and D. B. Rubin, "Maximum likelihood from incomplete data via the em algorithm," *Journal of the royal statistical society. Series B (methodological)*, pp. 1–38, 1977.

[14] G. McLachlan and D. Peel, *Finite mixture models*. John Wiley & Sons, 2004.

[15] F. Vaida, "Parameter convergence for em and mm algorithms," *Statistica Sinica*, vol. 15, no. 3, p. 831, 2005.

[16] M. Basseville, I. V. Nikiforov *et al.*, *Detection of abrupt changes: theory and application*. Prentice Hall Englewood Cliffs, 1993, vol. 104.

Paper B

Statistical modeling and calibration of triangulation Lidars

Authors:
Anas Alhashimi, Damiano Varagnolo and Thomas Gustafsson

Reformatted version of paper originally published in:
Proceedings of the 13th International Conference on Informatics in Control, Automation and Robotics (ICINCO 2016) - Volume 1, pages 308-317

Digital Object Identifier:

Statistical modeling and calibration of triangulation Lidars

Anas Alhashimi, Damiano Varagnolo and Thomas Gustafsson

Abstract: We aim at developing statistical tools that improve the accuracy and precision of the measurements returned by triangulation Light Detection and Rangings (Lidars). To this aim we: *i)* propose and validate a novel model that describes the statistics of the measurements of these Lidars, and that is built starting from mechanical considerations on the geometry and properties of their pinhole lens - CCD camera systems; *ii)* build, starting from this novel statistical model, a Maximum Likelihood (ML) / Akaike Information Criterion (AIC) - based sensor calibration algorithm that exploits training information collected in a controlled environment; *iii)* develop ML and Least Squares (LS) strategies that use the calibration results to statistically process the raw sensor measurements in non controlled environments. The overall technique allowed us to obtain empirical improvements of the normalized Mean Squared Error (MSE) from 0.0789 to 0.0046.

1 Introduction

Lidars are ubiquitously used for mapping purposes. Different types of Lidar technologies, such as ToF and triangulation, have different statistical performance. For example, ToF Lidars have generically lower bias and measurement noise variances than triangulation ones. At the same time, triangulation Lidars are generally cheaper than ToF ones. The market pull is then to increase the performance of cheaper Lidars in a cost-effective way.

Improving the accuracy and precision of sensors can then be done in different ways, e.g., by improving their mechanical properties. *In this paper we have a precise target: improve the performance indexes of triangulation Lidars by removing their biases and artifacts through opportune statistical manipulations of the raw information coming from the sensor.*

The following literature review analyzes a set of algorithms that are related to our aim.

Literature review It is convenient to categorize the algorithms in the existing and relevant literature as:

- procedures for the characterization or calibration of the devices. Here characterization means a thorough quantification of the measurement noisiness of the device, while calibration means an algorithm that aims at diminishing this noisiness level;
- when dealing with calibration issues, procedures for the intrinsic or extrinsic calibration. Here intrinsic means that the focus is on estimating the parameters of the Lidar itself, while extrinsic means that the focus is on estimating the parameters resulted from sensor positioning and installation.

Characterization issues: several papers discuss Lidar characterization issues for both ToF [1, 2, 3, 4, 5, 6, 7, 8, 9] and triangulation Lidars [10, 11]. Notice that, at the best of our knowledge, for triangulation Lidars there exist only two manuscripts: [10], that discusses the nonlinearity of Neato Lidars, and [11], that analyzes the effect of the color of the target on the measured distance. Importantly, [10] models nonlinear effects on the measurements and the variance of additive measurement noises as two independent effects that can be modeled with a second order polynomials on the actual distance. From a statistical perspectives the authors, therefore, decouple the learning process into two separate parts.

Calibration issues: as for the calibration issues there is a relatively large number of papers describing how to calibrate extrinsic parameters either using additional sensors (such as cameras) [12, 13, 14, 15], or just requiring knowledge on the motion of the Lidar itself [16, 17, 18, 19].

Still considering calibration issues, there has been also a big effort on how to perform intrinsic calibration for multi-beam Lidar systems, where the results from one beam is used to calibrate the intrinsic parameters of other beams [20, 21, 22, 23, 24, 25, 26, 27, 28, 29]. As for single-beam Lidar systems, instead, [27] proposes a method for the intrinsic calibration of a revolving-head 3D Lidar and the extrinsic calibration of the parameters with respect to a camera. The technique involves an analytical method for computing an initial estimate for both the Lidar's intrinsic parameters and the Lidar-camera transformation, that is then used to initialize an iterative nonlinear least-squares refinement of all of the calibration parameters.

We also mention the topic of on-line calibration of sensor parameters for mobile robots when doing Simultaneous localization and mapping (SLAM), very useful in navigation tasks. In this category, [30] proposes an approach to simultaneously estimate a map of the environment, the position of the on-board sensors of the robot, and its kinematic parameters. These parameters are subject to variations due to wear of the devices or mechanical effects like loading. An other similar methodology for the intrinsic calibration of depth sensor during SLAM is presented in [31].

Statement of Contributions We focus specifically on triangulation Lidars for robotic applications, and aim to increase their performance in a cost-effective way through statistical processing techniques. Our long term vision is to arrive at a on-line automatic calibration procedure for triangulation Lidars like in [30, 31]; before reaching this above long-term goal, we must nonetheless solve satisfactorily the problem of calibrating triangulation Lidars off-line.

In this paper we thus:

- propose and assess a model for the measurement process of triangulation Lidars (see Section 3 and model (1)). Our model not only generalizes the model proposed in [10, 11], but also motivates it starting from mechanical and physical interpretations;
- on top of this model, propose and assess a ML calibration procedure that uses data from a Motion Capture (MoCap) system. Importantly, our calibration procedure extends the one proposed in [10]: there authors decoupled the learning process into two separate stages (corresponding to estimate two different sets of parameters), while here the calibration is performed simultaneously on both sets of parameters;
- propose and assess novel ML and LS strategies for correcting the measurements from the sensor with the model inferred during the calibration stage.

As reported in (31) and (32), the overall strategy is then shown to be capable to improve the normalized MSE of the raw information from the sensor from 0.0789 to 0.0046.

1.1 Organization of the Manuscript

Section 2 describes the working principles of triangulation Lidars. Based on these working principles, Section 3 proposes a statistical model of the measurement process of the device. Section 4 then validates this statistical model using data acquired through a MoCap system. Section 5 then presents a calibration algorithm for sensors deployed in a test environment. Section 7 eventually concludes the paper with the description of future research issues.

2 The Triangulation Lidar Range Sensor

We now describe the functioning principle of the triangulation scanners; this discussion will be useful for explaining why the moments of the measurement noise depend on the actual measured distance. More details about the constructive details of triangulation Lidars can be found in [32, 33].

A prototypical triangulation Lidar is the one in Figure 1. Its working principles are then explained with the diagram in Figure 2 and its caption.

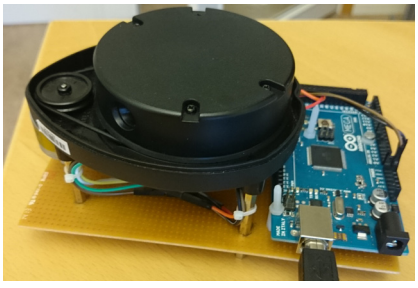

Figure 1: Photo of a triangulation Lidar.

This simple working principle helps keeping the cost of the sensor low[1], and making it commercially usable in low-cost devices like robotic vacuum cleaners. The low cost of the sensor comes nonetheless with some well-defined mechanical problems [33]:

- low-cost lens, that generate nonlinear distortion effects;
- imprecise pointing accuracy, that is known of at best 6 degrees;
- not rigid physical linkages among lens elements, camera, laser, and laser optics, that may suffer from distortion effects during the life of the device.

[1]Incidentally, the sensor was costing $\$135.00$ as of February 2016 in Ebay. Nonetheless, the original industrial goal was to reach an end user price of $\$30.00$.

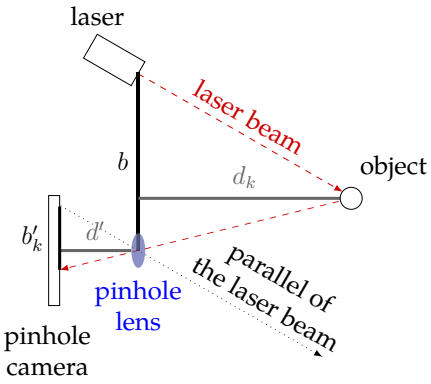

Figure 2: Diagram exemplifying the working principle of a triangulation Lidar . The laser emits an infra-red laser signal that is then reflected by the object to be detected. The beam passes through a pinhole lens and hits a CCD camera sensor. By construction, thus, the triangles defined by (b, d_k) and by (b'_k, d') are similar: this means that the distance to the object is nonlinearly proportional to the angle of the reflected light, and as soon as the camera measures the distance b'_k one can estimate the actual distance d_k using triangles similarities concepts.

As it can be seen in Figure 3, all these problems induce measurement errors; more precisely, triangulation Lidars suffer from strong nonlinearities in both the bias and the standard deviation of the measurement noise. This pushes towards finding some signal processing tools that can alleviate these problems, and keep the sensor cheap while improving its performance.

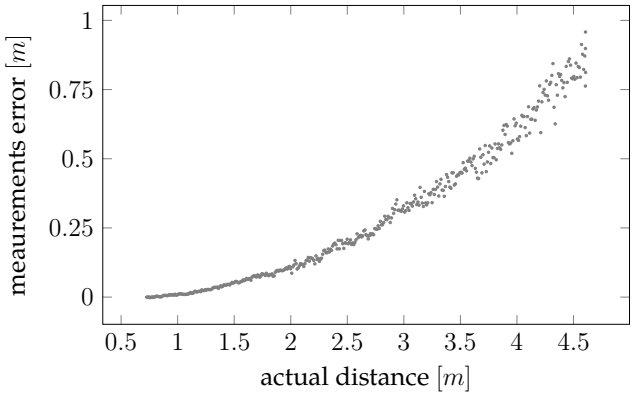

Figure 3: Dataset

3 A novel statistical model for the Lidar measurements

Let y_k be the k-th measurement returned by the Lidar when the true distance is d_k. Physically, y_k is computed by the logic of the sensor through a static transformation of b'_k in Figure 2; we assume here that this static transformation is unknown, that b'_k is not available, and that we want to improve the estimation for d_k from just y_k.

Our ansatz for the whole transformation from d_k to y_k is then

$$y_k = f(d_k) + f(d_k)^2 e_k \tag{1}$$

where

- $f(\cdot)$ is an unknown non-linear function;
- $e_k \sim \mathcal{N}(0, \sigma_e^2)$ is a Gaussian and white additive measurement noise.

In the following Section 3.1 we motivate the presence of $f(\cdot)$ from mechanical considerations, while in the following Section 3.2 we motivate the presence of the $f(\cdot)^2$ multiplying the noise e_k starting from physical considerations.

3.1 Explaining the presence of the nonlinear term $f(\cdot)$ in model (1)

The nonlinear term $f(\cdot)$ in (1) is related to what is called the *radial distortion* in camera calibration literature [34, 35, 36, 37]. Indeed camera lenses are notoriously nonlinear at their borders, with this nonlinearity increasing as the light beam passes closer to the lens edges. In our settings this thus happens when targets are very close or very far.

Radial distortions are usually modeled in the camera calibration literature as a series of odd powers, i.e., as

$$f(d_k) = \sum_{i=0}^{n} \alpha_i d_k^{2i+1} \tag{2}$$

where the α_i's are the model parameters.

As numerically shown during the validation of (1) in Section 4, model (2) does not describe well the evidence collected in our experiments. Indeed the specific case of triangulation Lidars lacks of the symmetries encountered in computer vision settings (see (4) and the discussion on that identity), and thus in our settings there is no need for odd symmetries in the model (in other words, doubling d does not lead to doubling b'). We thus propose to remove this constraint and use a potentially non-symmetric polynomial, i.e.,

$$f(d_k) = \sum_{i=0}^{n} \alpha_i d_k^{i}. \tag{3}$$

The numerical validations of model (3) shown in Section 4 confirm then our physical intuition.

3.2 Explaining the presence of the multiplicative term $f(d_k)^2$ in model (1)

Assume for now that there are no lens-distortion effects. The similarity between the triangles in Figure 2 then implies

$$\frac{d_k}{b} = \frac{d'}{b'_k}. \tag{4}$$

In (4) d_k and b'_k are generally time-varying quantities, while b and d' are constants from the geometry of the Lidar. Assume now that the quantity measured by the CCD at time k is corrupted by a Gaussian noise, so that $z_k = b'_k + w_k$ with $w_k \sim \mathcal{N}(0, \sigma^2_{\text{CCD}})$ and σ^2_{CCD} constant and independent of d_k. Thus $z_k \sim \mathcal{N}(b'_k, \sigma^2_{\text{CCD}})$; since

$$y_k = \frac{bd'}{z_k}, \tag{5}$$

assuming a Gaussian measurement noise on the CCD implies that y_k is a reciprocal Gaussian r.v. This kind of variable is notoriously difficult to treat (e.g., their statistical moments cannot be derived from closed form expressions starting from the original Gaussian variables). For this reason we perform a first order Taylor approximation of the nonlinear map (5) above. In general, if

$$\begin{cases} z_k \sim \mathcal{N}(b, \sigma^2) \\ y_k = \phi(z_k) \end{cases} \tag{6}$$

then the first order Taylor approximation of the distribution of y_k is [38, (A.16)]

$$y_k \sim \mathcal{N}\left(\phi(b), \phi'(b)^2\sigma^2\right) \tag{7}$$

where $\phi'(\cdot)$ is the first derivative of $\phi(\cdot)$ w.r.t. z_k. Substituting the values of our specific problem into formula (7) leads then to the novel approximated model

$$y_k \sim \mathcal{N}\left(\frac{bd'}{b'_k}, \left(\frac{-bd'}{b'^2_k}\right)^2 \sigma^2_{\text{CCD}}\right), \tag{8}$$

or, equivalently,

$$y_k = d_k + d_k^2 e_k \qquad e_k \sim \mathcal{N}\left(0, \sigma_e^2\right) \tag{9}$$

where $\sigma_e^2 = \dfrac{\sigma^2_{\text{CCD}}}{b^2 d'^2}$ is a scaled version of σ^2_{CCD} independent of d_k and to be estimated from the data.

Consider now that actually there are some lens distortion effects that imply the presence of the nonlinear term $f(d_k)$. We can then repeat the very same discussion above, and obtain model (1) by substituting d_k with $f(d_k)$ in (9).

4 Validation of the approximation (8)

The approximation introduced by the first order Taylor expansion in (8) can be seen as arbitrary. Nonetheless we show in this section that on the collected datasets it actually corresponds to the most powerful approximation in a statistical sense.

To this aim we perform this two-step validation:

1. *(check if the noises are independent and identically distributed (iid) and normal)* perform a normality test on the y_k's assuming that measurements are collected at a fixed distance (i.e., d_k is constant): indeed e_k is approximately Gaussian as much as y_k is;

2. *(check the order of the term multiplying e_k)* compare the following alternative statistical models for the measurements y_k:

$$\begin{aligned} H^0: &\quad y_k = f(d_k) + e_k \\ H^1: &\quad y_k = f(d_k) + f(d_k)e_k \\ H^2: &\quad y_k = f(d_k) + f(d_k)^2 e_k \\ H^3: &\quad y_k = f(d_k) + f(d_k)^3 e_k \end{aligned} \tag{10}$$

   and check which one describes better the collected information.

As for point 1 we can use standard iid tests (like the Wald-Wolfowitz runs [39]) and standard normality tests (like the Shapiro-Wilk normality test). These tests performed on our registered data showed p-values of 0.56 and 0.42, so we can safely consider the measurement noises to be iid and Gaussian.

As for point 2, we instead consider the following strategy: for every model above, assuming that measurements are collected at a fixed distance (i.e., d_k is constant), we can perform a simple algebraic manipulation of (1) to obtain

$$\frac{y_k - y_{k-1}}{f(d_k)^\star} = e_k - e_{k-1} \tag{11}$$

where $\star$ indicates the order of the model (that means $\star \in \{0, \dots, 3\}$). (11) in its turn indicates that, since e_k and e_{k-1} are assumed iid,

$$\frac{y_k - y_{k-1}}{f(d_k)^\star} \sim \mathcal{N}\left(0, 2\sigma_e^2\right), \quad \star \in \{0, \dots, 3\}. \tag{12}$$

Assume now that the dataset is composed by different batches each corresponding to d_k's that are constant in the batch, but different among batches. Moreover assume that each batch is sufficiently rich to make it is possible to estimate with good confidence the unknown $f(d_k)$ through the empirical mean of the y_k relative to that batch. By combining the information from different batches it is then possible to check which model $\star$ describes better the measured information.

Indicate then with B the number of batches in the dataset, with $b = 1, \dots, B$ the index of each batch, and with $\mathcal{B}_b$ the set of k's that are relative to that specific batch b. In formulas, we thus:

1. estimate, for each model batch $b = 1, \dots, B$, the distance

$$\widehat{f_b} = \frac{1}{|\mathcal{B}_b|} \sum_{k \in \mathcal{B}_b} y_k; \tag{13}$$

2. estimate, for each model $\star = 0, \dots, 3$, the variance of e_k as

$$\widehat{\sigma_e^2} := \frac{1}{B} \sum_{b=1}^{B} \left(\frac{1}{2|\mathcal{B}_b|} \sum_{k, k-1 \in \mathcal{B}_b} \left(\frac{y_k - y_{k-1}}{\widehat{f_b^\star}} \right)^2 \right). \tag{14}$$

3. compute, for each model $\star = 0, \dots, 3$, the log-likelihood of the data as

$$
\begin{aligned}
&-\log \mathbb{P}\left[\boldsymbol{y}\ ;\ \boldsymbol{d},\ \widehat{\sigma_e^2}\right] = \\
&\sum_{b=1}^{B}\left(|\mathcal{B}_b|\log\left(\widehat{f_b^{2\star}}\widehat{\sigma_e^2}\right) + \sum_{k=1}^{\mathcal{B}_b}\frac{\left(y_k - \widehat{f_b}\right)^2}{\widehat{f_b^{2\star}}\widehat{\sigma_e^2}}\right)
\end{aligned}
\tag{15}
$$

where $\boldsymbol{y} := [y_1, \dots, y_N]^T$ and $\boldsymbol{d} := [d_1, \dots, d_N]^T$.

In Figure 4 we then show the log-likelihoods for the different models. *As it can be seen, hypothesis H^2 is the one that best describes the collected evidence.*

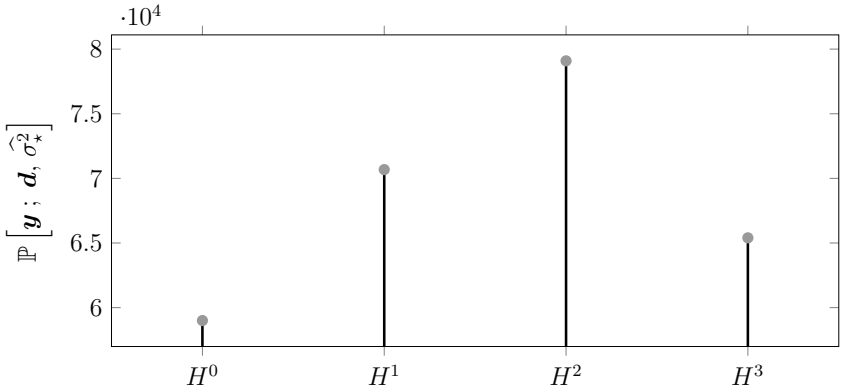

Figure 4: Evaluation of (15) on the collected datasets.

A non rigorous (but graphical and intuitive) argument supporting H^2 as the hypothesis best describing the evidence is then the one offered in Figure 5. The argument goes as follows: for the exact $\star \in \{0, \dots, 3\}$ the quantities

$$
\frac{y_k - y_{k-1}}{f(d_k)^\star} \qquad \star \in \{0, \dots, 3\}\,. \tag{16}
$$

should be iid independently of d_k. This iid-ness is indeed a necessary condition for iid-ness of the measurement noises (one of our assumptions).

Since $f(\cdot)$ is actually unknown, this iid-ness test must be performed by means of some estimate of $f(\cdot)$. In the following we use the estimator defined in Section 5 over an experiment where we manually increase the true distance d_k. As it can be seen, the hypothesis H^2 is the unique one for which the quantities $\dfrac{y_k - y_{k-1}}{\widehat{f}(d_k)^\star}$ are homoscedastic. Thus the normalizing factor $\star = 2$ is the unique one guaranteeing iid-ness for the measurement noises. Notice that this argument is a non rigorous wishful thinking, since we use some estimates as the ground truth; nonetheless the heteroscedasticity of the noises for $\star = 0, 1, 3$ indicates that these hypotheses are non-descriptive.

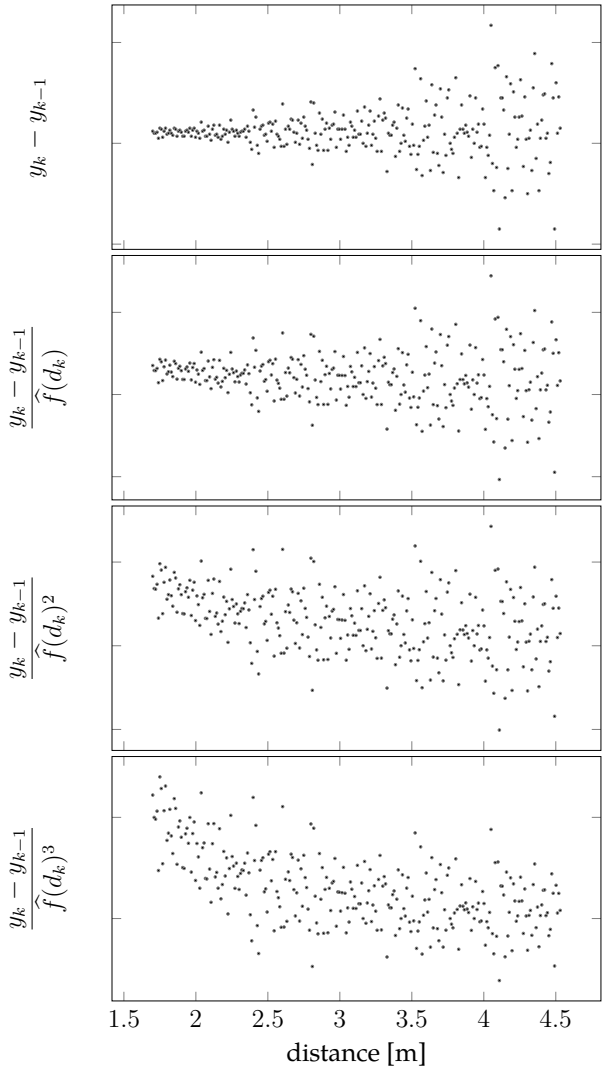

Figure 5: Plots of the quantities $\frac{y_k - y_{k-1}}{\widehat{f}(d_k)^\star}$ for $\star = 0, \ldots, 3$ and for increasing d_k and for $\widehat{f}(\cdot)$ computed as in Section 5. The results graphically suggest that $\widehat{f}(d_k)^2$ is the unique normalizing factor for which we obtain homoscedastic samples.

5 Calibrating the Lidar

Our overall goal is not just to propose the statistical model (1) describing the measurement process of the Lidar but also to find a calibration procedure for estimating the unknowns $f(\cdot)$ and σ_e^2 from some collected information.

Once again the long term goal is to calibrate (1) on-line and continuously using information from other sensors like odometry, ultrasonic sensors, etc. Instrumental to this future direction we now solve the first step, that is to estimate $f(\cdot)$ and σ_e^2 from a dataset $\mathcal{D} = \{y_k, d_k\}$ in which we know d_k (e.g., thanks to a MoCap system).

Given our Fisherian setting, we seek for the ML estimate for both $f(\cdot)$ and σ_e^2, where we recall that (due to the radial distortion hypothesis as the source of $f(\cdot)$, see Section 3.1) $f(\cdot)$ is modeled as a non-symmetric polynomial, i.e., as $f(d_k) = \sum_{i=0}^{n} \alpha_i d_k^i$ as in (3). Since now model (1) implies

$$y_k - f(d_k) \sim \mathcal{N}\left(0, f(d_k)^4 \sigma_e^2\right), \tag{17}$$

it follows immediately that the corresponding negative log-likelihood is proportional to

$$\mathcal{L} := \log\left(\det \Sigma\right) + \big(\boldsymbol{y} - \boldsymbol{f}(\boldsymbol{d})\big)^T \Sigma^{-1} \big(\boldsymbol{y} - \boldsymbol{f}(\boldsymbol{d})\big) \tag{18}$$

where

- $\boldsymbol{y} := [y_1, \ldots, y_N]^T$;
- $\boldsymbol{d} := [d_1, \ldots, d_N]^T$;
- $\boldsymbol{f}(\boldsymbol{d}) := [f(d_1), \ldots, f(d_N)]$;
- $\Sigma := \text{diag}\left(f(d_1)^4 \sigma_e^2, \ldots, f(d_N)^4 \sigma_e^2\right)$.

Finding the ML estimates in our settings thus means:

1. solving

$$\arg\min_{\theta \in \Theta} \mathcal{L}\left(\theta\right) \tag{19}$$

for several different n, with

$$\theta := \left[\alpha_0, \ldots, \alpha_n, \sigma_e^2\right] \tag{20}$$

and Θ the set of $\theta \in \mathbb{R}^{n+1}$ for which $\sigma_e^2 > 0$;

2. deciding which n is the best one using some model order selection criterion, e.g., AIC.

Unfortunately problem (19) is not convex, so it neither admits a closed form solution nor it can be easily computed using numerical procedures. Solving problem (19) is thus numerically difficult. Keeping in mind that our long-term goal is the development of on-line calibration procedures, where numerical problems will be even more complex, we strive for some alternative calibration procedure.

5.1 An approximate calibration procedure

We here propose an alternative estimator that trades off statistical performance for solvability in a closed form. We indeed propose to seek an estimate for θ in (20) by using the alternative model

$$y_k = f(d_k) + d_k^2 e_k, \tag{21}$$

that differs from (1) only for the fact that the noise is multiplied by d_k^2 instead of $f(d_k)^2$. This approximation is intuitively meaningful, since $f(d_k)$ represents a distortion term induced by the pinhole lens: ideally, indeed, $f(d_k)$ should be equal to d_k.

Assuming model (21) it is now possible do derive a ML estimator of θ. Indeed dividing both sides of (21) by d_k^2 we get

$$\frac{y_k}{d_k^2} = g(d_k) + e_k \tag{22}$$

where (cf. (3))

$$g(d_k) = \sum_{i=0}^{n} \alpha_i d_k^{i-2}. \tag{23}$$

This means that the estimation problem can be cast as the problem of estimating the parameters $\boldsymbol{\alpha} := [\alpha_0, \dots, \alpha_n]^T$ and the noise variance σ_e^2 describing the linear system

$$\frac{y_k}{d_k^2} = \begin{bmatrix} d_k^{-2} & \dots & d_k^{n-2} \end{bmatrix} \begin{bmatrix} \alpha_0 \\ \vdots \\ \alpha_n \end{bmatrix} + e_k, \tag{24}$$

for which the ML solution is directly

$$\begin{aligned} \widehat{\boldsymbol{\alpha}} &= \left(H^T H\right)^{-1} H^T \widetilde{\boldsymbol{y}} \\ \widehat{\sigma_e^2} &= \frac{1}{N} \left(\widetilde{\boldsymbol{y}} - H\widehat{\boldsymbol{\alpha}}\right)^T \left(\widetilde{\boldsymbol{y}} - H\widehat{\boldsymbol{\alpha}}\right) \end{aligned} \tag{25}$$

with

$$H := \begin{bmatrix} d_1^{-2} & \cdots & d_1^{n-2} \\ \vdots & & \vdots \\ d_N^{-2} & \cdots & d_N^{n-2} \end{bmatrix} \quad \widetilde{\boldsymbol{y}} := \begin{bmatrix} \frac{y_1}{d_1^2} \\ \vdots \\ \frac{y_N}{d_N^2} \end{bmatrix}. \tag{26}$$

Notice that the procedure above does not determine the model complexity n. For inferring this parameter we then propose to rely on classical model order selection criteria such as AIC.

5.2 Using the calibration results to estimate d_k

Once the sensor has been calibrated, i.e., a $\widehat{\boldsymbol{\alpha}}$ and $\widehat{\sigma_e^2}$ have been computed, it is possible to invert the process and use the learned information for testing purposes. This means that given some measurements y_k collected in an unknown environment we can, through $\widehat{\boldsymbol{\alpha}}$ and $\widehat{\sigma_e^2}$, estimate d_k.

Computing the ML estimate of d_k

Rewriting model (3) as

$$f(d_k) = \boldsymbol{d}_k^T \boldsymbol{\alpha} \qquad \boldsymbol{d}_k := \begin{bmatrix} d_k^0 \\ d_k^1 \\ \vdots \\ d_k^n \end{bmatrix} \tag{27}$$

and equating the score of y_k parametrized by $\boldsymbol{\alpha}$ and σ_e^2 to zero leads to the equation

$$\left(y_k - \boldsymbol{d}_k \boldsymbol{\alpha}\right)\left(y_k - \boldsymbol{d}_k \left(I - K\right) \boldsymbol{\alpha}\right) = \sigma_e^2 d_k^4 \tag{28}$$

with

$$K := \operatorname{diag}\left(0, \frac{1}{2}, \ldots, \frac{n}{2}\right). \tag{29}$$

This means that estimating d_k from y_k, $\widehat{\boldsymbol{\alpha}}$ and $\widehat{\sigma_e^2}$ can be performed by solving (28) in d_k after substituting the real values $\boldsymbol{\alpha}$ and σ_e^2 with their estimates.

Since polynomial (28) is quartic for $n = 0, 1, 2$, and of order at least 6 for any other n, the ML estimate for d_k must then either rely on complex algebraic formulas or numerical roots finding methods.

Computing the LS estimate of d_k

Given our assumption (3) on the structure of $f(\cdot)$, and given an estimate $\widehat{f}$ for f, the problem of estimating d_k from y_k is the one of minimizing the squared loss $\left(y_k - \widehat{f}\left(d_k\right)\right)^2$. Once again, the problem is of finding the roots of a polynomial, since the solutions of the LS problem above are directly

$$\widehat{d}_k \in \left\{ \widetilde{d} \text{ s.t. } y_k - \widehat{f}\left(\widetilde{d}\right) = 0 \right\}. \tag{30}$$

Thus if the Lidar has heavy nonlinear radial distortions (that means that it requires high order polynomials $f\left(\cdot\right)$) then one is again required to compute polynomial roots.

Notice also that some of the roots above may not belong to the measurement range of the sensor (e.g., some roots may be negative); these ones can safely be discarded from the set of plausible solutions. The other ones, instead, are equally plausible.

This raises a question on how to decide which root should be selected among the equally plausible ones. This question is actually non-trivial, and cannot be solved by means of the frequentist approach used in this manuscript. We thus leave this question unanswered for now, and leave it as a future research question. Bayesian formulations will be explored to see if they solve the multiple plausible roots problem.

6 Numerical experiments

Our experiments consist of a robot with the Lidar mounted on top moving with piecewise constant speeds towards a target. We recorded several datasets for training and testing purposes, consisting of the Lidar measurements and a ground truth information collected by a MoCap system (see Figure 6). Training datasets were thus initially used to estimate $\boldsymbol{\alpha}$ and

Figure 6: Experimental setup used for recording the dataset. The Lidar was mounted over a Pioneer 3AT robot facing an obstacle; the photo moreover shows some of the cameras of the MoCap system.

σ_e^2 as described in Equation (25). As for the model order selection, we empirically detected that $n = 2$ was always the best choice when using AIC measures. E.g., for the dataset shown in Figure 7 we obtained the AIC scores reported in Table 1.

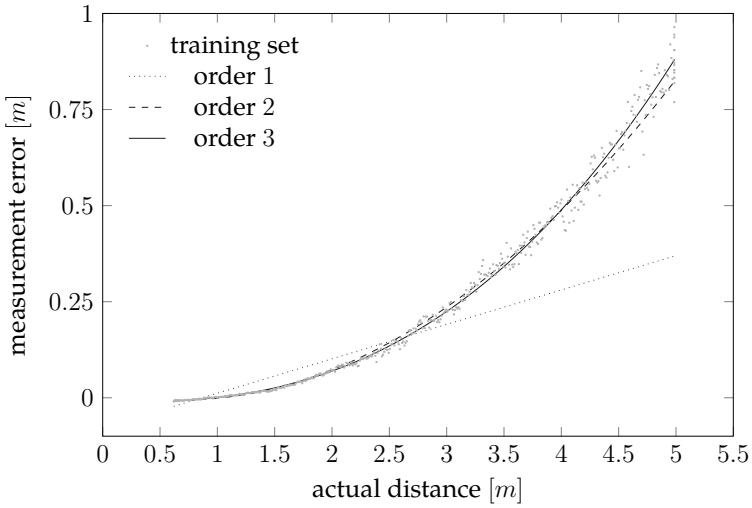

Figure 7: A typical training set collected in our experiments. The plotted quantities correspond to the measurement errors and to the polynomial models fitting these errors.

The estimated $\boldsymbol{\alpha}$ and σ_e^2 were also used for testing purposes to refine the estimate of the distances d_k in non-controlled environments. Notice that the selected model order was always 2, so it was always possible to solve the LS problem in a closed form and also discard one of the roots in (30), so that the set of roots was always a singleton. As shown in Figure 8, $\widehat{d}_k$ is much closer to d_k than y_k. For example, the empirical normalized MSEs for the test set in

Table 1: AIC scores for the different models complexities involved in the training set of Figure 7.

polynomial order	AIC score
1	-5.774
2	-7.380
3	-5.824
4	-3.890

Figure 8 were

$$\frac{1}{N}\sum_{k=1}^{N}\frac{\left\|\widehat{d}_k - d_k\right\|^2}{\|d_k\|^2} = 0.0046, \tag{31}$$

$$\frac{1}{N}\sum_{k=1}^{N}\frac{\|y_k - d_k\|^2}{\|d_k\|^2} = 0.0789. \tag{32}$$

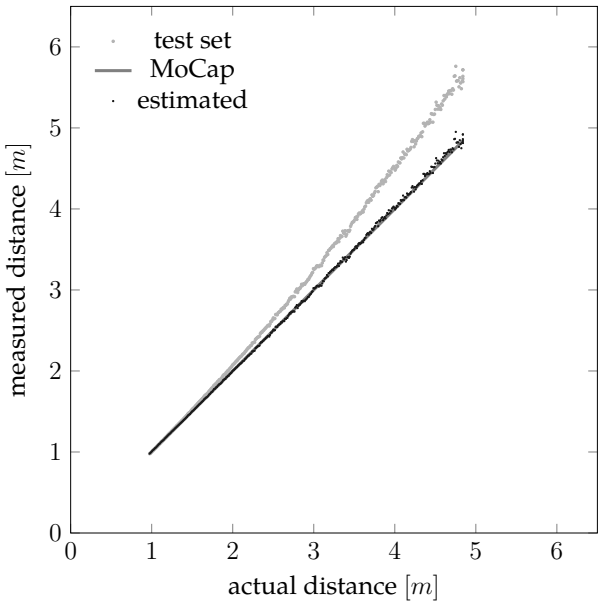

Figure 8: Effects of the estimation procedure on the original Lidar measurement. It can be noticed how the overall strategy removes the nonlinearities induced by the pinhole lens - CCD camera system.

7 Conclusions

We derived, starting from a combination of physical and statistical considerations, a model that describes the statistical behavior of the measurements returned by triangulation Lidars. This statistical model, given in (1), is based on two assumptions:

1. the effects of radial distortions in the pinhole lens can be captured by means of a polynomial function;

2. the nonlinearities induced by the geometry of the laser-CCD system can be captured by means of a heteroscedastic noise which standard deviation depends in first approximation quadratically with the measured distance.

This model, validated through some experiments on real devices, allows to build tailored triangulation Lidars calibration strategies that follow the classical training-testing paradigm:

- in the training phase, collect information in a controlled environment and use it to estimate through ML paradigms the parameters defining the statistical behavior of the sensor;

- in the test phase, use this information and some statistical inference techniques such as ML or LS to correct the measurements from the sensor when this is in a non-controlled environment.

It turns then out that both the ML and LS estimation strategies may be numerically demanding, specially for sensors suffering from strong radial distortions in the pinhole camera. In this case, indeed, the estimators may require to use numerical root finding procedures and lead to some computational disadvantages.

Irrespectively of these issues, that can in any case be mitigated by limiting the complexity of the polynomials describing the radial distortions, the estimation strategies above have been proved to be effective in our tests. Real-life experiments indeed showed that the techniques allow to reduce the empirical MSE of the sensor of a factor 17.15.

Despite this promising result, the research associated to triangulation Lidars is not finished. First of all, the techniques should be modified so to be implementable using recursive estimation schemes. Moreover, by following a classical training-testing approach, the techniques above present some limitations. Different sensors may in fact differ even if nominally being constructed in the same way. Moreover sensors may change their statistical behavior in time, due to aging or mechanical shocks. This means that techniques based on results from a controlled environment on just one sensor and just once are eventually not entirely meaningful.

A robust approach must indeed perform continuous learning for each sensor independently in a non-controlled environment by performing information fusion steps, e.g., combining also information from other sensors like odometry, ultrasonic and accelerometers.

This information-fusion continuous-learning algorithm nonetheless must be based on some preliminary results on what are the statistical models of triangulation Lidars and on how inference can be performed on them. This paper can thus be seen as the first step towards more evolved strategies.

References

[1] L. Kneip, F. Tâche, G. Caprari, and R. Siegwart, "Characterization of the compact hokuyo urg-04lx 2d laser range scanner," in *Robotics and Automation, 2009. ICRA'09. IEEE International Conference on*. IEEE, 2009, pp. 1447–1454.

[2] A. Reina and J. Gonzales, "Characterization of a radial laser scanner for mobile robot navigation," in *Intelligent Robots and Systems, 1997. IROS'97., Proceedings of the 1997 IEEE/RSJ International Conference on*, vol. 2. IEEE, 1997, pp. 579–585.

[3] K.-H. Lee and R. Ehsani, "Comparison of two 2d laser scanners for sensing object distances, shapes, and surface patterns," *Computers and electronics in agriculture*, vol. 60, no. 2, pp. 250–262, 2008.

[4] R. Sanz-Cortiella, J. Llorens-Calveras, J. R. Rosell-Polo, E. Gregorio-Lopez, and J. Palacin-Roca, "Characterisation of the lms200 laser beam under the influence of blockage surfaces. influence on 3d scanning of tree orchards," *Sensors*, vol. 11, no. 3, pp. 2751–2772, 2011.

[5] P. Tang, B. Akinci, and D. Huber, "Quantification of edge loss of laser scanned data at spatial discontinuities," *Automation in Construction*, vol. 18, no. 8, pp. 1070–1083, 2009.

[6] J. Tuley, N. Vandapel, and M. Hebert, "Analysis and removal of artifacts in 3-d ladar data," in *Robotics and Automation, 2005. ICRA 2005. Proceedings of the 2005 IEEE International Conference on*. IEEE, 2005, pp. 2203–2210.

[7] C. Ye and J. Borenstein, "Characterization of a 2-d laser scanner for mobile robot obstacle negotiation," in *ICRA*, 2002, pp. 2512–2518.

[8] D. Anderson, H. Herman, and A. Kelly, "Experimental characterization of commercial flash ladar devices," in *International Conference of Sensing and Technology*, vol. 2, 2005.

[9] A. Alhashimi, D. Varagnolo, and T. Gustafsson, "Joint temperature-lasing mode compensation for time-of-flight lidar sensors," *Sensors*, vol. 15, no. 12, pp. 31 205–31 223, 2015.

[10] J. Lima, J. Gonçalves, and P. J. Costa, "Modeling of a low cost laser scanner sensor," in *CONTROLO'2014–Proceedings of the 11th Portuguese Conference on Automatic Control*. Springer, 2015, pp. 697–705.

[11] D. Campos, J. Santos, J. Gonçalves, and P. Costa, "Modeling and simulation of a hacked neato xv-11 laser scanner," in *Robot 2015: Second Iberian Robotics Conference*. Springer, 2016, pp. 425–436.

[12] Q. Zhang and R. Pless, "Extrinsic calibration of a camera and laser range finder (improves camera calibration)," in *Intelligent Robots and Systems, 2004.(IROS 2004). Proceedings. 2004 IEEE/RSJ International Conference on*, vol. 3. IEEE, 2004, pp. 2301–2306.

[13] C. Mei and P. Rives, "Calibration between a central catadioptric camera and a laser range finder for robotic applications," in *Robotics and Automation, 2006. ICRA 2006. Proceedings 2006 IEEE International Conference on*. IEEE, 2006, pp. 532–537.

[14] O. Jokinen, "Self-calibration of a light striping system by matching multiple 3-d profile maps," in *3-D Digital Imaging and Modeling, 1999. Proceedings. Second International Conference on*. IEEE, 1999, pp. 180–190.

[15] B. Tiddeman, N. Duffy, G. Rabey, and J. Lokier, "Laser-video scanner calibration without the use of a frame store," in *Vision, Image and Signal Processing, IEE Proceedings-*, vol. 145, no. 4. IET, 1998, pp. 244–248.

[16] H. Andreasson, R. Triebel, and W. Burgard, "Improving plane extraction from 3d data by fusing laser data and vision," in *Intelligent Robots and Systems, 2005.(IROS 2005). 2005 IEEE/RSJ International Conference on*. IEEE, 2005, pp. 2656–2661.

[17] G.-Q. Wei and G. Hirzinger, "Active self-calibration of hand-mounted laser range finders," *Robotics and Automation, IEEE Transactions on*, vol. 14, no. 3, pp. 493–497, 1998.

[18] A. M. McIvor, "Calibration of a laser stripe profiler," in *3-D Digital Imaging and Modeling, 1999. Proceedings. Second International Conference on*. IEEE, 1999, pp. 92–98.

[19] Q. Zhang and R. Pless, "Constraints for heterogeneous sensor auto-calibration," in *Computer Vision and Pattern Recognition Workshop, 2004. CVPRW'04. Conference on*. IEEE, 2004, pp. 38–38.

[20] C.-Y. Chen and H.-J. Chien, "On-site sensor recalibration of a spinning multi-beam lidar system using automatically-detected planar targets," *Sensors*, vol. 12, no. 10, pp. 13 736–13 752, 2012.

[21] N. Muhammad and S. Lacroix, "Calibration of a rotating multi-beam lidar," in *Intelligent Robots and Systems (IROS), 2010 IEEE/RSJ International Conference on*. IEEE, 2010, pp. 5648–5653.

[22] G. Atanacio-Jiménez, J.-J. González-Barbosa, J. B. Hurtado-Ramos, F. J. Ornelas-Rodríguez, H. Jiménez-Hernández, T. García-Ramirez, and R. González-Barbosa, "Lidar velodyne hdl-64e calibration using pattern planes," *International Journal of Advanced Robotic Systems*, vol. 8, no. 5, pp. 70–82, 2011.

[23] C. Glennie and D. D. Lichti, "Static calibration and analysis of the velodyne hdl-64e s2 for high accuracy mobile scanning," *Remote Sensing*, vol. 2, no. 6, pp. 1610–1624, 2010.

[24] ——, "Temporal stability of the velodyne hdl-64e s2 scanner for high accuracy scanning applications," *Remote Sensing*, vol. 3, no. 3, pp. 539–553, 2011.

[25] C. Glennie, "Calibration and kinematic analysis of the velodyne hdl-64e s2 lidar sensor," *Photogrammetric Engineering & Remote Sensing*, vol. 78, no. 4, pp. 339–347, 2012.

[26] M. Gordon and J. Meidow, "Calibration of a multi-beam laser system by using a tls-generated reference," *ISPRS Annals of Photogrammetry, Remote Sensing and Spatial Information Sciences II-5 W*, vol. 2, pp. 85–90, 2013.

[27] F. M. Mirzaei, D. G. Kottas, and S. I. Roumeliotis, "3d lidar–camera intrinsic and extrinsic calibration: Identifiability and analytical least-squares-based initialization," *The International Journal of Robotics Research*, vol. 31, no. 4, pp. 452–467, 2012.

[28] X. Gong, Y. Lin, and J. Liu, "3d lidar-camera extrinsic calibration using an arbitrary trihedron," *Sensors*, vol. 13, no. 2, pp. 1902–1918, 2013.

[29] Y. Park, S. Yun, C. S. Won, K. Cho, K. Um, and S. Sim, "Calibration between color camera and 3d lidar instruments with a polygonal planar board," *Sensors*, vol. 14, no. 3, pp. 5333–5353, 2014.

[30] R. Kümmerle, G. Grisetti, and W. Burgard, "Simultaneous calibration, localization, and mapping," in *Intelligent Robots and Systems (IROS), 2011 IEEE/RSJ International Conference on*. IEEE, 2011, pp. 3716–3721.

[31] A. Teichman, S. Miller, and S. Thrun, "Unsupervised intrinsic calibration of depth sensors via slam." in *Robotics: Science and Systems*. Citeseer, 2013.

[32] F. Blais, "Review of 20 years of range sensor development," *Journal of Electronic Imaging*, vol. 13, no. 1, 2004.

[33] K. Konolige, J. Augenbraun, N. Donaldson, C. Fiebig, and P. Shah, "A low-cost laser distance sensor," in *Robotics and Automation, 2008. ICRA 2008. IEEE International Conference on*. IEEE, 2008, pp. 3002–3008.

[34] Z. Zhang, "A flexible new technique for camera calibration," *Pattern Analysis and Machine Intelligence, IEEE Transactions on*, vol. 22, no. 11, pp. 1330–1334, 2000.

[35] J. Weng, P. Cohen, and M. Herniou, "Camera calibration with distortion models and accuracy evaluation," *IEEE Transactions on Pattern Analysis & Machine Intelligence*, vol. 14, no. 10, pp. 965–980, 1992.

[36] D. C. Brown, "An advanced reduction and calibration for photogrammetric cameras," DTIC Document, Tech. Rep., 1964.

[37] C. B. Duane, "Close-range camera calibration," *Photogrammetric engineering*, vol. 37, no. 8, pp. 855–866, 1971.

[38] F. Gustafsson, *Statistical sensor fusion*. Studentlitteratur,, 2010.

[39] C. Croarkin and P. Tobias, "Nist/sematech e-handbook of statistical methods," *NIST/SEMATECH, July. Available online: http://www.itl.nist.gov/div898/handbook*, 2006.

Paper C

Calibrating triangulation Lidars without groundtruth information in terrestrial applications

Authors:
Anas Alhashimi, Damiano Varagnolo, Thomas Gustafsson

Reformatted version of paper submitted to:
IEEE Sensors Journal

Calibrating triangulation Lidars without groundtruth information in terrestrial applications

Anas Alhashimi, Damiano Varagnolo, Thomas Gustafsson

Abstract: We aim at improving the usability of triangulation Lidar ranging sensors through developing and testing a groundtruth-less calibration procedure that does not require tests in controlled environments for estimating the intrinsic parameters of these sensors. The calibration procedure corresponds to an approximated EM scheme exploiting statistical heteroscedastic models for the triangulation Lidar measurement process plus a simplified model for the dynamics of terrestrial robots. The procedure can also integrate other common sensors in robotic applications, such as odometers and sonar rangers, and can simultaneously learn the parameters of all these sensors. The standing assumption in the calibration procedure is then that the robot moves on a straight line (and is thus suitable only for terrestrial applications where robots move on a flat surface).
The procedure has also been tested by moving a robot in a controlled environment so to be able to compute the performance indexes of the various estimators. Results show that the proposed approximated EM strategy leads to effective calibrations that diminish the MSE of measurements returned by our triangulation Lidar by a factor between 3 and 6, comparable to the efficiency of state-of-the-art groundtruth-based calibration procedures. Surprisingly, adding odometric and ultrasonic information further improved the performance index of the overall estimation strategy, but only by a factor up to 1.2.

Expectation Maximization, Lidar , Calibration

1 Introduction

The easiest way to calibrate a sensor is to compare it with a more precise sensor (the "groundtruth") and learn through this comparison how the original sensor is affected by bias and measurement noises. This strategy unfortunately requires a controlled environment (the groundtruth), something that may be expensive and time consuming. Moreover the sensor may change its characteristics in time, and thus require periodical calibrations. One may thus want to avoid using groundtruth information to calibrate sensors; the questions are then *is it possible* and *how is it possible*.

Different specific applications have obviously different specific answers. Here we focus on terrestrial robotic applications and thus consider the problem of how to calibrate sensors in typical terrestrial robots without using groundtruth information.

More precisely we focus on triangulation Lidar distance rangers [1, 2, 3], a relatively novel cheap and lightweight Lidar technology for measuring distances in the range of meters which favorable economical and structural properties are counterbalanced by a strong need

for calibration steps. As the example in Figure 1 shows, indeed, the raw data from a non-calibrated triangulation Lidar look like suffering from a non-linear bias and a heteroscedastic measurement noise.

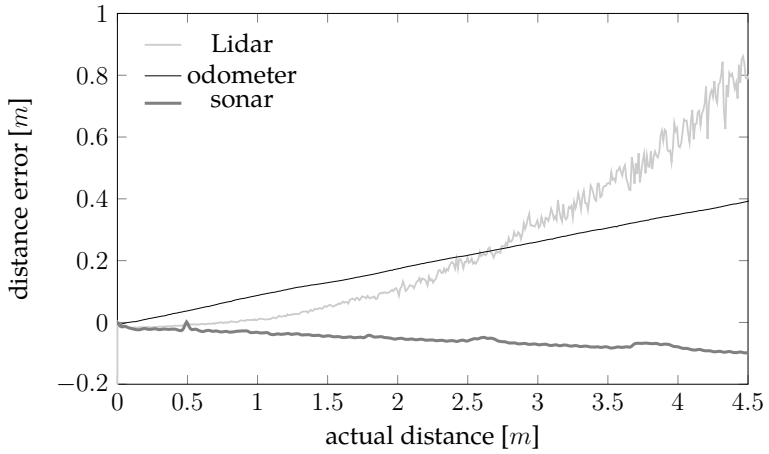

Figure 1: Example of the errors committed by a non-calibrated triangulation Lidar / odometer / sonar in measuring the distance between a robot hosting these sensors and a frontal wooden obstacle. The robot was moving on a flat floor in an indoor artificially illuminated room.

Before stating our contributions, we review some literature dedicated to calibration of sensors, specially of Lidars .

Literature review

It is convenient to distinguish between *characterizing* and *calibrating* a sensor: the former means to quantify the measurement noisiness of the device, while the latter means finding how to process the raw information so to diminish its bias and noisiness levels. The raw information processing algorithm in its turn may depend on two different types of information: the *intrinsic* parameters of the sensor, or the *extrinsic* ones, i.e., that parameters that result from how the sensor interacts with the environment (e.g., relative positioning distances).

There is then a relatively large number of papers describing how to calibrate extrinsic parameters either using additional sensors (such as cameras) [4, 5, 6, 7], or just requiring knowledge on the motion of robots [8, 9, 10, 11]; all of these nonetheless require groundtruth information *and* refer to extrinsic calibration problems, while we deal with intrinsic ones.

There is of course also literature dedicated specially to the intrinsic calibration of multi-beam Lidar systems, where the technique is often to use one beam to calibrate the intrinsic parameters of the other beams [12, 13, 14, 15, 16, 17, 18, 19, 20, 21]. Also this branch of literature is only partially related to our case, since in our set-up we consider single-beam Lidar systems.

Specific types of Lidars have then specific statistical models, and thus require specific calibration algorithms. E.g., ToF Lidars have been analyzed in [22, 23, 24, 25, 26, 27, 28, 29, 30], while triangulation Lidars (the ones we are interested in) have been studied in [1, 2, 3, 31].

To the best of our knowledge, triangulation Lidars have been analyzed in only the 4 manuscripts cited above: [1], that proposes the technology and performs an early-assessment of its potential; [2], that discusses the nonlinearities affecting the triangulation Lidars produced by Neato; [3], that analyzes the effect of the color of the target on the raw data returned by triangulation Lidars ; and [31], where we proposed a groundtruth-based calibration procedure based on a statistical model that generalizes the one in [2]. As it will be clear in the following statement of contributions, our paper differentiates from all the manuscripts above by proposing the first groundtruth-less calibration procedure dedicated to this type of sensors.

1.1 Statement of contributions

In brief we start from the statistical model proposed in [31] to construct groundtruth-less intrinsic parameters calibration procedure based on an approximated EM algorithm.

In more details we ignore temporal calibration problems (i.e., considering also the effects of uncertainties in the timings of the measurements, see [32]), plus focus explicitly on the terrestrial robots case. The standing assumptions that ensure the feasibility of the estimation strategy are indeed:

1. the robot moves on a line (even with a time varying speed; the important is that the movement is a line);

2. the robot has knowledge of the actuation signals it gave to its motors (this precludes doing calibrations *by hand*).

We also propose two ancillary results: the first is a description of how to integrate in the calibration scheme also other ranging sensors like odometry and ultrasonic, so to perform simultaneous calibration (and thus enjoy of the potential synergies in the information that these sensors provide). The second is a description of how to use the results coming from a groundtruth-less calibration procedure to perform Kalman smoothing during the normal operations of these sensors.

We eventually quantify and compare how these novel groundtruth-less calibration strategies perform compared to the groundtruth-based strategies proposed in [31], plus investigate the gains obtained combining Lidars , odometers and sonars. The results indicate that:

1. the groundtruth-less leads to results that are similar to the ones obtained with groundtruth-based strategies (sometimes even better!). This is not totally surprising: we indeed postulate that the information on the actuation signal given to the robots' wheels (that was not used in [31]) compensates for the loss of the groundtruth;

2. adding odometers and sonars tend to improve the overall estimation performance, but the improvement also tends to be quite contained, indicating that the additional information brought from these sensors is minimal.

1.2 Organization of the manuscript

Section 2 formulates precisely the problem that we consider. Section 3 presents the statistical models of the sensors that we considered here, plus generalizes these models so that other

authors with other sensors may tailor our strategy to their particular case. Section 4 models the dynamics of the robot. Section 5 derives our calibration procedure. Section 6 presents a Kalman smoothing based strategy useful to exploit the results from the calibration procedure during the normal operations of the sensors. Section 7 numerically compares the statistical performances of the various estimators. Section 8 draws some conclusions and describes our future research efforts.

2 Problem formulation

We consider the practical need of calibrating a triangulation Lidar mounted on an autonomous terrestrial robot. We assume that: *i)* we do not have access to groundtruth information; *ii)* we have access to the inputs given from the robot to the wheels' motors; *iii)* the robot moves on a straight line; *iv)* the surrounding environment does not change. (Optionally, the robot may also be endowed with other non-calibrated distance-measuring sensors such as odometers and ultrasound rangers.) In practice, we consider the archetypal situation of an autonomous vacuum cleaning robot that makes straight moves in an unknown environment.

An other (mild) assumption is that we know the structure of the statistical models of the various sensors, so that we frame the solution of the calibration problem as a statistical inference problem. I.e., how to transform a dataset of distances measured by the sensors plus commands given to the robot's wheels into a (meaningful) estimate of the sensors' intrinsic parameters, under the assumption that the robot moved on a straight line.

3 Sensors Modeling

Sections 3.1, 3.3 and 3.2 describe the specific statistical models of the various sensors used in our EM calibration strategy. Section 3.4 instead generalizes the statistical models of Sections 3.1, 3.3 and 3.2 and presents information useful to re-derive the equations of our EM calibration strategy for other types of ranging sensors.

3.1 Triangulation Lidar sensors models

In [31] we derived and validated, starting from a combination of physical and statistical considerations, a model of the measurements produced by triangulation Lidars that accounts for pinhole lens radial distortions effects and nonlinearities induced by the geometry of the laser-CCD system. The model is then

$$y_k^l = \underbrace{\alpha_0^l + \alpha_1^l d_k + \alpha_2^l d_k^2}_{\text{nonlinear bias}} + \underbrace{\beta_2^l d_k^2 e_k^l}_{\text{heteroscedastic noise}} \tag{1}$$

where y_k^l is the measurement at time k, d_k is the true distance, $\alpha_0^l, \alpha_1^l, \alpha_2^l$ are the parameters defining the (nonlinear) sensor bias, $e_k^l \sim \mathcal{N}(0,1)$ is iid, and the term $\beta_2^l d_k^2$ implies that the measurement noise is heteroscedastic.

3.2 Odometry sensors model

Several different models describe the statistical properties of the odometers' measurements, e.g., [33, 34]. There seems to be consensus in considering, in the common case where robots have two independent traction wheels, separate errors in the translation of each wheel that increase linearly with the distance traveled and with the number of input commands given to the robot, i.e., heteroscedastic models.

Unfortunately our experiments suggest to use a homoscedastic noises (see, e.g., Figure 1). For this reason we considered in our calibration procedure the model

$$y_k^o = \underbrace{\alpha_0^o + \alpha_1^o d_k}_{\text{linear bias}} + \underbrace{\beta_0^o e_k^o}_{\text{homoscedastic noise}} \tag{2}$$

with $e_k^o \sim \mathcal{N}(0,1)$. Notice that this choice has been driven by our specific hardware, and thus has no claim of generality; nonetheless we derived our procedure using general formulas, so that if readers need to change (2) in favor of more complicated dependencies on e_k^o they can easily do so.

3.3 Ultrasonic ranging sensors model

Ultrasonic sensors are affected by an affine bias accounting for installation offsets and scaling of the actual distance induced by the dependency of the sound propagation speed in air on the air temperature (safely assumable constant during a calibration procedure). The measurement noise is instead typically generated from robot shaking and floor surface variations effects that generate mechanical vibration of the robot body [35]. Thus the statistical model that we consider is

$$y_k^u = \underbrace{\alpha_0^u + \alpha_1^u d_k}_{\text{affine bias}} + \underbrace{\beta_0^u e_k^u}_{\text{homoscedastic noise}} \tag{3}$$

where the notation and assumptions on e_k^u are similar to the ones in 1.

3.4 Generic sensor model

Generalizing the results obtained in Sections 3.1, 3.3 and 3.2, we may consider a generic heteroscedastic sensor model

$$y_k^{(s)} = \underbrace{\sum_{i=0}^{N_\alpha^{(s)}-1} \alpha_i^{(s)} d_k^i}_{\text{bias}} + \underbrace{\sum_{i=0}^{N_\beta^{(s)}-1} \beta_i^{(s)} d_k^i e_k^{(s)}}_{\text{noise}} \tag{4}$$

where d_k is the noiseless distance, (s) is the sensor label, $e_k^{(s)} \sim \mathcal{N}(0,1)$ i.i.d., and the coefficients $\alpha_i^{(s)}$, $\beta_i^{(s)}$, $N_\alpha^{(s)}$ and $N_\beta^{(s)}$ define the type of bias and noise affecting that specific sensor type.

4 Model of the dynamics of the robot

Consider the case of a robot endowed with S different sensors each satisfying a measurement model like (4). Since calibrating these sensors means to estimate the coefficients of the polynomials in (4), the model of the dynamics of the robot should be sufficiently rich to capture these polynomials.

Let then the transition model for the actual distance d_k be linear Gaussian, i.e.,

$$d_{k+1} = d_k + u_k + \nu_k \tag{5}$$

with u_k the scalar input representing the motion commands given to the robot, $\nu_k \sim \mathcal{N}(0, \sigma_d^2)$ with σ_d^2 for simplicity assumed known. Define thus p as the maximum order of the polynomials appearing in (4), i.e.,

$$p := \max_s \left\{ N_\alpha^{(s)}, N_\beta^{(s)} \right\}_{s \in \{1,\dots,S\}}, \tag{6}$$

and let the (redundant) state vector describing the robot's motion as $x_k := [1, d_k, \cdots, d_k^{p-1}]^T$. The associated (non-minimal) dynamical model is thus

$$\begin{bmatrix} x_{k+1} \\ y_k \end{bmatrix} = \begin{bmatrix} A_k & B_k \\ C & \mathbb{0} \end{bmatrix} \begin{bmatrix} x_k \\ \mathbb{1} \end{bmatrix} + \begin{bmatrix} w_k \\ v_k(x_k) \end{bmatrix} \tag{7}$$

with $y_k := [y_k^{(1)}, \dots, y_k^{(S)}]^T$ the measurements vector, $\mathbb{0}$ a matrix of zeros and $\mathbb{1}$ a vector of ones both with opportune dimensions, and with (padding when necessary the various coefficients with zeros)

$$A_k := \begin{bmatrix} 1 & 0 & 0 & 0 & \cdots \\ 0 & 1 & 0 & 0 & \cdots \\ 0 & 2u_k & 1 & 0 & \cdots \\ 0 & 3u_k^2 & 3u_k & 1 & \cdots \\ \vdots & \vdots & \ddots & \ddots & \ddots \end{bmatrix} \qquad B_k := \begin{bmatrix} 0 \\ u_k \\ \vdots \\ u_k^{p-1} \end{bmatrix} \tag{8}$$

$$C := \begin{bmatrix} \alpha_1^{(1)} & \cdots & \alpha_p^{(1)} \\ \vdots & & \\ \alpha_1^{(S)} & \cdots & \alpha_p^{(S)} \end{bmatrix} \tag{9}$$

with

- u_k (assumed known) conveniently absorbed into the various model matrices;
- the i-th row of A_k exhibiting the coefficients of the binomial formula $(d_k + u_k)^{i-1}$ (but the first element, that is always 0);
- the measurement noise v_k satisfying, given model (4), $v_k \sim \mathcal{N}(0, R(x_k))$ with

$$R(x_k) := \operatorname{diag}\left(r^{(1)}(x_k), \dots, r^{(S)}(x_k) \right) \tag{10}$$

and

$$r^{(s)}(x_k) := \left(\begin{bmatrix} \beta_0^{(s)} & \cdots & \beta_{p-1}^{(s)} \end{bmatrix} x_k \right)^2. \tag{11}$$

We notice that the definition of x_k and the assumption $\nu_k \sim \mathcal{N}(0, \sigma_d^2)$ in (5) implies that the process noise w_k in (7) should not be Gaussian. This, unfortunately, hinders numerical tractability of the estimation processes based on (7). To overcome this problem we simplify w_k and assume it to be Gaussian, $w_k \sim \mathcal{N}(0, Q)$ with Q known and diagonal with small entries. Moreover, again for the same sake of simplification, we assume the initial state to be Gaussian too, i.e., $x_1 \sim \mathcal{N}(\mu_d, \Sigma_d)$ with μ_d and $\Sigma_d = \mathbb{0}$.

We also notice that we may have alternatively defined x_k as $[d_k, \cdots, d_k^{p-1}]^T$, but this would have led us into the need for estimating the matrices B_k (and thus system identifiability problems).

5 An EM-based groundtruth-less calibration procedure

Let $\boldsymbol{u} := [u_1, \ldots, u_N]^T$, and

$$y_k := \begin{bmatrix} y_k^{(1)} \\ \vdots \\ y_k^{(S)} \end{bmatrix}, \; k = 1, \ldots, N, \qquad \boldsymbol{y} := [y_1, \ldots, y_N] \tag{12}$$

$$x_k := \begin{bmatrix} 1 \\ d_k \\ \vdots \\ d_k^{p-1} \end{bmatrix}, \; k = 1, \ldots, N+1, \qquad \boldsymbol{x} := [x_1, \ldots, x_{N+1}]. \tag{13}$$

Assuming $\boldsymbol{u}$ to be known, model (7) is fully described by the set of parameters

$$\theta := \left\{ \begin{array}{c} \left\{ \alpha_0^{(s)}, \ldots, \alpha_{p-1}^{(s)} \right\}_{s \in \{1,\ldots,S\}}, \\ \left\{ \beta_0^{(s)}, \ldots, \beta_{p-1}^{(s)} \right\}_{s \in \{1,\ldots,S\}} \end{array} \right\}. \tag{14}$$

Our first aim is thus to estimate θ from a dataset of measurements $\boldsymbol{y}$, $\boldsymbol{u}$ collected in a non-controlled environment. In other words, we want to find a statistically meaningful map of the kind

$$\{\boldsymbol{y}, \boldsymbol{u}\} \mapsto \widehat{\theta} \tag{15}$$

where the unique additional assumption that we pose is that the robot follows a straight line and the surrounding environment does not change in the while.

We assume a frequentist framework for which θ is a deterministic and unknown quantity. Given this assumption we strive for finding the ML estimator for θ given $\{\boldsymbol{y}, \boldsymbol{u}\}$ in (15) (and thus without assuming that sequence $\boldsymbol{x}$ of the actual states is known at some point). Since the likelihood $p(\boldsymbol{y}, \boldsymbol{x}\,;\,\theta)$ depends on the unknown $\boldsymbol{x}$, the natural strategy would then be to maximize the marginal likelihood of the outputs $\boldsymbol{y}$ with respect to θ, i.e., solve

$$\widehat{\theta}_{ML} := \arg\max_{\theta \in \Theta} p(\boldsymbol{y}\,;\,\theta) \tag{16}$$

where Θ is the (assumed closed) set of admissible candidate parameters vectors, and where $p(\boldsymbol{y}\ ;\ \theta)$ is obtained integrating out from $p(\boldsymbol{y},\boldsymbol{x}\ ;\ \theta)$ the latent r.v. $\boldsymbol{x}$. Since solving numerically (16) in our specific case is not trivial (given that the marginalization task is not trivial) we attempt to solve (16) numerically by means of an opportune EM scheme. Before presenting the specific equations of our strategy in Sections 5.2 and 5.3, and for completeness of the treatment, we briefly discuss the basic machineries behind EM algorithms in the following Section 5.1. For more details on the EM algorithm see, e.g., [36].

5.1 The Expectation Maximization (EM) algorithm in the general case

The strategy is founded on the basic relationship

$$p(\boldsymbol{y}\ ;\ \theta) = \frac{p(\boldsymbol{y},\boldsymbol{x}\ ;\ \theta)}{p(\boldsymbol{x}\,|\boldsymbol{y}\ \ ;\ \theta)} \tag{17}$$

and computes $\widehat{\theta}$ iterating the two steps (with t being the iteration index):

E step: given $\widehat{\theta}^{(t)}$ i.e., the estimate of the parameters at iteration t, compute

$$\ell\left(\theta,\ \widehat{\theta}^{(t)}\right) = \mathbb{E}_{p\left(\boldsymbol{x}|\boldsymbol{y}\ ;\ \widehat{\theta}^{(t)}\right)}\left[\log p(\boldsymbol{y},\boldsymbol{x}\ ;\ \theta)\right]; \tag{18}$$

M step: compute

$$\widehat{\theta}^{(t+1)} = \arg\max_{\theta}\ell\left(\theta,\ \widehat{\theta}^{(t)}\right). \tag{19}$$

The EM algorithm is ensured to make $\widehat{\theta}^{(t)}$ asymptotically converge, by iterating the two steps above, to a potentially local maximum of $p(\boldsymbol{y}\ ;\ \theta)$. Among the various plausible stopping criteria, the most common ones are to stop either when $\left\|\widehat{\theta}^{(t+1)}-\widehat{\theta}^{(t)}\right\|$ is below a given threshold, or after a pre-fixed number of iterations. The following two subsections explicit then the two previous generic EM steps to our specific case.

5.2 The Expectation step in our specific case

Computing $\ell\left(\theta,\ \widehat{\theta}^{(t)}\right)$ requires to find $\log p(\boldsymbol{y},\boldsymbol{x}\ ;\ \theta)$; consider thus that model (7) implies

$$\begin{bmatrix} x_{k+1} \\ y_k \end{bmatrix} \sim \mathcal{N}\left(\begin{bmatrix} A_k & B_k \\ C & \mathbb{0} \end{bmatrix}\begin{bmatrix} x_k \\ \mathbb{1} \end{bmatrix}, \begin{bmatrix} Q & \mathbb{0} \\ \mathbb{0}^T & R(x_k) \end{bmatrix}\right). \tag{20}$$

with $x_1 \sim \mathcal{N}(\mu_1, \Sigma_1)$ and with μ_1 and Σ_1 known. Defining

$$\Sigma_k := \begin{bmatrix} Q & \mathbb{0} \\ \mathbb{0}^T & R(x_k) \end{bmatrix} \tag{21}$$

and using both the Bayes rule and the Markovianity of (7) we get

$$p(\boldsymbol{y},\boldsymbol{x}\ ;\ \theta) = p(x_1\ ;\ \theta)\prod_{k=2}^{N} p(y_k\,|x_k\ \ ;\ \theta)\,p(x_{k+1}\,|x_k\ \ ;\ \theta) \tag{22}$$

that leads immediately to

$$\begin{aligned}\log p\left(\boldsymbol{y},\boldsymbol{x}\ ;\ \theta\right) = \log p\left(x_1\ ;\ \theta\right) + \\ \sum_{k=2}^{N}\log p\left(y_k\left|x_k\right.\ ;\ \theta\right) + \sum_{k=2}^{N}\log p\left(x_{k+1}\left|x_k\right.\ ;\ \theta\right).\end{aligned} \tag{23}$$

Given (20) the joint log likelihood thus can be written as

$$\begin{aligned}\log p\left(\boldsymbol{y},\boldsymbol{x}\ ;\ \theta\right) \propto \mathcal{C} + \log\det\Sigma_1 - \left\|x_1-\mu_1\right\|_{\Sigma_1}^2 \\ + \sum_{k=2}^{N}\left(\log\det\Sigma_k - \left\|\begin{bmatrix}x_{k+1}\\ y_k\end{bmatrix} - \begin{bmatrix}A_k & B_k\\ C & \mathbb{0}\end{bmatrix}\begin{bmatrix}x_k\\ \mathbb{1}\end{bmatrix}\right\|_{\Sigma_k}^2\right)\end{aligned} \tag{24}$$

where $\left\|\star\right\|_{\diamond}^2 := \star^T\diamond^{-1}\star$ and $\mathcal{C}$ is a constant independent of the variables $\boldsymbol{y}$, $\boldsymbol{x}$, and θ. Applying then the conditional expectation $\mathbb{E}_{p\left(\boldsymbol{x}\left|\boldsymbol{y}\right.\ ;\ \widehat{\theta}^{(t)}\right)}\left[\cdot\right]$ on both sides, expanding the norms opportunely and ignoring multiplicative factors yields to (see also [37])

$$\ell\left(\theta,\ \widehat{\theta}^{(t)}\right) = \mathcal{C} + \sum_{k=1}^{N}\left(\log\det\Sigma_k - \operatorname{tr}\left(\mathcal{E}_k\right)\right) \tag{25}$$

with, for $k=1$,

$$\mathcal{E}_1 := \mathbb{E}_{p\left(\boldsymbol{x}\left|\boldsymbol{y}\right.\ ;\ \widehat{\theta}^{(t)}\right)}\left[\Sigma_1^{-1}\left(x_1-\mu_1\right)\left(x_1-\mu_1\right)^T\right] \tag{26}$$

and, for $k=2,\dots,N$,

$$\begin{aligned}\mathcal{E}_k := \ \mathbb{E}_{p\left(\boldsymbol{x}\left|\boldsymbol{y}\right.\ ;\ \widehat{\theta}^{(t)}\right)}\Bigg[\Sigma_k^{-1}\left(\begin{bmatrix}x_{k+1}\\ y_k\end{bmatrix} - \begin{bmatrix}A_k & B_k\\ C & \mathbb{0}\end{bmatrix}\begin{bmatrix}x_k\\ \mathbb{1}\end{bmatrix}\right) \\ \left(\begin{bmatrix}x_{k+1}\\ y_k\end{bmatrix} - \begin{bmatrix}A_k & B_k\\ C & \mathbb{0}\end{bmatrix}\begin{bmatrix}x_k\\ \mathbb{1}\end{bmatrix}\right)^T\Bigg].\end{aligned} \tag{27}$$

Exploiting the fact that Σ_k in (21) is block diagonal and expanding opportunely we eventually find that computing $\operatorname{tr}\left(\mathcal{E}_k\right)$ requires computing quantities of the kind

$$\begin{aligned}&\mathbb{E}_{p\left(\boldsymbol{x}\left|\boldsymbol{y}\right.\ ;\ \widehat{\theta}^{(t)}\right)}\left[x_{k+1}x_k^T\right]\\ &\mathbb{E}_{p\left(\boldsymbol{x}\left|\boldsymbol{y}\right.\ ;\ \widehat{\theta}^{(t)}\right)}\left[x_kx_k^T\right]\\ &\mathbb{E}_{p\left(\boldsymbol{x}\left|\boldsymbol{y}\right.\ ;\ \widehat{\theta}^{(t)}\right)}\left[R\left(x_k\right)^{-1}C_kx_kx_k^TC_k^T\right]\\ &\mathbb{E}_{p\left(\boldsymbol{x}\left|\boldsymbol{y}\right.\ ;\ \widehat{\theta}^{(t)}\right)}\left[R\left(x_k\right)^{-1}y_kx_k^TC_k^T\right].\end{aligned} \tag{28}$$

Given that $R\left(x_k\right)$ in (28) depend on x_k, the quantities above cannot be computed in closed form, but rather requires numerical integration procedures. Since we aim at algorithms that can be implemented on cheap hardware, we seek for approximating $\ell\left(\theta,\ \widehat{\theta}^{(t)}\right)$ in (25) with an alternative approximated version $\widetilde{\ell}\left(\theta,\ \widehat{\theta}^{(t)}\right)$ with closed-form computability qualities.

To this point we notice that if the covariances $R\left(\cdot\right)$ were independent of x_k then we would be in the very same situation of [37], and thus we would be able to compute (28) by means of

a dedicated Kalman smoother. *We thus follow this approach, and approximate $R(\cdot)$ by considering x_k being equal to its past estimated value.*

More precisely, assume to be at iteration t of the EM algorithm; this means that at time $t-1$ we have computed both an estimate of the parameters $\widehat{\theta}^{(t)}$ and an estimate of the state $\widehat{x}_k^{(t-1)}$ (with initial condition $\widehat{x}_k^{(0)} = [1, \text{mean}(y_k), \ldots, \text{mean}(y_k)^{p-1}]$). Define thus

$$R_k^{(t)} := \text{diag}\left(r^{(1)^{(t)}}\left(\widehat{x}_k^{(t-1)}\right), \ldots, r^{(S)^{(t)}}\left(\widehat{x}_k^{(t-1)}\right)\right) \tag{29}$$

$$r^{(s)^{(t)}}\left(\widehat{x}_k^{(t-1)}\right) := \left(\left[\beta_0^{(s)^{(t)}} \ \cdots \ \beta_{p-1}^{(s)\ (t)}\right]\widehat{x}_k^{(t-1)}\right)^2 \tag{30}$$

and $\beta_0^{(s)^{(t)}}, \ldots, \beta_{p-1}^{(s)\ (t)}$ the set of parameters modeling sensor s estimated at time t by the EM algorithm. $R_k^{(t)}$ is thus a statistically meaningful approximation of the actual noise covariance $R(x_k)$, and with this we can approximate the quantities in (28) (and thus $\ell\left(\theta,\ \widehat{\theta}^{(t)}\right)$) by means of the following Algorithm 3. For convenience we indicate with $C^{(t)}$ the estimate of matrix C in (9) and the process noise covariance defined by the current estimate of the parameters $\widehat{\theta}^{(t)}$.

Exploiting the results in [38], thus, we can claim that

$$\begin{aligned}
\mathbb{E}_{p\left(\boldsymbol{x}|\boldsymbol{y}\ ;\ \widehat{\theta}_t\right)}\left[x_k x_k^T\right] &\approx \widehat{x}_{k|N}\widehat{x}_{k|N}^T + P_{k|N} \\
\mathbb{E}_{p\left(\boldsymbol{x}|\boldsymbol{y}\ ;\ \widehat{\theta}_t\right)}\left[x_{k+1} x_k^T\right] &\approx \widehat{x}_{k+1|N}\widehat{x}_{k|N}^T + M_{k+1|N} \\
\mathbb{E}_{p\left(\boldsymbol{x}|\boldsymbol{y}\ ;\ \widehat{\theta}_t\right)}\left[y_k x_k^T\right] &\approx y_k \widehat{x}_{k|N}^T.
\end{aligned} \tag{42}$$

Approximating $R(x_k)$ with $R_k^{(t)}$ thus leads to approximate the expectations (28) with (42), and thus to approximate $\ell\left(\theta,\ \widehat{\theta}^{(t)}\right)$ with an opportune $\widetilde{\ell}\left(\theta,\ \widehat{\theta}^{(t)}\right)$ obtainable expanding $\mathcal{E}_k$ in (27) into single factors and exploiting the fact that $R_k^{(t)}$ does not depend on x_k. Moreover when Algorithm 3 terminates we can also set $\widehat{\boldsymbol{x}}^{(t)} = \left[\widehat{x}_{1|N}, \ldots, \widehat{x}_{N|N}\right]$.

We notice that approximating ℓ with $\widehat{\ell}$ may theoretically disrupt the convergence properties of our EM strategy (something that we never experienced, though); proving the stability of the proposed scheme is nonetheless out of scope here and currently under analytical investigation.

5.3 The Maximization step in our specific case

Given the discussion above, we solve the M step by search for that parameter vector that maximizes $\widetilde{\ell}\left(\theta,\ \widehat{\theta}^{(t)}\right)$, i.e., compute

$$\widehat{\theta}^{(t+1)} = \arg\max_{\theta\in\Theta} \widetilde{\ell}\left(\theta,\ \widehat{\theta}^{(t)}\right). \tag{43}$$

by means of closed form equations and considering the latent variables $\boldsymbol{x}$ to be equal to that $\boldsymbol{x}^{(t)}$ computed in the Expectation step. Given definition (14), estimating θ means finding the matrix C (that contains the various $\left\{\alpha_0^{(s)}, \ldots, \alpha_{p-1}^{(s)}\right\}_{s\in\{1,\ldots,S\}}$), and the matrix $R\left(x_k^{(t)}\right)$ (that contains the various $\left\{\beta_0^{(s)}, \ldots, \beta_{p-1}^{(s)}\right\}_{s\in\{1,\ldots,S\}}$).

As shown in the next subsections, the actual equations for solving (43) depend on which combination of sensors one uses.

Algorithm 3 Kalman smoother for the Expectation step

1: Requires: $C^{(t)}$, $R_1^{(t)}, \ldots, R_N^{(t)}$
2: set (initial conditions for the forward pass)

$$P_{1|1} = \Sigma_1 \qquad \widehat{x}_{1|1} = \mu_1 \tag{31}$$

3: compute, for $k = 2, \ldots, N$ (forward pass)

$$P_{k|k-1} = A_k P_{k-1|k-1} A_k^T + Q \tag{32}$$

$$K_k = P_{k|k-1} C^{(t)^T} \left(C^{(t)} P_{k|k-1} C^{(t)^T} + R_k^{(t)} \right)^{-1} \tag{33}$$

$$P_{k|k} = P_{k|k-1} - K_k C^{(t)} P_{k|k-1} \tag{34}$$

$$\widehat{x}_{k|k-1} = A_k \widehat{x}_{k-1|k-1} + B_k \mathbb{1} \tag{35}$$

$$\widehat{x}_{k|k} = \widehat{x}_{k|k-1} + K_k \left(y_k - C^{(t)} \widehat{x}_{k|k-1} \right) \tag{36}$$

4: set (initial conditions for the backwards pass)

$$M_{N|N} = \left(I - K_N C^{(t)} \right) A_k P_{N-1|N-1} \tag{37}$$

5: compute, for $k = N, \ldots, 1$ (backwards pass)

$$J_k = P_{k|k} A^T P_{k+1|k}^{-1} \tag{38}$$

$$P_{k|N} = P_{k|k} + J_k \left(P_{k+1|N} - P_{k+1|k} \right) J_k^T \tag{39}$$

$$\widehat{x}_{k|N} = \widehat{x}_{k|k} + J_k \left(\widehat{x}_{k+1|N} - A_k \widehat{x}_{k|k} - B_k \mathbb{1} \right) \tag{40}$$

$$M_{k|N} = P_{k|k} J_{k-1}^T + J_k \left(M_{k+1|N} - A_k P_{k|k} \right) J_{k-1}^T \tag{41}$$

(the last equation being performed only when $k \neq N$)

The Maximization step when using just a triangulation Lidar

Having just a triangulation Lidar only, and considering model (1), our aim is to estimate $C = \left[\alpha_0^l, \alpha_1^l, \alpha_2^l\right]$ and β_2^l. Given the current estimate of the state provided by the E step, i.e., $\widehat{\boldsymbol{x}}^{(t)}$ with each element $\widehat{x}_k^{(t)}$ being the 3-dimensional vector $\left[\widehat{x}_k^{(t)}[1] \quad \widehat{x}_k^{(t)}[2] \quad \widehat{x}_k^{(t)}[3]\right]$, we can rewrite model (1) as

$$y_k^l = \begin{bmatrix}\alpha_0^l & \alpha_1^l & \alpha_2^l\end{bmatrix} \begin{bmatrix}\widehat{x}_k^{(t)}[1] \\ \widehat{x}_k^{(t)}[2] \\ \widehat{x}_k^{(t)}[3]\end{bmatrix} + \beta_2^l \widehat{x}_k^{(t)}[3] e_k^l. \tag{44}$$

Dividing every term by $\widehat{x}_k^{(t)}[3]$ we find the alternative model homoscedastic model

$$\widetilde{y}_k^l = \begin{bmatrix}\alpha_0^l & \alpha_1^l & \alpha_2^l\end{bmatrix} \begin{bmatrix}\widehat{x}_k^{(t)}[1]\widehat{x}_k^{(t)}[3]^{-1} \\ \widehat{x}_k^{(t)}[2]\widehat{x}_k^{(t)}[3]^{-1} \\ 1\end{bmatrix} + \beta_2^l e_k^l \tag{45}$$

where $\widetilde{y}_k^l := y_k^l \widehat{x}_k^{(t)}[3]$. Estimating the parameters from (45) is now immediate, since the estimation step can be performed immediately using ML considerations as

$$\begin{aligned} C^{(t+1)} &= \left(\left(\widetilde{\boldsymbol{y}}^l\right)^T H^l\right)\left(H^{lT} H^l\right)^{-1} \\ \beta_2^{l\,(t+1)} &= \frac{1}{N}\left(\widetilde{\boldsymbol{y}}^l - H^l C^{(t+1)}\right)^T \left(\widetilde{\boldsymbol{y}}^l - H^l C^{(t+1)}\right) \end{aligned} \tag{46}$$

with

$$\widetilde{\boldsymbol{y}}^l := \begin{bmatrix}\dfrac{y_1^l}{\widehat{x}_1^{(t)}[3]} \\ \vdots \\ \dfrac{y_N^l}{\widehat{x}_N^{(t)}[3]}\end{bmatrix} \qquad H^l := \begin{bmatrix}\dfrac{\widehat{x}_1^{(t)}[1]}{\widehat{x}_1^{(t)}[3]} & \dfrac{\widehat{x}_1^{(t)}[2]}{\widehat{x}_1^{(t)}[3]} & 1 \\ \vdots & & \vdots \\ \dfrac{\widehat{x}_N^{(t)}[1]}{\widehat{x}_N^{(t)}[3]} & \dfrac{\widehat{x}_N^{(t)}[2]}{\widehat{x}_N^{(t)}[3]} & 1\end{bmatrix}^T . \tag{47}$$

The Maximization step when using both a triangulation Lidar and an odometer

In this case the matrix C is equal to

$$C = \begin{bmatrix}C[1] \\ C[2]\end{bmatrix} = \begin{bmatrix}\alpha_0^l & \alpha_1^l & \alpha_2^l \\ \alpha_0^o & \alpha_1^o & \alpha_2^o\end{bmatrix} \tag{48}$$

where the parameters of the triangulation Lidar are given by $C[1]$ and β_2^l, and the ones of the odometer are given by $C[2]$ and β_0^o.

Given that $\widehat{\boldsymbol{x}}^{(t)}$ is given by the E step and that the two sensors are independent the estimation of the two sets of parameters can be performed independently. Thus for $C[1]$ and β_2^l we can proceed as in Section 5.3, while for $C[2]$ and β_0^o we proceed considering that, given model (2) and using again ML interpretations,

$$\begin{aligned} C^{(t+1)}[2] &= \left(\left(\boldsymbol{y}^o\right)^T H^o\right)\left(H^{oT} H^o\right)^{-1} \\ \beta_2^{o\,(t+1)} &= \frac{1}{N}\left(\boldsymbol{y}^o - H^o C^{(t+1)}[2]\right)^T \left(\boldsymbol{y}^o - H^o C^{(t+1)}[2]\right) \end{aligned} \tag{49}$$

where

$$H^o := \begin{bmatrix} \widehat{x}_1^{(t)}[1] & \widehat{x}_1^{(t)}[2] & \widehat{x}_1^{(t)}[3] \\ \vdots & & \vdots \\ \widehat{x}_N^{(t)}[1] & \widehat{x}_N^{(t)}[2] & \widehat{x}_N^{(t)}[3] \end{bmatrix}^T \tag{50}$$

The Maximization step when using a triangulation Lidar , an odometer and a sonar

In this case the matrix C is equal to

$$C = \begin{bmatrix} C[1] \\ C[2] \\ C[3] \end{bmatrix} = \begin{bmatrix} \alpha_0^l & \alpha_1^l & \alpha_2^l \\ \alpha_0^o & \alpha_1^o & \alpha_2^o \\ \alpha_0^u & \alpha_1^u & \alpha_2^u \end{bmatrix} \tag{51}$$

where the parameters of the triangulation Lidar are given by $C[1]$ and β_2^l, the ones of the odometer are given by $C[2]$ and β_0^o, and the ones of the ultrasonic ranger are given by $C[3]$ and β_0^u. The situation is as before, where sensors' parameters can be learned independently; one may then repeat the procedures in Sections 5.3 and 5.3, and then apply strategy (49)-(50) for the particular case of the ultrasonic data $\boldsymbol{y}^u$, H^u and $C[3]$.

6 Using the results of the EM calibration algorithm for testing purposes

The EM algorithm in Section (5) returns two different quantities:

- an estimate $\widehat{\boldsymbol{x}}$ of the latent variables $\boldsymbol{x}$, from which one can also estimate the various d_ks;
- an estimate $\widehat{\theta}$ of the calibration parameters θ.

The EM strategy thus can be directly used to transform the raw measurements $\boldsymbol{y}$ into some statistical estimate of the distances d_k. Nonetheless the EM algorithm may be computationally demanding, and one may prefer to run it only when strictly necessary.

Assume thus to have run the EM calibration algorithm fully once, and to want now to process some new raw data with a more lightweight estimation strategy. Given that we have $\widehat{\theta}$, at this point to obtain an estimated $\widehat{\boldsymbol{x}}$ (and thus $\widehat{d}_k$s) one simply has to run just once the Kalman smoother defined in Algorithm 3 (again with initial conditions $\widehat{x}_k^{(0)} = [1, \text{mean}(y_k), \ldots, \text{mean}(y_k)^{p-1}]$).

As will be shown in Section 7, this heuristic is fast and provides results similar to a dedicated complete EM algorithm when applied to a dataset with small sample size.

7 Numerical results

We consider datasets where the same robot moves with different constant speeds (0.1, 0.2, and 0.3 m/s) towards a fixed wooden target starting at a distance of 0.5m and ending at a distance of 4 m (two datasets per each speed). The robot mounts a Lidar, an odometer, and a sonar sensors, and we collect the groundtruth distances d_ks using a Vicon motion capture

system. We measure the statistical performance of an estimate $\widehat{d}_1, \ldots, \widehat{d}_N$ with the normalized empirical MSE

$$\text{NMSE} := \frac{1}{N} \sum_{k=1}^{N} \frac{\left\| \widehat{d}_k - d_k \right\|^2}{\|d_k\|^2}. \tag{52}$$

7.1 Testing the strategy in Section 5

We now analyze how the groundtruth-less EM calibration procedure compares w.r.t. a groundtruth-based one, and what is the influence of using more than one sensor. We thus plot in Figure 2 the normalized MSE for the full EM strategy in Section 5 for different speeds and different combinations of sensors (*raw Lidar data* indicating the MSE of the Lidar measurements y_k^l, while *groundtruth-based* indicates the MSE obtained when training[1] the estimator proposed in [31]). The collected evidence indicates that combining odometry measurements does not improve the estimation outcomes while adding the sonar does. Moreover increasing the speed (that corresponds to diminish the number of samples in the dataset) as expected leads to a generalized worsening of the estimation performance.

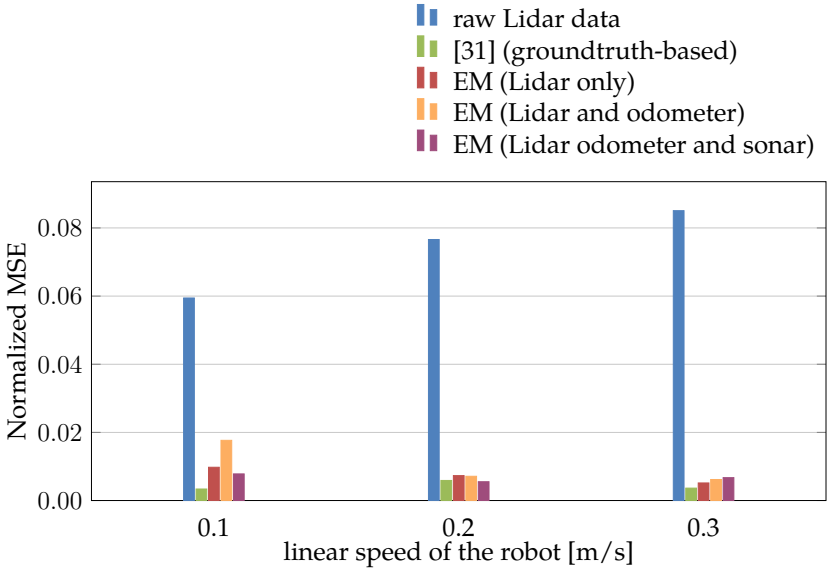

Figure 2: Comparison of the normalized empirical MSE for various types of estimators testing using different combinations of Lidar, odometer and sonar sensors.

To give a rough indication of how the computational complexity of our EM strategy depends on the number of samples in the dataset and on the number of sensors used, we plot in Figure 3 the convergence time of the algorithm implemented in Matlab on a standard laptop.

[1] We considered the training MSE and not the test one so to be even more unfavorable comparisons against our novel procedure.

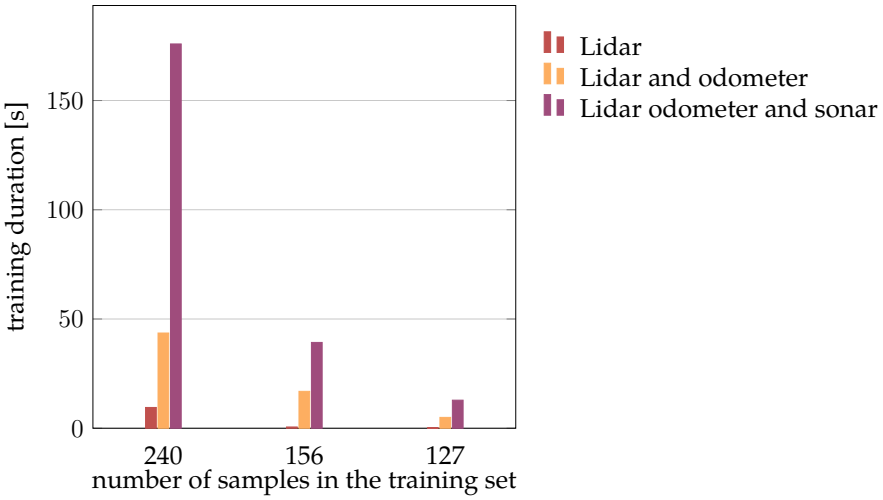

Figure 3: Dependency of the convergence time of the algorithm on the number of samples in the dataset used for training purposes.

7.2 Testing the strategy in Section 6

We then analyze if it is necessary to run the full EM algorithm every time, or if we can one do just one calibration once and after that use the Kalman smoother, and (in case) how the performance of the Kalman smoother based strategy depend on the size of the test dataset.

To answer these questions we use one dataset recorded at 0.1 m/s for the full EM training step (i.e., the richest dataset in terms of number of samples) and then apply the Kalman smoother as indicated in Section 6 in the other datasets.

Figure 4 then shows the normalized empirical MSE indices obtained for the various speeds and estimators (*raw Lidar data* indicating once again the MSE of the raw Lidar measurement y_k^l, and *groundtruth-based* indicating the MSE obtained testing the estimator proposed in [31] and trained as in Figure 2). The other three entries instead refer to using the Kalman smoother on test sets windows that are 12 samples long; for these estimators each bar in the plot thus represents the average of the MSEs calculated along the whole dataset at a given speed. We notice how the novel strategy compares favorably against the groundtruth-based one, indicating that it reaches good generalization capabilities. Also in this plot, combining the odometer measurements with the Lidar measurements does not improve the MSE in most of the cases.

Figure 5 eventually answers the question about how the performance of the Kalman smoother depends on the size of the training set, focusing just on the case where one uses only the Lidar sensor. We see that larger sample sizes almost always return a smaller MSE, and that also increasing the robot linear speed seems to decrease the normalized MSE for speeds smaller than 0.4 m/s.

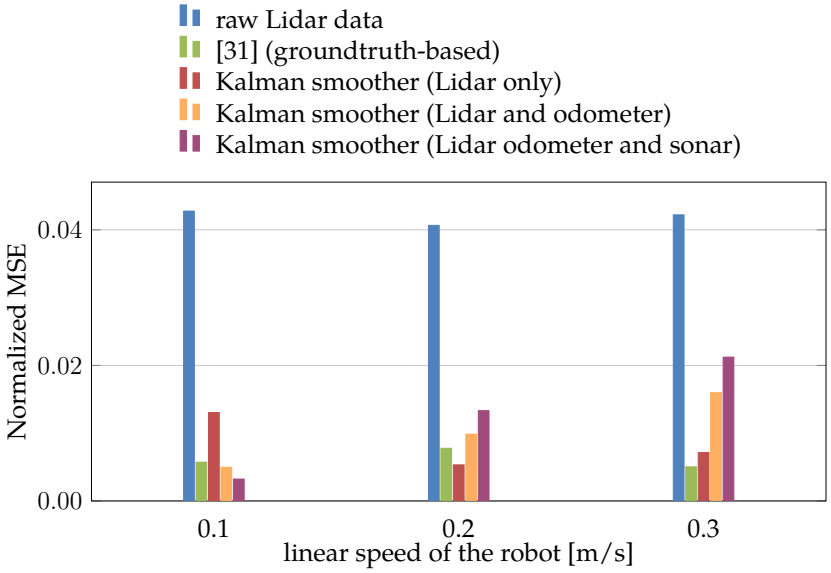

Figure 4: Comparison of the test-set performance of various estimators.

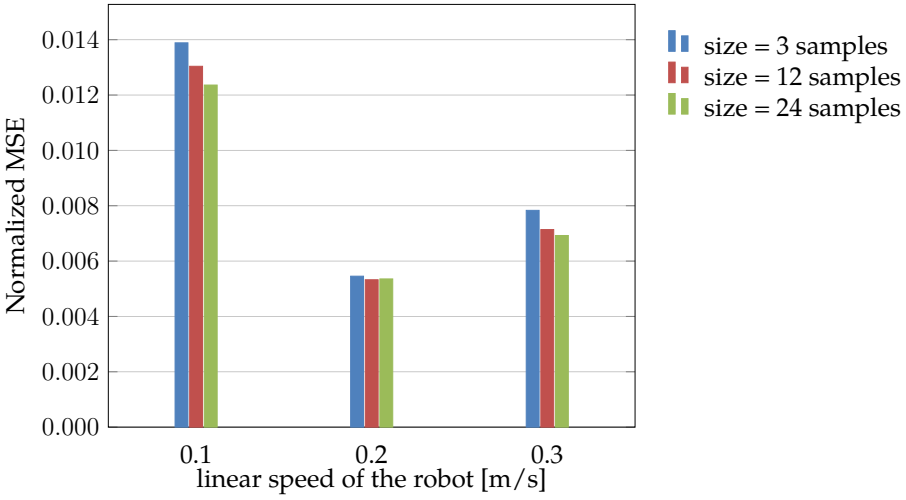

Figure 5: Dependency of the performance of the Kalman smoothing strategy on the size of the test set.

8 Conclusions

We designed and tested approximated EM plus Kalman smoother-based estimation strategies that allow, under the assumptions of linear motion and knowledge of which actuation inputs have been given to the motors of the robot, to jointly (or separately) calibrate sets of homoscedastic and heteroscedastic sensors such as triangulation Lidars , sonars and odometers without the need for groundtruth information.

The purpose of our effort is to make possible (and computationally cheap) for terrestrial robots to autonomously recalibrate their sensors whenever they feel they need, without having to go back to the factory or requiring the aid of technicians.

The proposed calibration procedure has also been shown to compete with alternative groundtruth-based strategies, validating thus our efforts at least in our experimental setup.

Despite promising, the strategy hasn't been fully developed yet: future research efforts are then directed to both prove the theoretical convergence properties of the overall EM scheme, plus generalize the strategy towards also aerial robotic applications, where our assumptions on the robot moving on a line are not valid anymore.

References

[1] K. Konolige, J. Augenbraun, N. Donaldson, C. Fiebig, and P. Shah, "A low-cost laser distance sensor," in *Robotics and Automation, 2008. ICRA 2008. IEEE International Conference on*. IEEE, 2008, pp. 3002–3008.

[2] J. Lima, J. Gonçalves, and P. J. Costa, "Modeling of a low cost laser scanner sensor," in *CONTROLO'2014–Proceedings of the 11th Portuguese Conference on Automatic Control*. Springer, 2015, pp. 697–705.

[3] D. Campos, J. Santos, J. Gonçalves, and P. Costa, "Modeling and simulation of a hacked neato xv-11 laser scanner," in *Robot 2015: Second Iberian Robotics Conference*. Springer, 2016, pp. 425–436.

[4] Q. Zhang and R. Pless, "Extrinsic calibration of a camera and laser range finder (improves camera calibration)," in *Intelligent Robots and Systems, 2004.(IROS 2004). Proceedings. 2004 IEEE/RSJ International Conference on*, vol. 3. IEEE, 2004, pp. 2301–2306.

[5] C. Mei and P. Rives, "Calibration between a central catadioptric camera and a laser range finder for robotic applications," in *Robotics and Automation, 2006. ICRA 2006. Proceedings 2006 IEEE International Conference on*. IEEE, 2006, pp. 532–537.

[6] O. Jokinen, "Self-calibration of a light striping system by matching multiple 3-d profile maps," in *3-D Digital Imaging and Modeling, 1999. Proceedings. Second International Conference on*. IEEE, 1999, pp. 180–190.

[7] B. Tiddeman, N. Duffy, G. Rabey, and J. Lokier, "Laser-video scanner calibration without the use of a frame store," in *Vision, Image and Signal Processing, IEE Proceedings-*, vol. 145, no. 4. IET, 1998, pp. 244–248.

[8] H. Andreasson, R. Triebel, and W. Burgard, "Improving plane extraction from 3d data by fusing laser data and vision," in *Intelligent Robots and Systems, 2005.(IROS 2005). 2005 IEEE/RSJ International Conference on*. IEEE, 2005, pp. 2656–2661.

[9] G.-Q. Wei and G. Hirzinger, "Active self-calibration of hand-mounted laser range finders," *Robotics and Automation, IEEE Transactions on*, vol. 14, no. 3, pp. 493–497, 1998.

[10] A. M. McIvor, "Calibration of a laser stripe profiler," in *3-D Digital Imaging and Modeling, 1999. Proceedings. Second International Conference on*. IEEE, 1999, pp. 92–98.

[11] Q. Zhang and R. Pless, "Constraints for heterogeneous sensor auto-calibration," in *Computer Vision and Pattern Recognition Workshop, 2004. CVPRW'04. Conference on*. IEEE, 2004, pp. 38–38.

[12] C.-Y. Chen and H.-J. Chien, "On-site sensor recalibration of a spinning multi-beam lidar system using automatically-detected planar targets," *Sensors*, vol. 12, no. 10, pp. 13 736–13 752, 2012.

[13] N. Muhammad and S. Lacroix, "Calibration of a rotating multi-beam lidar," in *Intelligent Robots and Systems (IROS), 2010 IEEE/RSJ International Conference on*. IEEE, 2010, pp. 5648–5653.

[14] G. Atanacio-Jiménez, J.-J. González-Barbosa, J. B. Hurtado-Ramos, F. J. Ornelas-Rodríguez, H. Jiménez-Hernández, T. García-Ramirez, and R. González-Barbosa, "Lidar velodyne hdl-64e calibration using pattern planes," *International Journal of Advanced Robotic Systems*, vol. 8, no. 5, pp. 70–82, 2011.

[15] C. Glennie and D. D. Lichti, "Static calibration and analysis of the velodyne hdl-64e s2 for high accuracy mobile scanning," *Remote Sensing*, vol. 2, no. 6, pp. 1610–1624, 2010.

[16] ——, "Temporal stability of the velodyne hdl-64e s2 scanner for high accuracy scanning applications," *Remote Sensing*, vol. 3, no. 3, pp. 539–553, 2011.

[17] C. Glennie, "Calibration and kinematic analysis of the velodyne hdl-64e s2 lidar sensor," *Photogrammetric Engineering & Remote Sensing*, vol. 78, no. 4, pp. 339–347, 2012.

[18] M. Gordon and J. Meidow, "Calibration of a multi-beam laser system by using a tls-generated reference," *ISPRS Annals of Photogrammetry, Remote Sensing and Spatial Information Sciences II-5 W*, vol. 2, pp. 85–90, 2013.

[19] F. M. Mirzaei, D. G. Kottas, and S. I. Roumeliotis, "3d lidar–camera intrinsic and extrinsic calibration: Identifiability and analytical least-squares-based initialization," *The International Journal of Robotics Research*, vol. 31, no. 4, pp. 452–467, 2012.

[20] X. Gong, Y. Lin, and J. Liu, "3d lidar-camera extrinsic calibration using an arbitrary trihedron," *Sensors*, vol. 13, no. 2, pp. 1902–1918, 2013.

[21] Y. Park, S. Yun, C. S. Won, K. Cho, K. Um, and S. Sim, "Calibration between color camera and 3d lidar instruments with a polygonal planar board," *Sensors*, vol. 14, no. 3, pp. 5333–5353, 2014.

[22] L. Kneip, F. Tâche, G. Caprari, and R. Siegwart, "Characterization of the compact hokuyo urg-04lx 2d laser range scanner," in *Robotics and Automation, 2009. ICRA'09. IEEE International Conference on*. IEEE, 2009, pp. 1447–1454.

[23] A. Reina and J. Gonzales, "Characterization of a radial laser scanner for mobile robot navigation," in *Intelligent Robots and Systems, 1997. IROS'97., Proceedings of the 1997 IEEE/RSJ International Conference on*, vol. 2. IEEE, 1997, pp. 579–585.

[24] K.-H. Lee and R. Ehsani, "Comparison of two 2d laser scanners for sensing object distances, shapes, and surface patterns," *Computers and electronics in agriculture*, vol. 60, no. 2, pp. 250–262, 2008.

[25] R. Sanz-Cortiella, J. Llorens-Calveras, J. R. Rosell-Polo, E. Gregorio-Lopez, and J. Palacin-Roca, "Characterisation of the lms200 laser beam under the influence of blockage surfaces. influence on 3d scanning of tree orchards," *Sensors*, vol. 11, no. 3, pp. 2751–2772, 2011.

[26] P. Tang, B. Akinci, and D. Huber, "Quantification of edge loss of laser scanned data at spatial discontinuities," *Automation in Construction*, vol. 18, no. 8, pp. 1070–1083, 2009.

[27] J. Tuley, N. Vandapel, and M. Hebert, "Analysis and removal of artifacts in 3-d ladar data," in *Robotics and Automation, 2005. ICRA 2005. Proceedings of the 2005 IEEE International Conference on*. IEEE, 2005, pp. 2203–2210.

[28] C. Ye and J. Borenstein, "Characterization of a 2-d laser scanner for mobile robot obstacle negotiation," in *ICRA*, 2002, pp. 2512–2518.

[29] D. Anderson, H. Herman, and A. Kelly, "Experimental characterization of commercial flash ladar devices," in *International Conference of Sensing and Technology*, vol. 2, 2005.

[30] A. Alhashimi, D. Varagnolo, and T. Gustafsson, "Joint temperature-lasing mode compensation for time-of-flight lidar sensors," *Sensors*, vol. 15, no. 12, pp. 31 205–31 223, 2015.

[31] ——, "Statistical modeling and calibration of triangulation lidars," in *ICINCO*, 2016.

[32] J. Kelly and G. S. Sukhatme, "A general framework for temporal calibration of multiple proprioceptive and exteroceptive sensors," in *Experimental Robotics*. Springer, 2014, pp. 195–209.

[33] K. S. Chong and L. Kleeman, "Accurate odometry and error modelling for a mobile robot," in *Robotics and Automation, 1997. Proceedings., 1997 IEEE International Conference on*, vol. 4. IEEE, 1997, pp. 2783–2788.

[34] A. Martinelli, N. Tomatis, and R. Siegwart, "Simultaneous localization and odometry self calibration for mobile robot," *Autonomous Robots*, vol. 22, no. 1, pp. 75–85, 2007.

[35] L. Kleeman, "Advanced sonar and odometry error modeling for simultaneous localisation and map building," in *Intelligent Robots and Systems, 2003.(IROS 2003). Proceedings. 2003 IEEE/RSJ International Conference on*, vol. 1. IEEE, 2003, pp. 699–704.

[36] S. Gibson and B. Ninness, "Robust maximum-likelihood estimation of multivariable dynamic systems," *Automatica*, vol. 41, no. 10, pp. 1667–1682, 2005.

[37] R. H. Shumway and D. S. Stoffer, "An approach to time series smoothing and forecasting using the em algorithm," *Journal of time series analysis*, vol. 3, no. 4, pp. 253–264, 1982.

[38] ——, *Time series analysis and its applications: with R examples*. Springer Science & Business Media, 2006.